UC-413

LBL-27878

Lawrence Berkeley Laboratory

UNIVERSITY OF CALIFORNIA

Delayed-Fission Properties of Neutron-Deficient Americium Nuclei

H.L. Hall

(Ph.D. Thesis)

October 1989

NUCLEAR SCIENCE DIVISION

For Reference

Not to be taken from this room

Prepared for the U.S. Department of Energy under Contract Number DE-AC03-76SF00098.

DISCLAIMER

This document was prepared as an account of work sponsored by the United States Government. Neither the United States Government nor any agency thereof, nor The Regents of the University of California, nor any of their employees, makes any warranty, express or implied, or assumes any legal liability or responsibility for the accuracy, completeness, or usefulness of any information, apparatus, product, or process disclosed, or represents that its use would not infringe privately owned rights. Reference herein to any specific commercial products process, or service by its trade name, trademark, manufacturer, or otherwise, does not necessarily constitute or imply its endorsement, recommendation, or favoring by the United States Government or any agency thereof, or The Regents of the University of California. The views and opinions of authors expressed herein do not necessarily state or reflect those of the United States Government or any agency thereof or The Regents of the University of California and shall not be used for advertising or product endorsement purposes.

Lawrence Berkeley Laboratory is an equal opportunity employer.

LBL-27878

Delayed-Fission Properties of Neutron-Deficient Americium Nuclei

Howard L. Hall

Ph. D. Thesis

Department of Chemistry
University of California
Berkeley, CA 94720

and

Nuclear Science Division
Lawrence Berkeley Laboratory
Berkeley, CA 94720

October 23, 1989

This work was supported in part by the Director, Office of Energy Research, Division of Nuclear Physics of the Office of High Energy and Nuclear Physics of the U.S. Department of Energy under Contract DE-AC03-76SF00098.

Delayed-Fission Properties of Neutron-Deficient Americium Nuclei

by

Howard L. Hall

Abstract

Characteristics of the delayed-fission decay mode in light americium nuclei have been investigated. Measurements on the unknown isotopes ^{230}Am and ^{236}Am were attempted, and upper limits on the delayed-fission branches of these nuclei were determined. Evidence of the existence of ^{236}Am was observed in radiochemical separations. Total kinetic energy and mass-yield distributions of the electron-capture delayed-fission mode were measured for ^{232}Am ($t_{1/2} = 1.31 \pm 0.04$ min) and for ^{234}Am ($t_{1/2} = 2.32 \pm 0.08$ min), and delayed-fission probabilities of 6.9×10^{-4} and 6.6×10^{-5}, respectively, were determined. The total kinetic energy and the asymmetric mass-yield distributions are typical of fission of mid-range actinides. No discernible influence of the anomalous triple-peaked mass division characteristic of the thorium-radium region was detected. Measurements of the time correlation between the electron-capture x-rays and the subsequent fission confirm that the observed fissions arise from the electron-capture delayed-fission mechanism. Delayed fission has provided a unique opportunity to extend the range of low-energy fission studies to previously inaccessible regions.

Dedication

This thesis is dedicated to those people who have contributed significantly to my development as a scientist:

- My parents, Harvey Eugene Hall and the late Marie Wavilee Hall, who instilled in me a basic curiosity about the workings of the world in which we live.
- Dr. Gary Asleson of the College of Charleston, who sparked my interest in chemistry during the summer of 1984 at the South Carolina Governor's School.
- Dr. Carl Likes, who caused me to major in chemistry.
- The DOE/ACS Summer School in Nuclear and Radiochemistry, which lead me to chose the University of California for graduate school, and nuclear chemistry as a speciality.
- Dr. Darleane Hoffman, whose wisdom, experience, and guidance have been invaluable in the performance of this work.
- Finally, my wife Mary, whose continual support and encouragement made the work bearable and this accomplishment possible.

Acknowledgements

The author is grateful to the other members of the LBL Heavy Ion Radiochemistry Group (D. C. Hoffman, D. M. Lee, M. J. Nurmia, K. E. Gregorich, R. A. Henderson, C. M. Gannett, D. A. Bennett, J. D. Leyba, R. B. Chadwick, K. R. Czerwinski, B. Kadkhodayan, S. A. Kreek, and N. J. Hannink) and collaborators (G. T. Seaborg, C. E. A. Palmer, and P. A. Baisden) for their assistance.

This work was supported in part by the Director, Office of Energy Research, Division of Nuclear Physics of the Office of High Energy and Nuclear Physics of the U.S. Department of Energy under Contract DE-AC03-76SF00098.

This work was supported in part by a National Science Foundation Graduate Fellowship. The results, views, and findings of this work are those of the author only and do not necessarily reflect those of the National Science Foundation.

The author wishes to thank the staff and crew of the LBL 88" Cyclotron for their patience and assistance.

Contents

1 Introduction **1**

2 Experimental Precedent **4**

3 Theory of Delayed Fission **8**

4 Targets and Irradiations **15**

4.1 ^{237}Np Targets 15

4.1.1 Development of the Multiple Target System 15

4.1.2 Preparation of ^{237}Np Targets 22

4.2 ^{207}Pb Targets 26

4.3 Irradiations 29

5 Experimental Procedures **32**

5.1 On-line Procedures 32

5.2 Chemical Procedures 38

5.2.1 Chemical Procedure for Elemental Assignment 38

5.2.2 Chemical Procedure for P_{DF} and σ_ε Measurement 39

5.3 Correlation Study Procedures 45

6 Results **49**

6.1 ^{230}Am Results 49

6.2 ^{232}Am Results 54

6.2.1 Elemental Assignment 54
6.2.2 On-line Results 55
6.2.3 P_{DF} and σ_ε Results 59
6.2.4 X-ray–Fission Results 66
6.3 ^{234}Am Results 69
6.3.1 Elemental Assignment 69
6.3.2 On-line Results 69
6.3.3 P_{DF} and σ_ε Results 76
6.3.4 X-ray–Fission Results 83
6.4 ^{236}Am Results 85
6.4.1 On-line Measurements 85
6.4.2 Radiochemical Measurements 89

7 Conclusions **99**

A X-ray - Fission Code **104**

List of Figures

1.1 Schematic illustration of delayed fission 2

3.1 Potential DF regions in the heavy elements 12

3.2 Fermi functions 14

4.1 Low-energy recoil ranges of americium in helium 18

4.2 **LIM** Target System schematic 20

4.3 Horizontal cross-section of the **LIM** Target System 21

4.4 α + ^{237}Np predicted cross sections 27

4.5 ^{27}Al + ^{207}Pb predicted cross sections 28

4.6 Single-target recoil chamber 30

5.1 **MG** Detector Schematic 34

5.2 **MG** α calibration spectrum 35

5.3 **MG** fission calibration 36

5.4 Overview of **MG-RAGS** 37

5.5 Elemental assignment chemistry 40

5.6 Elemental assignment chemistry: Tracers 41

5.7 Gamma measurement chemistry 43

5.8 Gamma measurement chemistry: Tracers 44

5.9 X-ray–fission correlation set-up 47

6.1 α particles from ^{230}Am search 50

6.2 ^{230}Am $\sigma_{<f>}$ versus $t_{1/2}$ 53

6.3 ^{232}Am fission decay curve 56
6.4 ^{232}Am TKE and mass-yield distributions 58
6.5 ^{232}Am TKE contour plot 60
6.6 ^{232}Am x-rays 63
6.7 ^{232}Am EC decay curve 64
6.8 ^{232}Am x-rays with fission 67
6.9 ^{234}Am fission decay curve 71
6.10 ^{234}Am TKE and mass-yield distributions 73
6.11 ^{234}Am TKE contour plot 74
6.12 ^{234}Am α spectrum 75
6.13 ^{234}Am 6.46 MeV α decay curve 77
6.14 Gamma rays observed in ^{234}Am samples 78
6.15 ^{234}Am x-rays 80
6.16 ^{234}Am EC decay curve 81
6.17 ^{234}Am x-rays with fission 84
6.18 ^{236}Am α spectrum 87
6.19 ^{236}Am 6.41-MeV α group decay curve 88
6.20 ^{236}Am $\sigma_{<f>}$ versus $t_{1/2}$ 91
6.21 γ rays in the ^{236}Am sample 93
6.22 K x-ray region of ^{236}Am γ spectrum 94
6.23 Calculated ^{236}Am excitation function 95
6.24 ^{236}Am x-ray half-life fit 97

7.1 $\overline{\mathrm{TKE}}$ versus $Z^2/A^{1/3}$ 101
7.2 Possible peaks from shape isomeric levels 102

List of Tables

2.1 Reported εDF activities 6

2.2 Reported βDF activities 7

4.1 ^{237}Np Targets - Set A 23

4.2 ^{237}Np Targets - Set B 25

6.1 ^{230}Am fissions 51

6.2 ^{232}Am εDF properties 61

6.3 ^{232}Am P_{DF} measurements 65

6.4 ^{232}Am X-F intensities 68

6.5 ^{234}Am εDF properties 72

6.6 ^{234}Am P_{DF} measurements 82

6.7 ^{234}Am X-F intensities 90

6.8 ^{236}Am fissions 90

6.9 ^{236}Am $t_{1/2}$ determinations 96

Chapter 1

Introduction

Delayed fission (DF) is a nuclear decay process in which a decaying nucleus populates excited states in its daughter nucleus, which then fission. These states can be above the fission barrier(s) of the daughter (yielding prompt fission), within the second well of the potential energy surface (a fission shape isomer), or within the first well of the potential energy surface (an electromagnetic isomer). This process is illustrated schematically in Figure 1.1. β or EC decay from a parent which has a Q-value smaller than the height of the fission barrier in the daughter should predominately populate states in the first well, since feeding into the second well would involve a collective rearrangement occurring simultaneously with the EC (or β) decay. Once the high-lying states in the daughter nucleus are populated, tunnelling through the barrier to the second well must compete with γ transitions leading to low-lying states in the inner well for fission to be observed. Once the nucleus has tunnelled into the second well (and formed a shape isomer), tunnelling through the second barrier must again compete with γ decay and tunnelling through the inner barrier (returning to the first well).

Delayed fission is believed to influence the production yields of heavy elements in multiple neutron capture processes [Burbidge 57,Wene 74,Wene 75, Klapdor 81,Meyer 89] followed by β decay, such as the astrophysical **r**-process

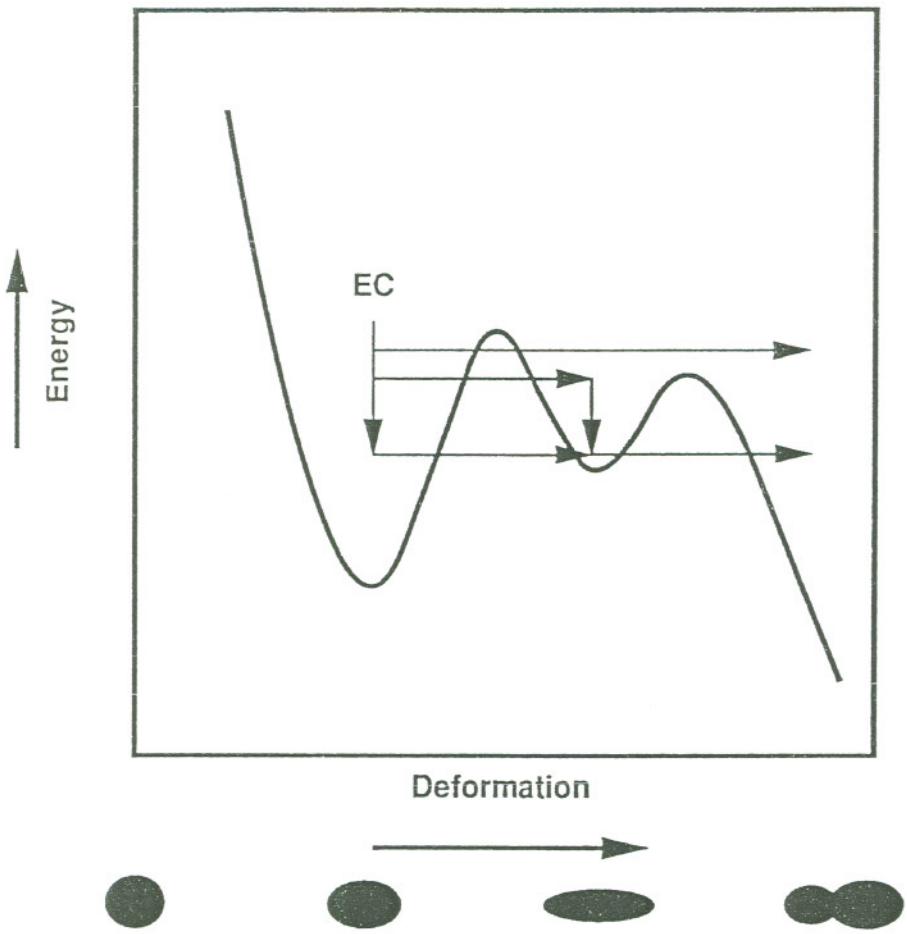

Figure 1.1: Two-dimensional illustration of the delayed-fission process. The potential energy curve of the daughter nucleus is shown, displaying the double-humped fission barrier prevalent in the actinide region.

and the production of heavy elements in nuclear devices. Both of these events produce extremely high neutron fluxes in the vicinity of heavy elements for a short period of time. In the case of the r-process, the flux is found in the heart of a star as it undergoes an explosive supernova. Since the heavier elements tend to concentrate in the center of stars due to gravitational and thermal forces, they are exposed to this huge neutron flux for a brief period. In the case of nuclear explosives, similarly large neutron fluxes can be generated upon detonation of the device. In both supernovae and nuclear weapons detonations, the combination of high neutron flux and available heavy targets lead to multiple neutron-capture events which can produce neutron-rich nuclei all the way to the neutron-drip line. Following neutron capture, these neutron-rich nuclei begin to β decay towards stability, producing higher atomic number elements. If this chain of β decays were to continue, the very heavy actinides (and possibly superheavy elements) would be produced in amounts that are not observed in nature nor in weapons-tests products [HOFF 86]. It is believed that delayed fission terminates the β-decay chain, diminishing the production of the higher Z elements [BURBIDGE 57,MEYER 89], while prompt fission and very short spontaneous fission half-lives terminate the neutron-capture process.

Delayed-fission processes may also provide a sensitive probe of fission barriers in the heavy element region [LAZAREV 80], since, if the parent Q-value is well known or can be accurately calculated, information about the structure of the fission barriers can be extracted from the probability of delayed fission. This would allow investigation of the fission barriers in nuclei well outside the range of normal experiments such as (n, f) and charged particle reactions. Delayed fission also has the potential to greatly expand the number of nuclei whose fission properties may be measured, since the electron-capture daughters usually have spontaneous fission partial half-lives which are much too long relative to their overall half-lives to allow detailed study.

Chapter 2

Experimental Precedent

Fission tracks from EC-delayed fission (εDF) were first observed [KUZNETSOV 66, KUZNETSOV 67] in the light americium and neptunium regions as early as 1966. In 1969, Berlovich and Novikov [BERLOVICH 69] noted that the nuclei in question met the conditions required for delayed fission, although the observed fissions were not specifically attributed [SKOBELEV 72] to delayed-fission processes until 1972. A fission mode in ^{232}Am was confirmed by Habs *et al.* [HABS 78] in 1978, and the P_{DF} for this isotope was reported to be on the order of one percent. An εDF branch has been tentatively assigned [HINGMANN 85] to ^{242}Es, again with a P_{DF} on the order of one percent. Recently, εDF has been reported [LAZAREV 87] outside the actinide elements, in the region of ^{180}Hg.

Most studies have reported only half-life and fission cross-section (σ_f) data measured without any separation of the delayed-fissile species from other reaction products. The cross section for producing the nuclei which decay by electron capture, ($\sigma_\varepsilon = \sigma B_\varepsilon$, where σ is the overall production cross section and B_ε is the EC branching ratio), when reported, has generally been extracted from theoretical calculations or systematics (such as evaporation codes), not measured experimentally. ^{242}Es-^{242}Cf is an exceptional case in that it was separated from most other reaction products using the velocity filter, **SHIP**, at GSI, but Hingmann *et al.* were

unable to unambiguously identify the fissioning species and have not reported their measurement in the reviewed literature. They report the observation of the α particles emitted from the EC daughter, ^{242}Cf, and hence estimate σ_ε. Gangrskiĭ *et al.* [GANGRSKIĬ 80] report delayed-fission probabilities for several trans-curium nuclei using the measured α decay of the EC daughter to estimate σ_ε. All reports of εDF are summarized in Table 2.1.

β-delayed fission (βDF) has been postulated to play a role in multiple neutron-capture processes since the 1950's. βDF was proposed by Burbidge, Burbidge, Fowler and Hoyle [BURBIDGE 57] as a route for depleting the yield of heavy elements produced in supernovae. βDF is also one possible explanation of why superheavy elements are not found in nature [WENE 74,WENE 75]. βDF had been predicted to significantly influence heavy-element yields in nuclear weapons tests [WENE 74,WENE 75]; however, a recent reexamination of these data shows that the predicted delayed-fission effects are seriously overestimated [HOFF 86, HOFF 88].

The first report of an observed fission activity attributable to β-delayed fission appeared in 1978. Gangrskiĭ *et al.* [GANGRSKIĬ 78] reported that ^{236}Pa and ^{238}Pa exhibited βDF with delayed-fission probabilities of about 10^{-10} and $10^{-6.2}$, respectively. Gangrskiĭ *et al.* performed no chemical separation after producing the two protactinium isotopes in irradiated uranium foils, simply measuring fissions with track detectors following the irradiations. Subsequently, Baas-May *et al.* [BAAS-MAY 85] studied ^{238}Pa using automated chemical separation procedures and observed no fission mode in this isotope. They set an upper limit on the delayed fission probability for ^{238}Pa of $P_{DF} \leq 2.6 \times 10^{-8}$, a factor of 25 lower than the measurement by Gangrskiĭ *et al.* This failure to confirm βDF in ^{238}Pa cast considerable doubt on the earlier report [GANGRSKIĬ 78] of a βDF branch in ^{236}Pa, since both ^{236}Pa and ^{238}Pa were measured in a similar fashion. ^{256m}Es is the most recently identified [HALL 89B] β-delayed fissile species. This isotope was identified chemically and βDF was observed using β-fission time correlations. ^{256m}Es is also

Table 2.1: Summary of reported observations of EC-delayed fission.

Nuclide[a]	$t_{1/2}$[b]	P_{DF}[c]	Reference
^{250}Md	52 sec.	2×10^{-4}	[GANGRSKIĬ 80]
^{248}Es	28 min.	3×10^{-7}	[GANGRSKIĬ 80]
^{246}Es	8 min.	3×10^{-5}	[GANGRSKIĬ 80]
^{244}Es	37 sec.	10^{-4}	[GANGRSKIĬ 80]
^{242}Es?	5 - 25 sec.	$(1.4 \pm 0.8) \times 10^{-2}$	[HINGMANN 85]
^{240}Bk	4 min.	10^{-5}	[GANGRSKIĬ 80]
^{234}Am	2.6 ± 0.2 min.	NR[d,e]	[SKOBELEV 72]
^{234}Am	2.6 ± 0.2 min.	NR	[SOMERVILLE 77]
^{232}Am	1.4 ± 0.25 min.	NR[e]	[SKOBELEV 72]
^{232}Am	0.92 ± 0.12 min.	$1.3^{+4}_{-0.8} \times 10^{-2}$	[HABS 78]
^{228}Np	60 ± 5 sec.	NR	[SKOBELEV 72]
^{180}Tl?	$0.70^{+0.12}_{-0.09}$ sec.	$\sim 10^{-6}$	[LAZAREV 87]

[a]The parent nuclide undergoing EC decay to a daughter which then fissions is given.
[b]Half-life is given as reported, or converted to a common unit when multiple references exist.
[c]Errors are given if reported.
[d]Not reported.
[e]Kuznetsov [KUZNETSOV 79] used the data from this report and estimated P_{DF} for ^{232}Am and ^{234}Am to be 6.96×10^{-2} and 6.95×10^{-5}, respectively.

Table 2.2: Summary of reported observations of β-delayed fission.

Nuclide[a]	$t_{1/2}$[b]	P_{DF}	Reference
^{256m}Es	7.6 hour	2×10^{-5}	[HALL 89B]
^{238}Pa[c]	2.3 min.	6×10^{-7}	[GANGRSKIĬ 78]
^{238}Pa[d]	2.3 min.	$\sim 10^{-8}$	[GANGRSKIĬ 78]
^{238}Pa[c]	2.3 min.	$\leq 2.6 \times 10^{-8}$	[BAAS-MAY 85]
^{236}Pa[e]	9.1 min.	$\sim 10^{-9}$	[GANGRSKIĬ 78]
^{236}Pa[f]	9.1 min.	3×10^{-10}	[GANGRSKIĬ 78]

[a]The parent nuclide undergoing β decay to a daughter which then fissions is given.
[b]Half-life is given as reported, or converted to a common unit when multiple references exist.
[c]Produced via ^{238}U(14.7-MeV n, p).
[d]Produced via ^{238}U(8–20-MeV n, p).
[e]Produced via ^{238}U(27-MeV γ, np).
[f]Produced via ^{238}U(18-MeV d, α).

---

the first case in which the fissioning isomeric level in the daughter nucleus has been assigned. A summary of experimental reports of βDF is presented in Table 2.2.

Chapter 3

Theory of Delayed Fission

The probability for the delayed-fission decay mode, P_{DF}, can be expressed in terms of experimentally measurable quantities as

$$P_{DF} = \frac{N_{if}}{N_i} = \frac{\sigma_{if}}{\sigma_i} \tag{3.1}$$

where N_i is the number of the type of decays of interest (*e.g.*, β or EC) and N_{if} is the number of those decays leading to delayed fission. Similarly, σ_{if} and σ_i are the corresponding cross sections. P_{DF} can also be derived from theoretical considerations as

$$P_{DF} = \frac{\int_0^{Q_i} W_i(Q_i - E)\, \frac{\Gamma_f}{\Gamma_f + \Gamma_\gamma}(E)\, dE}{\int_0^{Q_i} W_i(Q_i - E)\, dE} \tag{3.2}$$

where $W_i(Q_i - E)$ is the transition probability function for the decay of interest, $\frac{\Gamma_f}{\Gamma_f+\Gamma_\gamma}(E)$ is the ratio of the fission width of excited levels within the daughter nucleus to the total depopulation width of these states, E is the excitation energy of the daughter nucleus, and Q_i is the Q-value for the decay of interest. It has been assumed in this equation that no decay channels are open to the excited nucleus except fission and γ decay. As a result, the term $\frac{\Gamma_f}{\Gamma_f+\Gamma_\gamma}(E)$ is taken as being equal to the fission width divided by the total decay width, $\frac{\Gamma_f}{\Gamma_{tot}}(E)$. To be strictly correct, $\Gamma_{tot}(E)$ should include terms for particle emission as well as fission and γ decay,

but these decay widths are small enough that their omission in the denominator is acceptable.

The transition probability function, $W_i(E)$, can be expressed as the product of the Fermi function, f, and the beta strength function, S_β, giving

$$W_i(E) \approx f(Q_i - E, Z)\, S_\beta(E). \tag{3.3}$$

The Fermi function may be approximated as

$$f \approx \begin{cases} (Q_\varepsilon - E)^2 & \text{for EC decay,} \\ (Q_\beta - E)^5 & \text{for } \beta \text{ decay,} \end{cases} \tag{3.4}$$

for the calculation of P_{DF} in Equation (3.2).

S_β can be treated in several different ways. It can be taken as being proportional to the nuclear level density [WENE 74,SHALEV 77], it can be generated from the gross theory of β decay [KODAMA 75], or it can be taken as a constant above a certain energy [KRATZ 73,HORNSHØJ 75]. Klapdor *et al.* [KLAPDOR 79] have pointed out that all three of these common techniques ignore low-lying structure in the beta strength function, S_β. Klapdor found inclusion of low-lying structure (generated from a shell model) in the calculation of P_{DF} to have a significant impact on the value obtained. Although only the gross theory of β decay and the microscopic model can be considered theoretically self-consistent, however, for a qualitative understanding of P_{DF}, treating S_β as a constant above a cut-off energy is acceptable.

It is important to remember, although, that the structural effects ignored by this approach can significantly influence P_{DF}. For example, βDF has been observed to occur in ^{256m}Es with a P_{DF} of 2×10^{-5} from a single level at 1425 keV above the ground state [HALL 89B]. The assumption of a constant S_β would predict no delayed-fission branch, but in this case γ decay from the 1425-keV level was highly hindered (level half-life = 70 ns) so that fission was able to compete. Likewise, a nucleus with a high Q_ε-value would be expected to have a large P_{DF}, but if electron capture to the daughter's ground state is superallowed ($\Delta I^{\Delta\pi} = 0^{\text{No}}$) no high-lying states may be populated, hence P_{DF} in this case may be nearly zero.

The large dependence of P_{DF} on the energy available for the decay and the structure of the fission barrier arises primarily from the fission-width term, $\frac{\Gamma_f}{\Gamma_f+\Gamma_\gamma}(E)$. It is assumed that no decay channels other than γ decay and fission are open to the daughter, so that $(\Gamma_\gamma + \Gamma_f)$ is the total decay width. Γ_γ, the width for gamma decay, can be estimated [GANGRSKIĬ 80] from the probability for γ transitions, P_γ, as

$$\Gamma_\gamma = \frac{P_\gamma}{2\pi\rho} = \frac{C_\gamma\,\Theta^4\,e^{(E/\Theta)}}{2\pi\rho}, \tag{3.5}$$

where ρ is the nuclear level density, C_γ is a constant with the value 9.7×10^{-7} MeV^{-4}, and Θ is the nuclear temperature (0.5 - 0.6 MeV). The fission width, Γ_f, derived from the penetrability of the fission barrier in a similar fashion, yields

$$\Gamma_f = \frac{P_f}{2\pi\rho} \tag{3.6}$$

where P_f is the penetrability of the fission barrier.

Since the fission barrier in the region of the actinide nuclei is reasonably complex, it is common [HABS 78,GANGRSKIĬ 80] to simplify the penetrability through the entire two-humped barrier by approximating P_f to be

$$P_f \approx P_A(E)\,R_B \tag{3.7}$$

where $P_A(E)$ is the penetrability for tunnelling through the inner barrier and R_B is the transmission coefficient for fission from the lowest state in the second well. This, in effect, requires the nuclear motion in the second well to be strongly damped, *i.e.* fission from the second well is not allowed to occur before γ decay to the lowest-lying state. Hence, the calculation of P_f becomes much simpler. Transmission through the inner barrier B_A is then approximated as a simple parabolic barrier problem using the Hill-Wheeler [HILL 53] formalism

$$P_A = (1 + e^{\frac{2\pi(B_f - E)}{h\omega_f}})^{-1} \tag{3.8}$$

where B_f is the height of the barrier and $h\omega_f$ is the energy associated with the barrier curvature. This allows Γ_f to be expressed as

$$\Gamma_f \approx \frac{R_B}{2\pi\rho}(1 + e^{\frac{2\pi(B_f - E)}{h\omega_f}})^{-1}. \tag{3.9}$$

One can then express the quantity $\frac{\Gamma_f}{\Gamma_\gamma+\Gamma_f}(E)$ as

$$\frac{\Gamma_f}{\Gamma_\gamma+\Gamma_f}(E) \approx \frac{R_B(1+e^{\frac{2\pi(B_f-E)}{\hbar\omega_f}})^{-1}}{C_\gamma\,\Theta^4\,e^{(E/\Theta)}+R_B(1+e^{\frac{2\pi(B_f-E)}{\hbar\omega_f}})^{-1}}, \tag{3.10}$$

which illustrates the strong dependence of this term in Equation (3.2) on the energy available for decay and the structure of the fission barrier.

Utilizing these approximations, it is possible to rewrite Equation (3.2) for electron capture in the following simplistic form,

$$P_{DF} \approx \frac{\int_C^{Q_\varepsilon}(Q_\varepsilon-E)^2\,\frac{\Gamma_f}{\Gamma_\gamma+\Gamma_f}(E)\,dE}{\int_C^{Q_\varepsilon}(Q_\varepsilon-E)^2\,dE}, \tag{3.11}$$

where C is the cut-off energy below which S_β is presumed to be zero. This value has been given [KRATZ 73] as $C = 26A^{-1/2}$ MeV. The integral in the denominator is trivial and may be evaluated directly to give a normalization function $N_\varepsilon(A)$,

$$[N_\varepsilon(A)]^{-1} \equiv \int_C^{Q_\varepsilon}(Q_\varepsilon-E)^2\,dE = \frac{(Q_\varepsilon-26A^{-1/2})^3}{3}. \tag{3.12}$$

For βDF, $N_\beta(A)$ can be likewise evaluated to yield

$$[N_\beta(A)]^{-1} \equiv \int_C^{Q_\beta}(Q_\beta-E)^5\,dE = \frac{(Q_\varepsilon-26A^{-1/2})^6}{6}. \tag{3.13}$$

The remaining form of P_{DF},

$$P_{DF} \approx N_\varepsilon(A)\int_C^{Q_\varepsilon}(Q_\varepsilon-E)^2\,\frac{\Gamma_f}{\Gamma_\gamma+\Gamma_f}(E)\,dE \tag{3.14}$$

is exponentially dependent on the difference between the fission barrier and the energy available for decay, the electron-capture Q-value. Hence, for delayed fission to become a prominent decay mode in the actinide region (where fission barriers are on the order of 4-6 MeV), it is necessary to choose nuclei in which Q_ε is comparable to the fission barrier. This requires study of nuclei far from the valley of

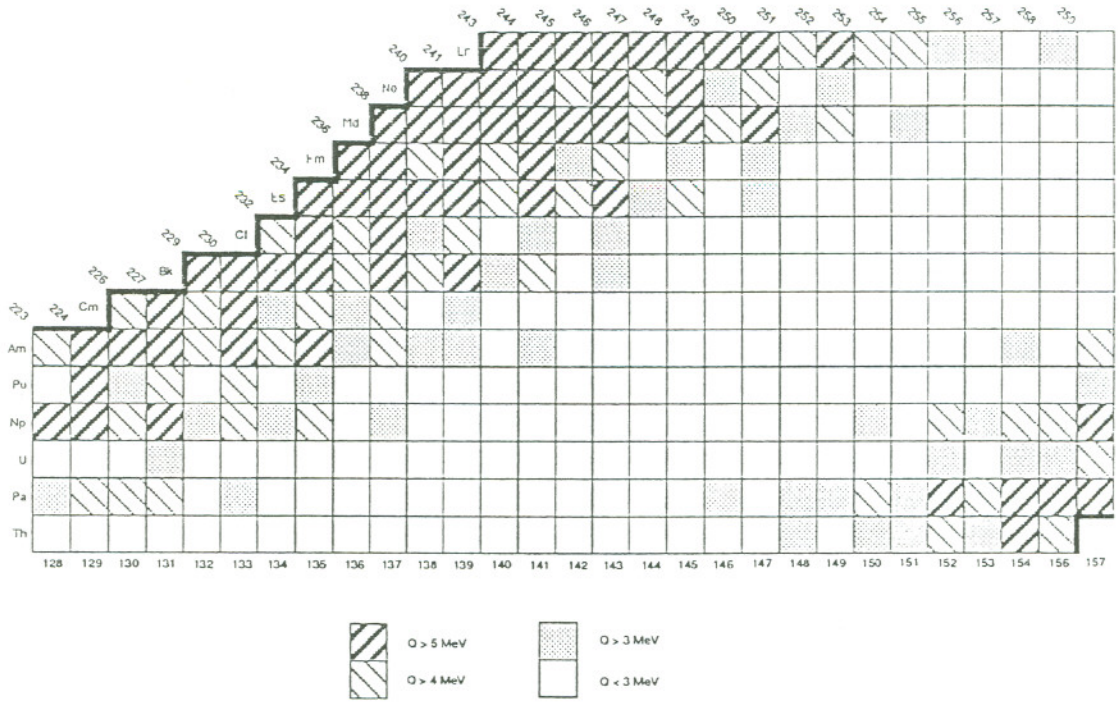

Figure 3.1: Regions in the heavy nuclei where delayed fission may occur due to high Q-values for EC or β decay. The heavy lines mark the proton and neutron drip lines, and Q-values are calculated from the masses of Möller *et al.* [MÖLLER 88].

β-stability (see Figure 3.1), which introduces a number of experimental difficulties in the production and characterization of these nuclei.

In a similar manner, the probability for βDF can be derived as

$$P_{DF} \approx N_\beta(A) \int_C^{Q_\beta} (Q_\beta - E)^5 \frac{\Gamma_f}{\Gamma_\gamma + \Gamma_f}(E)\, dE. \tag{3.15}$$

It should be noted that the term in the integral arising from the Fermi function, $(Q_\beta - E)^5$, shows that εDF is more likely to occur than βDF, all other things being equal. This is because the Fermi function for β decay approaches zero faster than that for electron capture at high energies. Since the high energy states have higher penetrabilities, the overall P_{DF} would be higher for εDF than for βDF. This behavior is shown in Figure 3.2. As a result, εDF in general should be easier to study than βDF, even if β-delayed fissile species were not so difficult to produce experimentally.

Of course, it should be emphasized that the form of the delayed-fission probability P_{DF} developed in Equation (3.14) is valid only for a qualitative understanding of the phenomenon of delayed fission. A quantitative model of P_{DF} would require a rigorous treatment of the structure of the beta strength function S_β as it appears in Equation (3.3), no doubt including the low-lying structure [KLAPDOR 79] imposed on S_β by levels within the daughter nucleus. A quantitative model should also include treatment of transmission through realistic fission barriers and avoid the oversimplification of 100% damping required for the approximation in Equation (3.7).

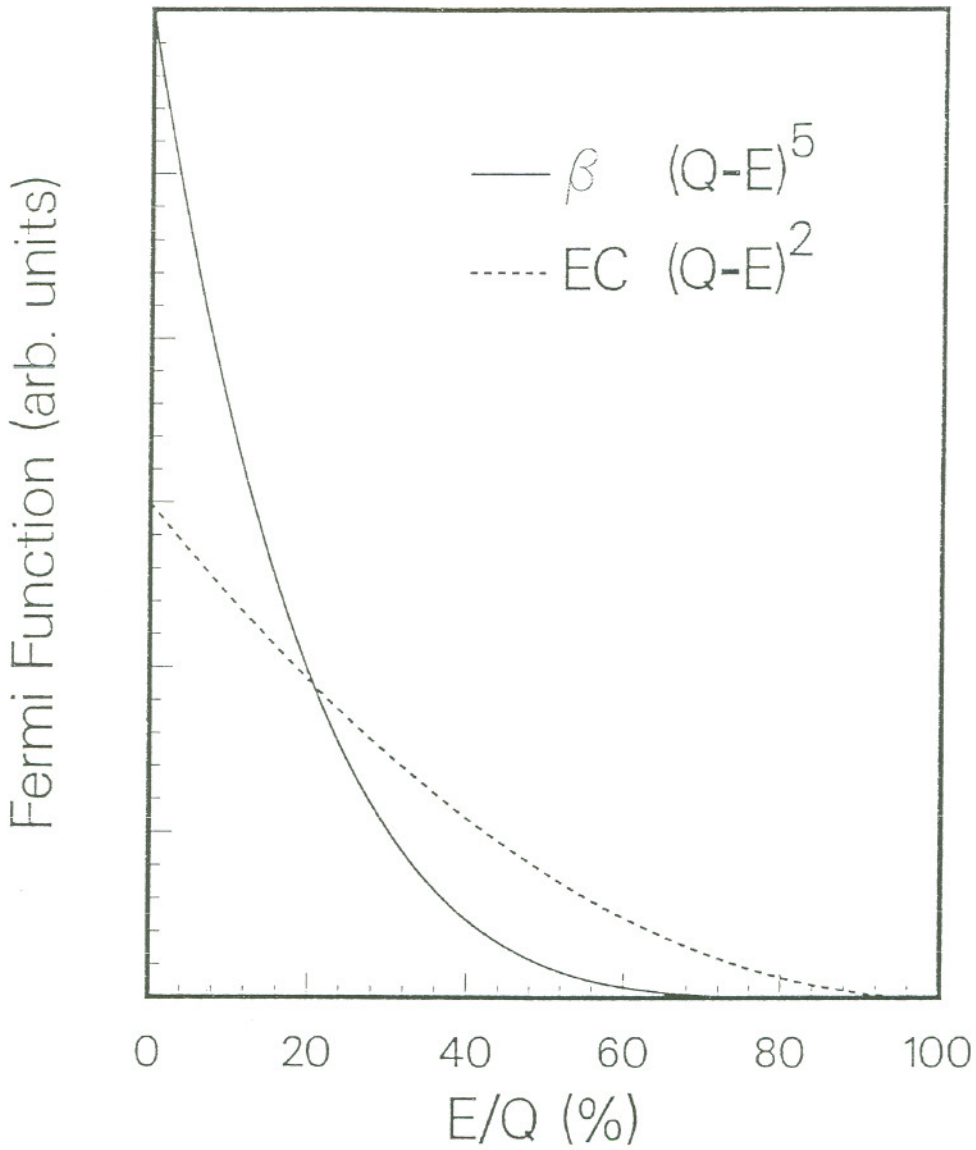

Figure 3.2: The Fermi functions from Equation (3.4) as a function of E/Q.

Chapter 4

Targets and Irradiations

In the production of the neutron-deficient americium nuclei chosen for this study, certain criteria and limitations had to be considered. Primarily, the nuclei of interest were either known to be short-lived, or were expected to be short-lived. For this reason and for safety concerns, production in thick targets followed by chemical separations from the bulk target material was not viable. Since it was necessary to perform chemical separations on the samples, in-beam techniques were not feasible. The use of thin targets with a gas-transport system is ideal for generating samples suitable for direct counting or fast radiochemical separations, so that technique was chosen for the production method.

4.1 ^{237}Np Targets

4.1.1 Development of the Multiple Target System

For the study of ^{232}Am and heavier isotopes of americium, light-ion reactions such as ^{237}Np(α,xn) are desirable for several reasons. Highly asymmetric nuclear reactions generally have much higher production cross-sections than the less asymmetric heavy ion reactions. The Coulomb barrier for the reaction is lower, increasing

the scope of reactions that can be carried out with a single accelerator. Most accelerators can give much higher beam fluxes of light ions than heavy ones. The $\frac{dE}{dx}$ for light ions is considerably lower than that of heavy ions [NORTHCLIFFE 70, HUBERT 80], thus reducing the problem of thermal damage to targets and vacuum windows. When a helium-jet technique is used to extract the product nuclei quickly, the helium carrier gas can provide cooling to the targets and windows as a beneficial side effect.

Disadvantages of light-ion reactions are few, but significant. Light ions by definition have small masses, hence they have small momenta for a given energy. Because of this, the recoil momentum transferred to the compound nucleus is very small. This quantity can be calculated from the conservation of momentum relationship,

$$p_{\text{projectile}} = p_{\text{compound nucleus}}, \tag{4.1}$$

where p is the particle momentum. Since momentum is conserved, the square of momentum is also conserved. Using this with the definition of the kinetic energy, $E = p^2/2m$, the square of the momentum is

$$p_i^2 = 2m_i E_i. \tag{4.2}$$

The following conservation relationship then holds for the projectile and the resulting compound nucleus (in the laboratory frame of reference, hence $p_{\text{target}} = 0$):

$$m_{\text{projectile}} E_{\text{projectile}} = m_{\text{CN}} E_{\text{CN}}, \tag{4.3}$$

where the subscript CN designates the compound nucleus.

From this relationship, the heavy compound nucleus can be calculated to have very little recoil energy for incident α-particle energies less than 100 MeV. This limits the effective thickness of the target material to approximately the recoil range of the compound nucleus in the target material. For a typical actinide oxide target, the recoil range is on the order of tens of micrograms per square centimeter [NORTHCLIFFE 70]. Also, the lower Coulomb barrier for light-ion reactions and the

higher available fluxes lead to an increase in the production of fission products and activation products from charged-particle reactions and capture of stray neutrons.

With this in mind, we sought to design a target system which would allow us to use all the advantages discussed above while minimizing the effect of the disadvantages. Since light ions lose very little energy while passing through thin targets and target backings, multiple targets can be bombarded concurrently with only a small spread in incident beam energy. A system using up to three light-heavy atom targets (*e.g.*, magnesium) has been reported [MOLTZ 80], but this has never been done with a large number of heavy targets where the recoil range becomes very small. Since an incident beam energy spread of a few MeV is acceptable for these experiments, ten or more actinide oxide targets on thin backings can be bombarded with the same beam. This multiplication of the targets compensates for the low recoil range of the compound nucleus, effectively yielding a thick target.

The low recoil range of the compound nucleus can also be exploited to suppress the collection efficiency of fission products. For example, the recoil range in helium of $^{241}Am^*$ produced by the bombardment of ^{237}Np with 100-MeV alpha particles can be estimated from Figure 4.1 to be about 70 $\mu g/cm^2$, or about 4 mm at atmospheric pressure. Typical fission fragments, with energies of about 1 MeV/A, have recoil ranges [NORTHCLIFFE 70] in helium of about 2500 $\mu g/cm^2$, or about 140 mm. Hence, by arranging the spacing between the targets to be greater than the recoil range of the compound nucleus but much less than that of fission fragments, most of the fission fragments will embed in the next target backing or the target holder rather than attach to aerosols. This severely decreases the gas-jet extraction yield of the fission products, and hence greatly reduces the β-γ background resulting from fission products.

The use of high beam fluxes is often desirable, so the target system design had to incorporate two primary safety features. First, the system had to accept high fluxes without suffering design failures due to the large amount of heat generated. Secondly, the amount of induced radioactivity, primarily in the beam stop, had to be

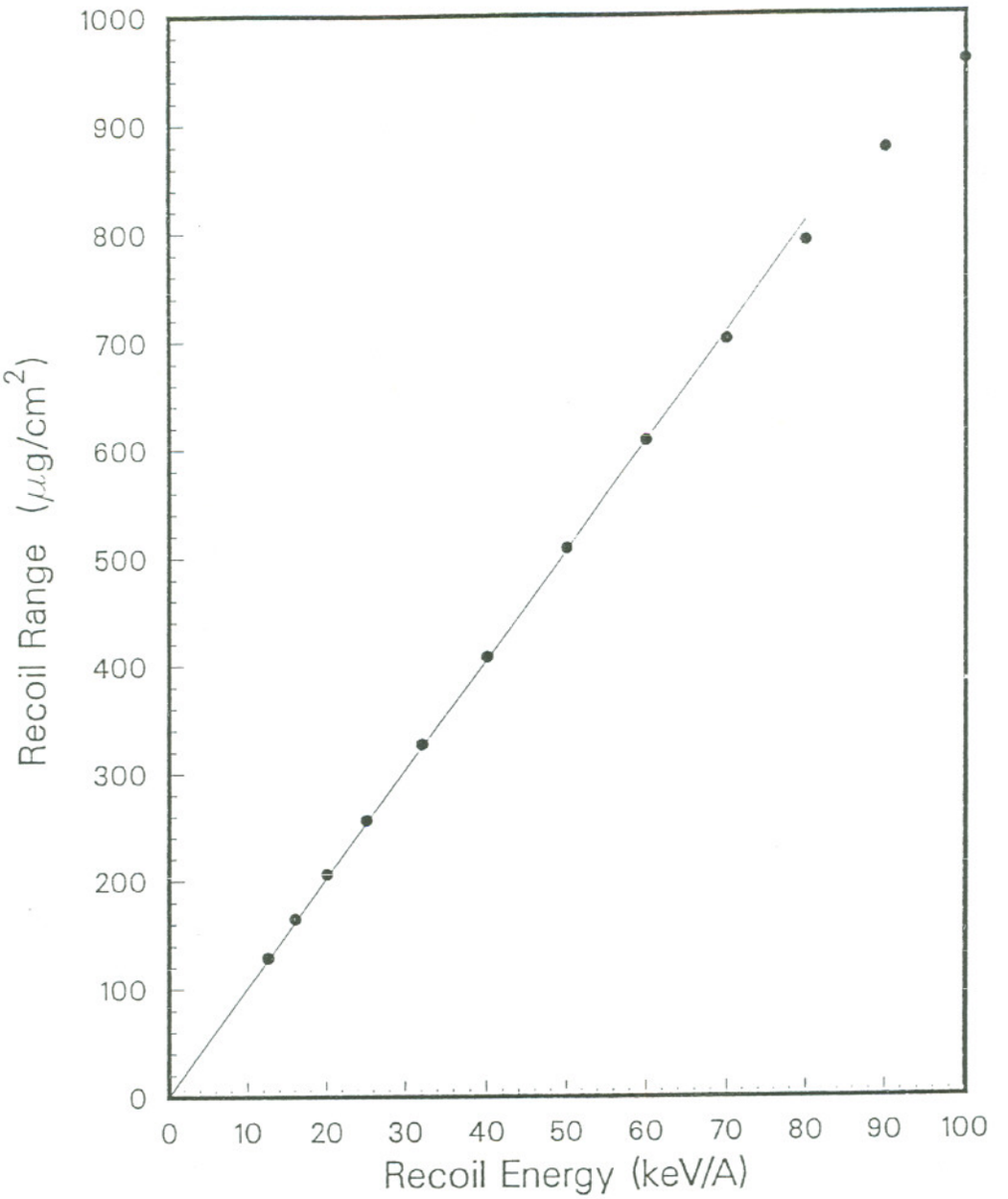

Figure 4.1: Estimation of low-energy recoil ranges for americium in helium by extrapolation of range data from [NORTHCLIFFE 70] to zero recoil energy.

minimized to reduce the hazards of handling the system following a bombardment. These criteria led to the use of a thick beryllium plug in a water-cooled copper heat sink as a beam stop. A large diameter collimator allowed large diameter (12.7-mm) targets to be used, hence reducing the risk of target failure due to localized heating. Fortunately, the energy deposition in the targets can be kept low enough by using suitably thin target backings so that the flow of helium in the KCl/He-jet provides adequate cooling.

The Light Ion Multiple Target System (**LIM** target system) that was designed [HALL 89A] for these irradiations is shown schematically in Figure 4.2. The target material is electrodeposited on thin foils by a standard technique [BEDOV 56, EVANS 72,AUMANN 74,MÜLLEN 75], as described below. These foils are attached to square target holder cards with epoxy adhesive. The target holder cards are then placed in the recoil chamber with the gas vents alternating so that the aerosol-laden helium gas has to pass behind each target. This configuration is shown in Figure 4.3. The number of targets, their composition, and their spacing can be varied in the target system. The beam, after passing through all the targets and the volume limiting foil after the last target, impinges on a 25-mm thick beryllium plug. This plug is press-fitted into a water-cooled copper jacket to dissipate the heat generated in a high-flux bombardment.

The transport efficiency of the gas jet through the target system was measured with an ^{225}Ac ($t_{1/2}$ = 10.0 days) recoil source by measuring the 4.8-minute daughter ^{221}Fr. The yield was measured as the ratio of ^{221}Fr collected per unit time after passing through the system to the amount of ^{221}Fr collected per unit time when bypassing the target system. This ratio was consistently 90% or better. Of course, the overall gas-jet yield is the product of the attachment efficiency, the transport efficiency, and the aerosol collection efficiency. In an on-line measurement using 100-MeV $^{4}He^{2+}$ to bombard ^{237}Np, we measured a ten-fold increase in the ^{232}Am activity collected when we switched from a single target with a large recoil volume ($\sim$100 cm^3) to a ten-target arrangement in the **LIM** target system with the targets

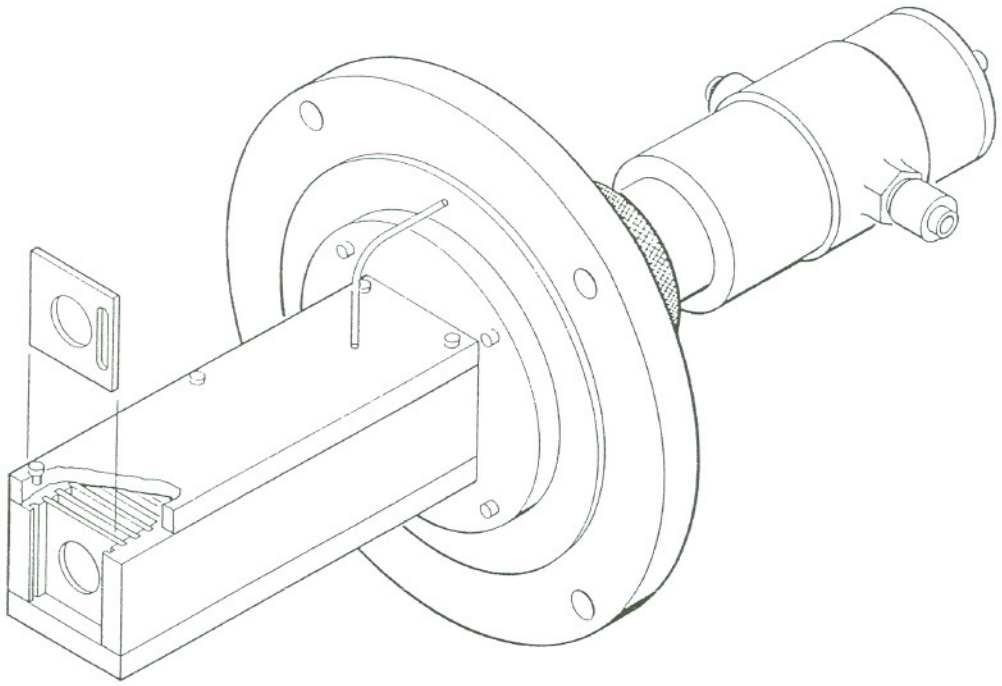

XBL 8811-3751

Figure 4.2: Schematic Representation of the **LIM** Target System.

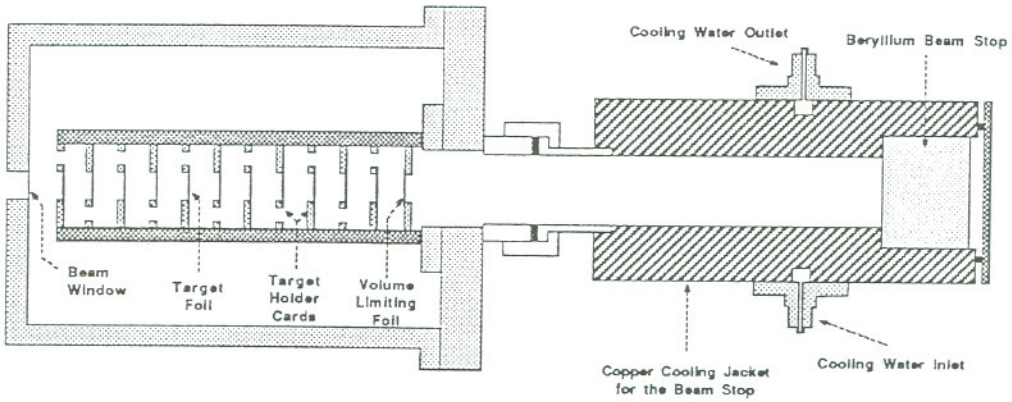

Figure 4.3: Horizontal cross-sectional view of the **LIM** target system. Note the alternating arrangement of the open gas vents, forcing the gas jet to sweep out the volume behind each target. The gas jet is extracted after the last target position through a single polyethylene capillary tube.

spaced 8.6 mm apart. This implies that the attachment efficiency in the **LIM** target system is as least as good as that of the traditional one-target, one-capillary system which had a measured overall efficiency of ~80%. The collection efficiency should remain constant since the same apparatus was used to collect the transported aerosols in each case. Comparison of our measured fission rate for this isotope with the published cross section [HABS 78] gives an overall gas-jet yield of 50–95%.

4.1.2 Preparation of ^{237}Np Targets

Approximately 50 mg of ^{237}Np in an aqueous solution was evaporated to dryness. The resulting salts were dissolved in conc. HCl and this solution was passed through an 8-mm × 160-mm anion exchange column (Bio-Rad AG-1-X8, 100-200 mesh, chloride form). Neptunium, plutonium, protactinium, and uranium were absorbed on the resin while cationic and monovalent anionic species passed through. The column was washed twice with conc. HCl to remove any residual unwanted material. The ^{233}Pa daughter of ^{237}Np was then removed from the column by elution with conc. HCl - 0.2 **M** HF and used for a separate experiment [BROWNE 89]. Plutonium contamination was removed by elution with a 7:1 solution of conc. HCl:5 **M** HI by volume. The column was again washed with conc. HCl (to remove residual HI), and the neptunium was removed from the column by elution with 2 **M** HCl. This fraction was evaporated to dryness.

The neptunium fraction was treated with fuming nitric and perchloric acids to destroy any organic residue, such as resin fines. The neptunium was converted to the nitrate by evaporating it to dryness twice with about 1 mL of conc. HNO_3, and the resulting neptunium nitrate was dissolved in isopropanol to form a stock solution. An aliquot of this solution was dried and assayed by α pulse-height-analysis (PHA). This assay revealed approximately 12 ppm plutonium (^{238,239}Pu) contamination by weight, which corresponds to about 20% of the total α rate in the neptunium. The concentration of neptunium was found to be 10 mg/mL.

For the initial study of the fission properties of ^{232}Am, 2.5-μm molybdenum foils

Table 4.1: ^{237}Np target data for **LIM** target set A.

Target	FAP[a] (cpm)	Thickness (μg/cm^2)[b]
NpA-1	146020 ± 341	118 ± 8
NpA-2	144165 ± 409	117 ± 8
NpA-3	153085 ± 491	124 ± 9
NpA-4	155172 ± 278	126 ± 9
NpA-5	175438 ± 296	132 ± 9
NpA-6	163512 ± 286	130 ± 9
NpA-7	160720 ± 283	142 ± 10
NpA-8	174648 ± 296	115 ± 8
NpA-9	141913 ± 266	133 ± 9
NpA-10	163930 ± 286	132 ± 9
NpA-11	163296 ± 286	142 ± 10

[a]Fission-Alpha-Preset (FAP) counters are windowless 2π gas-flow proportional counters.
[b]Calculated using a specific activity of 1.56×10^3 dpm/(μg/cm^2) for ^{237}Np, a target area of 1.27 cm^2, a FAP efficiency of 0.4983, and the experimentally determined ratio of 0.80 for the ^{237}Np α activity to total α activity. The quoted error includes an estimated error of ±7% due to non-uniformity in target thicknesses.

---

were used as target backings. An aliquot of the isopropanol solution containing 150–250 μg of ^{237}Np was electrodeposited [MÜLLEN 75] on each molybdenum foil in a 1.27-cm^2 area (12.5-mm diameter circle). Eleven targets (set A) were made, with thicknesses ranging from 118 μg/cm^2 to 142 μg/cm^2, as measured by gross α counts. Data on each target are given in Table 4.1. All errors quoted here and throughout this work are at the one standard deviation level, or 68% confidence level. Three targets from set A were used to measure the uniformity of the neptunium deposition. Each target was counted in a 2π windowless gas-flow proportional α counter with a mask covering the target. The mask had a 0.3-cm diameter hole in it, and this hole was positioned to sample the α radiation from five different areas of the target

in different counts. This data revealed an average spread in the target thicknesses from one section of the target to another of 7%. This spread is included in the error of the target thickness reported.

Each foil was then mounted on a target holder frame. Ten of the target holder frames were placed in the **LIM** [HALL 89A] Target System for the initial ^{232}Am experiment, with a spacing of approximately one centimeter between each target. A 25-μm beryllium foil served as the volume limiting foil for the **LIM** Target System, and another 25-μm beryllium foil served as the vacuum and beam-entrance window for the system. The fission properties of ^{232}Am were measured using these targets, and the results are given in **6.2**.

Unfortunately, the interactions of the α-particle beam with the molybdenum target backings produced a very high β-γ background ($\sim 10^{7-8}$ per second after a one-minute irradiation) for these experiments. With such a high sample activity, fast radiochemical separations followed by γ measurements are difficult due to the high background and high radiation dose to the experimenter. In order to reduce this high background from reactions of the beam with the target backings, a new set of targets was made on thin beryllium foil. These targets were used for all subsequent studies on ^{232}Am, ^{234}Am, and ^{236}Am.

For the second set (set B) of ^{237}Np targets, 25-μm beryllium foils were used as target backings. An aliquot of the isopropanol solution containing 150–250 μg of ^{237}Np was electrodeposited on a beryllium foil in a 1.27-cm^2 area (12.5-mm diameter circle) for each target. Fifteen targets were made, with thicknesses ranging from 124 μg/cm^2 to 197 μg/cm^2, as determined from gross α counts. Individual data on each target is given in Table 4.2. Target uniformity was comparable to set A.

Each foil was again mounted on a target holder frame, which was placed in the **LIM** Target System with a spacing of approximately one centimeter between each target. A 25-μm beryllium foil served as the volume limiting foil for the **LIM** Target System, and another 25-μm beryllium foil served as the vacuum window for the system. Twelve targets were used for the production of ^{232}Am and ^{234}Am, and

Table 4.2: ^{237}Np target data for **LIM** target set B.

Target	FAP[a] (cpm)	Thickness (μg/cm^2)[b]
NpB-1	167964 ± 205	124 ± 9
NpB-2	171393 ± 207	127 ± 9
NpB-3	214182 ± 231	158 ± 11
NpB-4	226181 ± 238	167 ± 12
NpB-5	266353 ± 258	197 ± 14
NpB-6	232169 ± 241	172 ± 12
NpB-7	248119 ± 249	184 ± 13
NpB-8	212721 ± 231	157 ± 11
NpB-9	222004 ± 236	164 ± 12
NpB-10	225591 ± 237	167 ± 12
NpB-11	227192 ± 238	168 ± 12
NpB-12	229102 ± 239	171 ± 12
NpB-13	221873 ± 236	164 ± 11
NpB-14	238134 ± 244	176 ± 12
NpB-15	216149 ± 232	160 ± 11

[a]Fission-Alpha-Preset (FAP) counters are windowless 2π gas-flow proportional counters.
[b]Calculated using a specific activity of 1.56×10^3 dpm/(μg/cm^2) for ^{237}Np, a target area of 1.27 cm^2, a FAP efficiency of 0.4983, and the experimentally determined ratio of 0.80 for the ^{237}Np α activity to total α activity. The quoted error includes an estimated error of ±7% due to non-uniformity in target thicknesses.

ten were used for the experiments with ^{236}Am.

4.2 ^{207}Pb Targets

The reaction ^{207}Pb(^{27}Al,$4n$)^{230}Am was chosen for experiments aimed at producing ^{230}Am. The advantage of this reaction over the light-ion reactions used to produce the other isotopes of americium is that the production of the heavier americium isotopes is strongly suppressed. If ^{230}Am were to be made by ^{237}Np(α,$11n$) or ^{237}Np(^{3}He,$10n$), fission from the ^{232}Am also produced would probably overwhelm the fission of ^{230}Am due to the very broad excitation functions expected by the time ten or eleven neutrons have been evaporated. On the other hand, in the reaction of ^{207}Pb with ^{27}Al, ^{230}Am is produced by a $4n$ reaction. ^{232}Am would be produced in this reaction by the $2n$ channel, which tends to have a very poor cross section. As a result, the interference from the heavier isotopes with the fission of ^{230}Am would be very small. The predicted excitation functions for the ^{237}Np(α,xn) and ^{207}Pb(^{27}Al,xn) reactions are shown in Figures 4.4 and 4.5, respectively.

The ^{207}Pb used to make the target for this experiment was obtained from the Isotope Sales Division of the Oak Ridge National Laboratory as lead carbonate. Isotopic analysis performed by ORNL determined that the material was enriched to 91.62% in ^{207}Pb, with 6.02% ^{208}Pb and 2.36% ^{206}Pb as the primary contaminants.

Since the target was to be made by vacuum evaporation of the lead, it was necessary to convert the lead carbonate to lead oxide, as the carbonate form tends to decompose quite violently under the conditions of the evaporation. This conversion was performed by heating the lead carbonate in air to 800°C in a palladium crucible. The lead carbonate is converted to lead oxide in the chemical reaction

$$\mathrm{PbCO_3(white)} \xrightarrow{\Delta} \mathrm{PbO(yellow)} + \mathrm{CO_2}\uparrow . \tag{4.4}$$

Since the material is cushioned by air at atmospheric pressure, the evolution of CO_2 does not occur violently as it does in vacuum.

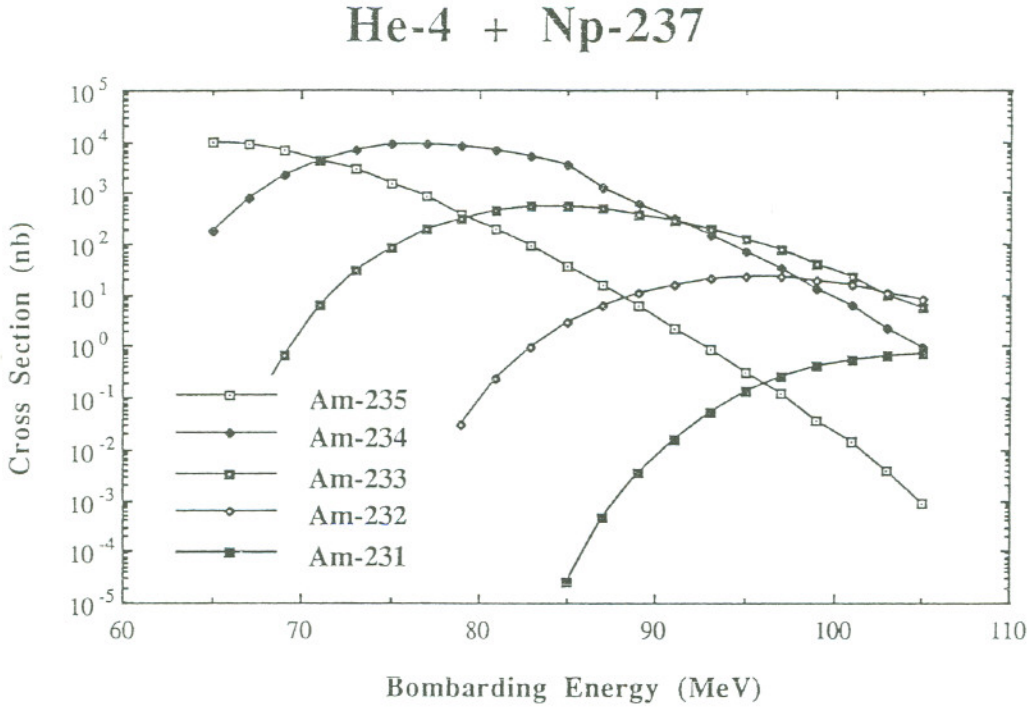

Figure 4.4: Predicted excitation functions for the reaction $^{237}\mathrm{Np}(\alpha,xn)^{241-x}\mathrm{Am}$. Cross-section data was calculated using **SPIT** [WILD 88], an evaporation code.

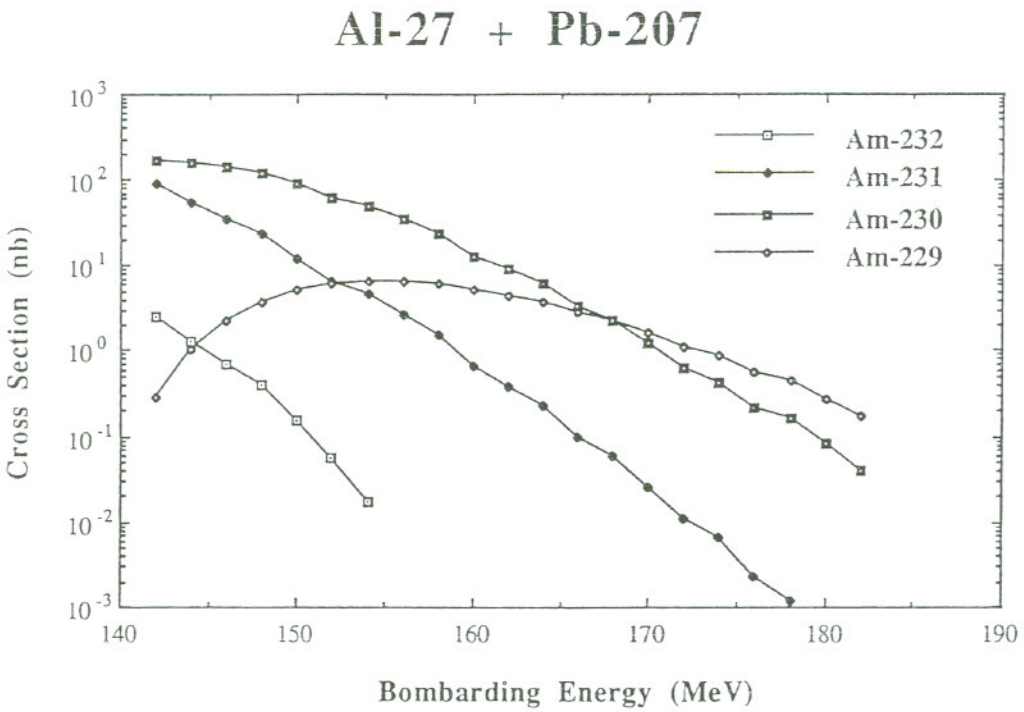

Figure 4.5: Predicted excitation functions for the reaction ^{207}Pb(^{27}Al,xn)$^{234-x}$Am. Cross-section data was calculated using **SPIT** [WILD 88], an evaporation code.

The lead oxide was then cooled and removed from the crucible. It was placed in a small tantalum cup in the vacuum evaporation apparatus and the evaporation cell was evacuated to about 10^{-6} torr. The tantalum cup was resistively heated to vaporize the lead oxide, which was deposited on 12.5-μm beryllium in an 11-mm diameter circle. After a suitable period, the tantalum cup was cooled to terminate the vaporization. The black color of the deposited lead oxide indicated that the target material had been deposited as Pb_2O, rather than PbO. The thickness of the target was measured by observing the energy shift in α particles from ^{244}Cm decay when the target was interposed between the source and the detector. The results of this measurement indicated that the target thickness was 2.76 mg/cm^2 (as lead). This was confirmed by comparing the weights of the beryllium foil before and after deposition.

The irradiation of this target was conducted in a single-target recoil chamber. In this apparatus, the target and vacuum window are cooled by a forced-flow of nitrogen gas between them, while the downstream side of the target is exposed to the KCl-laden helium used to transport the reaction products out of the recoil chamber. This configuration is shown schematically in Figure 4.6.

4.3 Irradiations

All ion beams used in this work were provided by the Lawrence Berkeley Laboratory 88-Inch Cyclotron. All energies are given in the laboratory frame of reference.

For the search for ^{230}Am, the projectile was $^{27}Al^{7+}$ at 178 MeV (machine) which corresponds to 156 MeV on target. This energy is not the maximum of the predicted excitation function, but it is in an energy region where ^{232}Am production should be strongly suppressed (See Figure 4.5) relative to the production of ^{230}Am. The aluminum beam intensity was normally about 2 eμA, but the aluminum generated a number of problems with the accelerator ECR ion source. As a result, the total beam dose for the ^{230}Am experiment was fairly low.

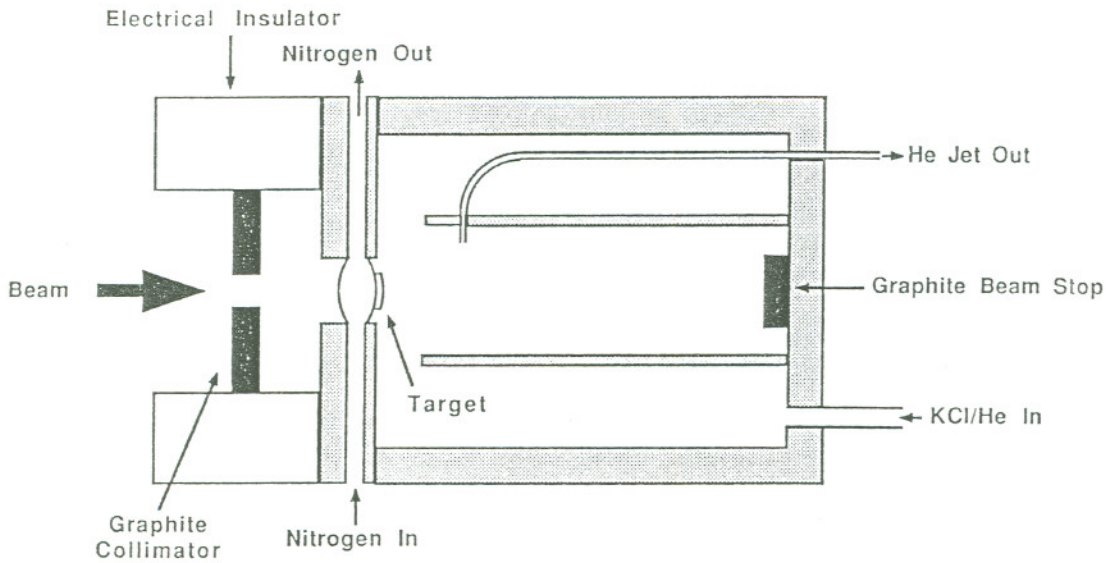

Figure 4.6: Schematic illustration of the single-target recoil chamber used in the irradiations of ^{207}Pb with ^{27}Al.

For the studies of ^{232}Am and ^{234}Am, the beam particle was $^{4}He^{+2}$. For ^{232}Am, the incident energy was 100 MeV (machine), corresponding to an energy spread in the targets of 94-98 MeV (using the range tables of Hubert [HUBERT 80] for the calculation). Beam intensities were 2-5 pμA for these irradiations. For ^{234}Am, the incident energy was 75 MeV (machine), corresponding to an α energy on the first target of 73.5 MeV, dropping to about 70 MeV after the last target in the stack. The beam intensity was 3-6 pμA for the ^{234}Am production irradiations.

The ^{237}Np(^{3}He,4n) reaction was used to search for the unknown isotope ^{236}Am. The energy of the $^{3}He^{+2}$ was 40 MeV (machine), which corresponds to an energy spread of 33-39 MeV on target. The beam intensity was about 6-7 pμA.

In all cases, the recoiling reaction products were collected on KCl aerosols in helium, which swept out the volume behind each target continuously. The activity-laden aerosols were transported via a polyvinyl chloride capillary tube to either the **MG-RAGS** (see **5.1** below) or to a chemistry laboratory (see **5.2** below).

Chapter 5

Experimental Procedures

5.1 On-line Procedures

For on-line measurements of the fission properties of ^{234}Am, the KCl aerosols were transported from the target system about five meters via a capillary tube and collected on thin ($40 \pm 15\,\mu g/cm^2$) polypropylene foils placed on the periphery of a wheel. At preset intervals, the wheel rotated 4.5°, passing the polypropylene foil through a series of six detector stations. The detector stations were placed so that the foil which had been in the aerosol collection position stepped immediately into station one, where it was counted for the preset interval. The foil subsequently passed through each detector station until it left station six, after which it was no longer counted. The wheel had 80 such foils along its perimeter, so at any given moment one sample could be collected while six others were being counted. After one full rotation of the wheel, the wheel and associated polypropylene foils were replaced with a clean set to minimize the build-up of any long-lived fission activities and thick KCl sources.

Each detector station consisted of a pair of ion-implanted passivated silicon (IIPS) semiconductor detectors mounted above and below the plane of the wheel,

as shown schematically in Figure 5.1. This arrangement allowed detection of coincident fission fragments with an efficiency of approximately 50%. Each detector station could also detect α-particles, again with a total efficiency of about 50%. Under the conditions of these experiments, the α-particle energy resolution was about 40 keV. The detectors were calibrated for the fission measurements with a ^{252}Cf source evaporated on a thin polypropylene foil. Sample α and fission calibration spectra are shown in Figures 5.2 and 5.3, respectively. The signals from the semiconductor detectors, after appropriate amplification and pulse-shaping, were digitized to 11-bit (2048 channels) accuracy by Ortec AD-811 analog-to-digital converters (ADCs) in a CAMAC crate. These ADCs were controlled by a Standard Engineering CAMAC crate controller interfaced to a Digital Equipment Corporation LSI-11/73 computer system. Each detected α or fission fragment was tagged with the time at which it occurred, a channel number (energy), and a detector marker, and then written to magnetic tape in list (event-by-event) mode. This process is schematically illustrated in Figure 5.4. Since each event has a time associated with it, the stepping interval of the wheel does not form the only time basis for half-life measurements. Subsequent sorting and histogramming was performed on the data to extract α spectra, fission fragment spectra, coincidence data, and decay information. The rotating wheel is known as the "Merry Go-'round (**MG**)," and the controlling computer system and its affiliated electronics are known as the Realtime Acquisition Graphics System (**RAGS**), hence the acronym **MG-RAGS**.

Each point on the decay curves generated from **MG** data has to be normalized to represent the same number of samples per detector station. This is necessary since, for each wheel, the first station sees 80 foils before the acquisition is stopped while the second station sees 79, the third 78, and so on. The correction is fairly small (0% for the first station, rising to 12% for the last), but can significantly affect the measured half-life. This normalization has been performed on all **MG** decay curves presented in this work.

Once the initial α or fission activities are determined, cross sections can be

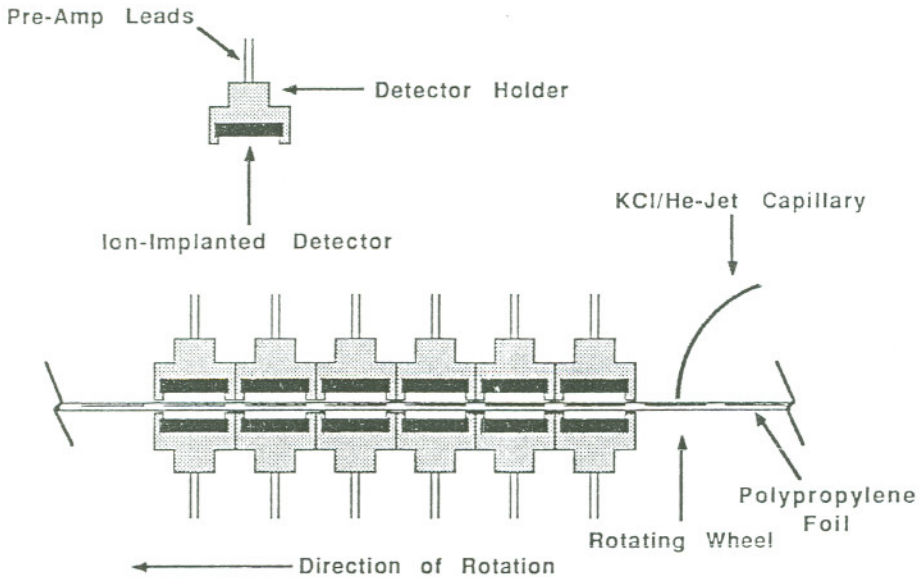

Figure 5.1: Schematic representation of the detector station configuration used in the MG for these irradiations.

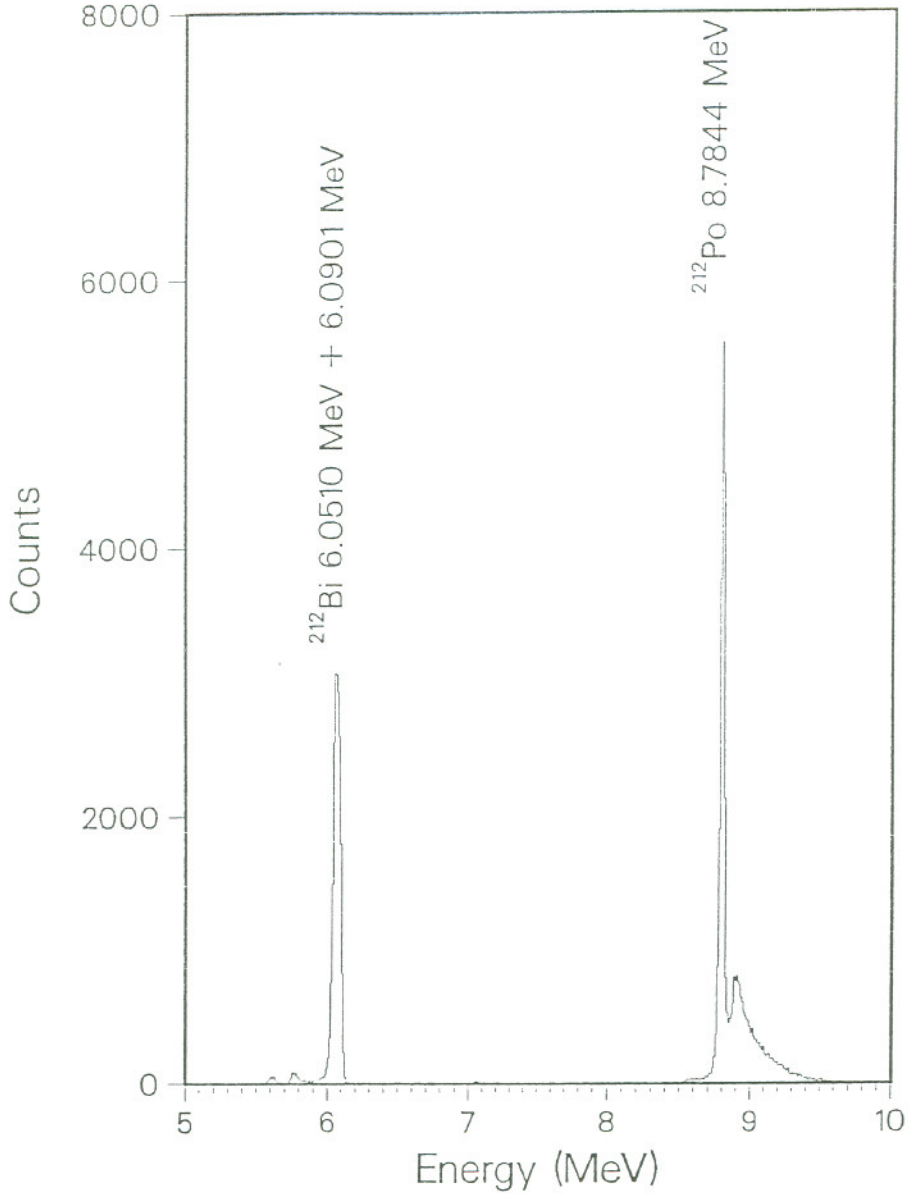

Figure 5.2: **MG** α calibration spectrum obtained using a ^{212}Pb source. The structure in the spectrum just above the 8.7844-MeV ^{212}Po α peak arises from summing of the ^{212}Bi β with the ^{212}Po ($t_{1/2} = 0.298\mu s$) α particle.

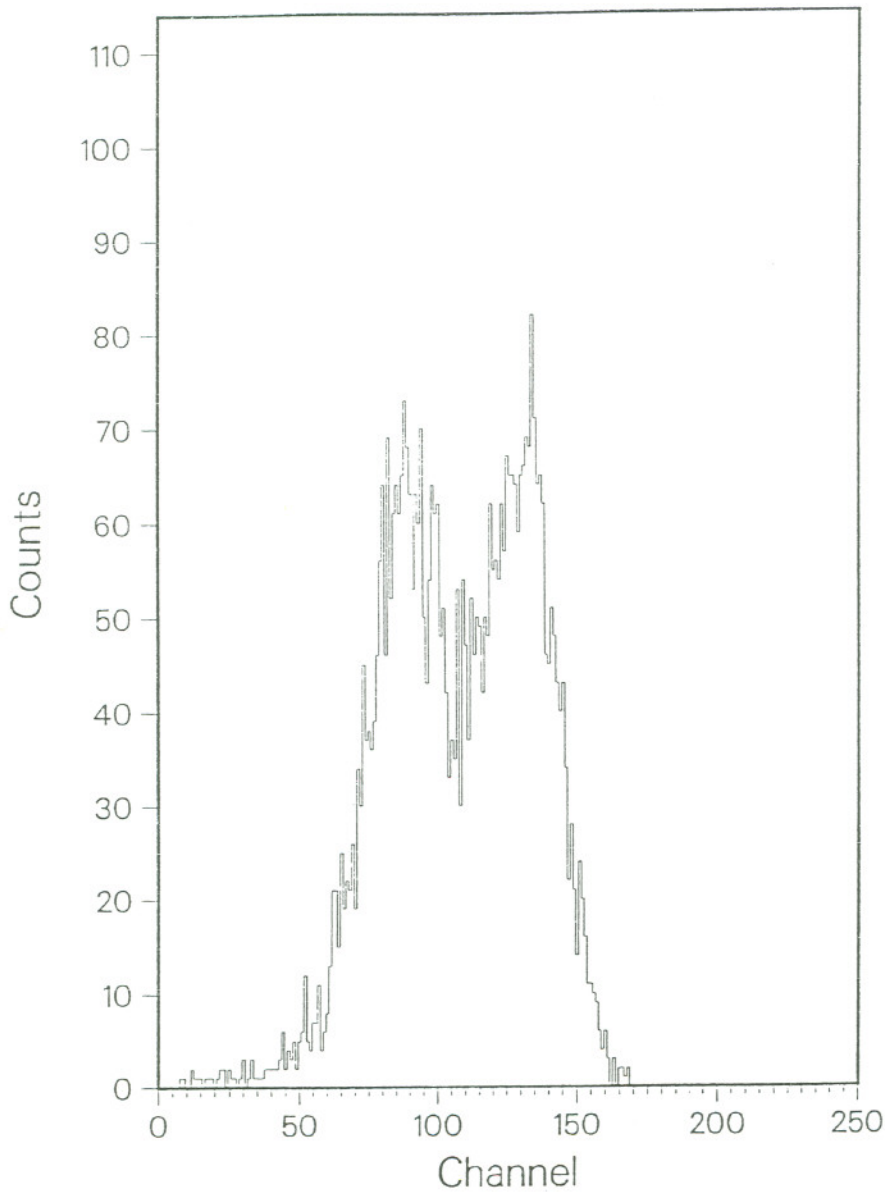

Figure 5.3: **MG** fission calibration spectrum using a ^{252}Cf source evaporated on thin polypropylene.

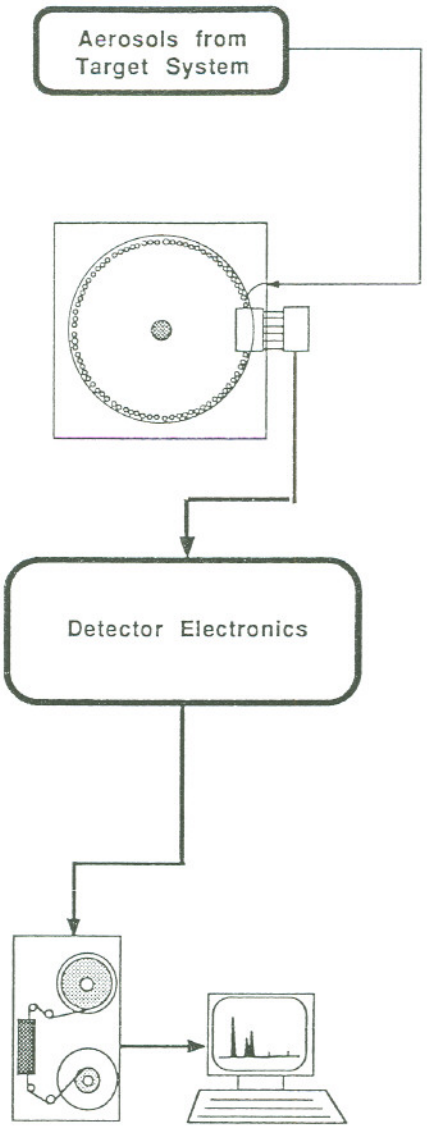

Figure 5.4: A schematic overview of the **MG-RAGS** on-line data acquisition system.

determined from MG data by

$$\sigma = \frac{A_0/\epsilon}{N_T\,\phi\,N_S\,(1-e^{-\lambda t_{irr}})}, \tag{5.1}$$

where A_0 is the initial activity determined from the decay curve, ϵ is the detection efficiency, N_T is the effective target thickness, ϕ is the beam flux, N_S is the number of samples measured, and t_{irr} is the length of the irradiation. ϕ can be accurately measured, but N_T often has to be estimated from the range of the compound nucleus in the target material (since the targets used in the light ion bombardments of ^{237}Np are thick compared to the range of the compound nucleus).

5.2 Chemical Procedures

Two different chemical separations were performed on the reaction products of these irradiations. The first separation was designed to determine the elemental assignment of the fission activity; the second was used to produce an americium sample suitable for measurement of the plutonium K x-rays from the EC decay of the americium isotopes of interest. Measurement of the EC decay in conjunction with the εDF allows determination of P_{DF} experimentally.

5.2.1 Chemical Procedure for Elemental Assignment

In the separation designed to assign the Z of the fissioning activity produced by the reaction of α particles with ^{237}Np, the activity-laden aerosols were transported about five meters via a capillary tube and collected on a tantalum foil. The activity and KCl were then dissolved in 20 μL of 8 **M** HNO_3. The resulting solution was passed through a 1-mm $\times$ 10-mm anion-exchange column (Bio-Rad AG 1-X8, 200-400 mesh). The column was washed with $\sim$ 100 μL of 8 **M** HNO_3. Under these conditions all trivalent actinides will pass through the column, while the higher valence actinides are adsorbed by the resin. The eluant was collected on a tantalum

foil, dried, flamed, and counted with a silicon surface barrier (SSB) detector for α particles and fissions. The column was then washed with $\sim 100\ \mu$L of 3 **M** HCl – 0.1 **M** HF to elute neptunium and plutonium. This second fraction was also collected on a tantalum foil, dried, flamed, and counted. A flow chart of this separation procedure is given in Figure 5.5. Figure 5.6 shows the result of this separation on a tracer mixture of ^{241}Am and ^{239}Pu. Tracer studies of this procedure showed cross-contamination of each fraction to be on the order of 2%. Data from the SSB detectors were stored using **RAGS**. The total time required for this separation was about 90 seconds.

5.2.2 Chemical Procedure for P_{DF} and σ_ε Measurement

This separation procedure had to be more specific for americium since it was necessary to separate americium from highly γ-active fission products, formed with production cross sections on the order of barns. High purity was achieved by using a stacked-column technique. In this technique, a single column is made with two types of resin packed sequentially into the column support. For this experiment, the column consisted of a 3-mm $\times$ 50-mm column of cation-exchange resin (Bio-Rad AG-MP-50, 200-400 mesh) atop a 3-mm $\times$ 10-mm column of anion-exchange resin (Bio-Rad AG 1-X8, 200-400 mesh). Elution with concentrated HCl allowed americium to be separated from monovalent fission products, divalent fission products, and the lanthanides using the top column, and then plutonium and neptunium were adsorbed by the bottom column.

For this procedure, the activity was transported via capillary about 80 meters to a collection site in the chemistry laboratory at the LBL 88-Inch Cyclotron. The activity and KCl were dissolved with 20 μL of 0.5 **M** HCl to which a known quantity of ^{241}Am ($t_{1/2} = 432$ a) had been added as a yield tracer. The resulting solution was passed through the stacked column. Concentrated HCl was then passed through the column to remove americium. For the longer-lived isotopes ^{234,236}Am, the fraction containing americium was collected, and americium was coprecipitated

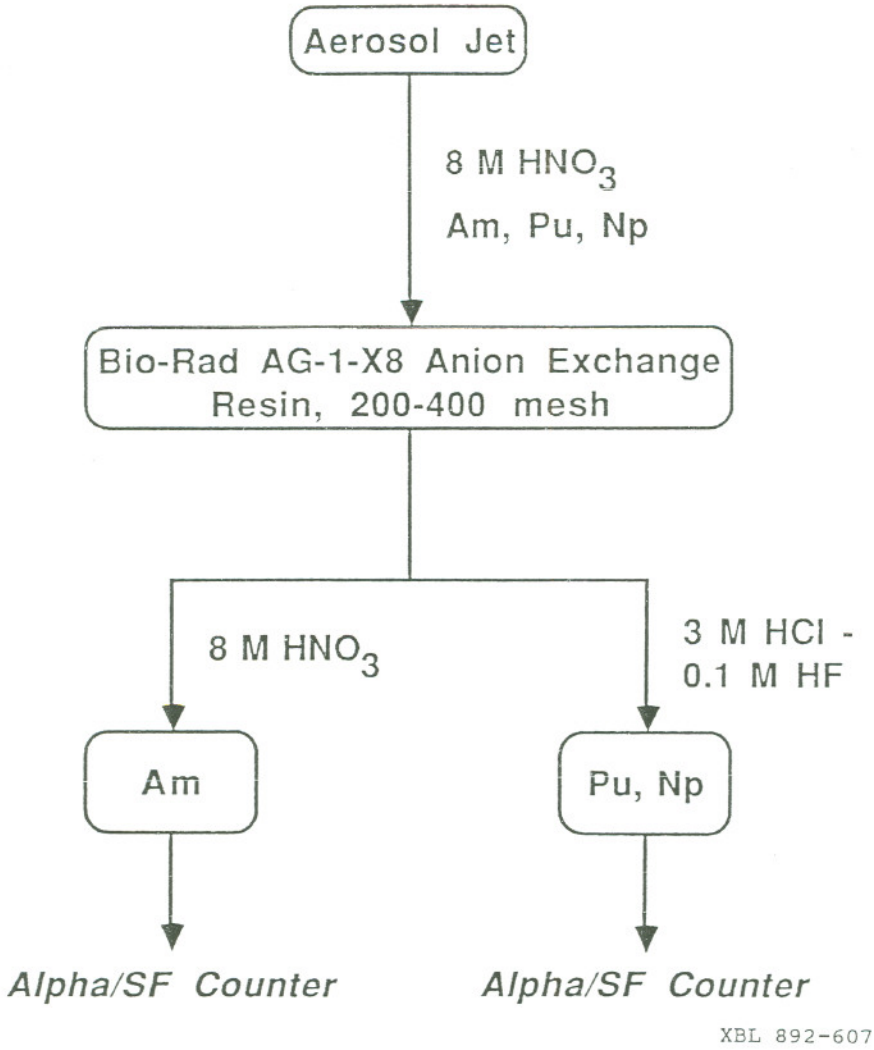

Figure 5.5: Flow chart of the chemical separation designed to confirm the assignment of the fission activities produced in the ^{237}Np + α reaction to americium.

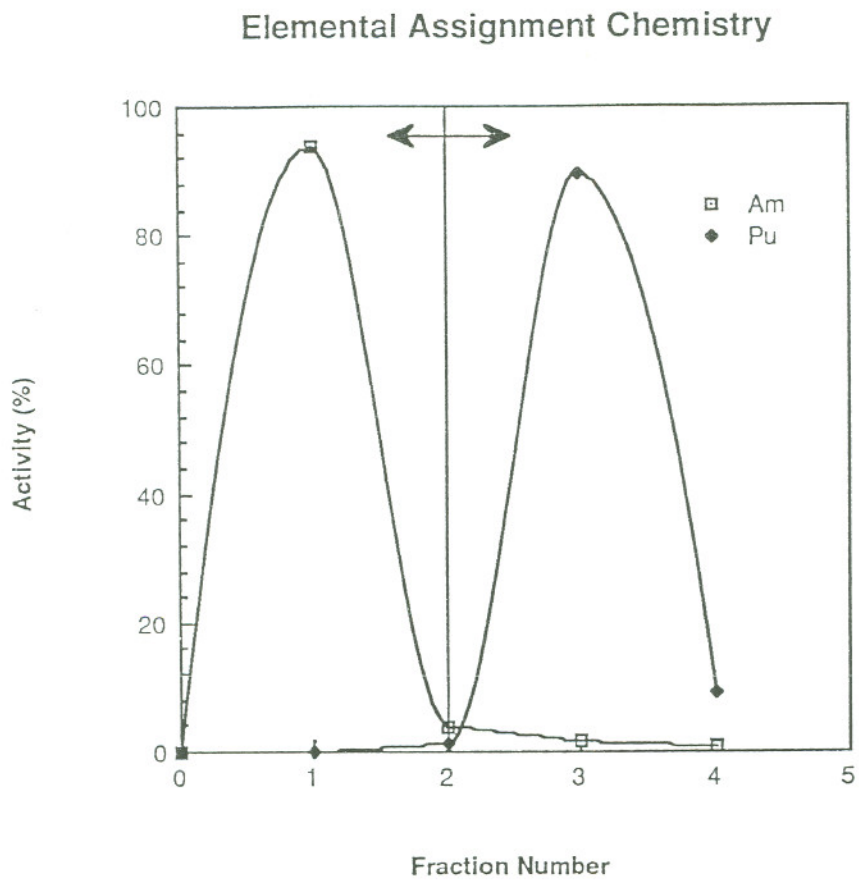

Figure 5.6: Results of the elemental assignment chemistry on a tracer mixture of ^{241}Am ($t_{1/2} = 432$ a) and ^{239}Pu ($t_{1/2} = 2.411 \times 10^4$ a).

with CeF_3. The precipitate was filtered, washed, and then counted with an intrinsic germanium γ spectroscopy system. For ^{232}Am, the americium fraction from the column was immediately counted (as a liquid sample) with an intrinsic germanium γ spectroscopy system because of the short half-life of ^{232}Am. A flow chart of this separation procedure is shown in Figure 5.7. Figure 5.8 shows the result of this separation on a tracer mixture of ^{241}Am and ^{239}Pu. The total time required for this procedure was approximately four minutes when the coprecipitation was performed, or approximately 90 seconds without it. Signals from the germanium detector were pulse-height analyzed by an Ortec ACE-4K card in an IBM-PC compatible computer. A series of 1.0 min γ spectra were taken and saved on the PC's hard disk for subsequent analysis.

Fission of the nuclei studied was measured on an alternating basis with the γ samples from the chemical separation. Samples for the fission measurements were produced by collecting the aerosols for an appropriate time period on a tantalum foil in the same collection apparatus as used in the chemical separations. The tantalum foil was flamed to red heat and counted in a windowless 2π gas flow proportional counter to measure the total number of fissions produced in a given collection. The efficiency of this detector for fissions was determined to be 98.6% with a calibrated ^{252}Cf source. By measuring the fission production rate and the EC decay of ^{234}Am on an alternating basis, any unknown values cancel out in the calculation of P_{DF} provided these values oscillate more slowly than the rate of the experiments. This increases the reliability of the measurement by removing possible sources of systematic error.

The delayed fission probability is then calculated from the electron-capture initial activities and the number of fissions observed in the subsequent (or preceding) fission sample. By measuring each quantity nearly simultaneously, experimental variables such as the target thickness, the beam flux (provided it is held constant), and the gas-jet yield all cancel out. This allows us to calculate P_{DF} with a variant

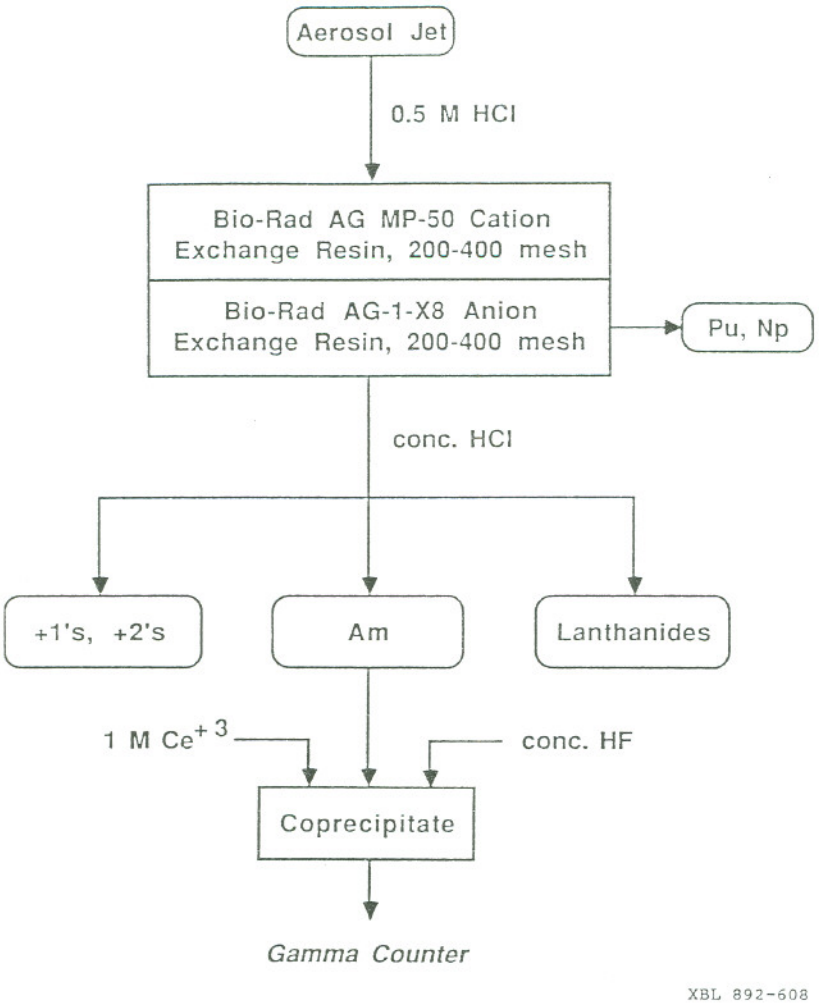

Figure 5.7: Flow chart of the procedure used to isolate americium from the reaction products in a form suitable for γ counting.

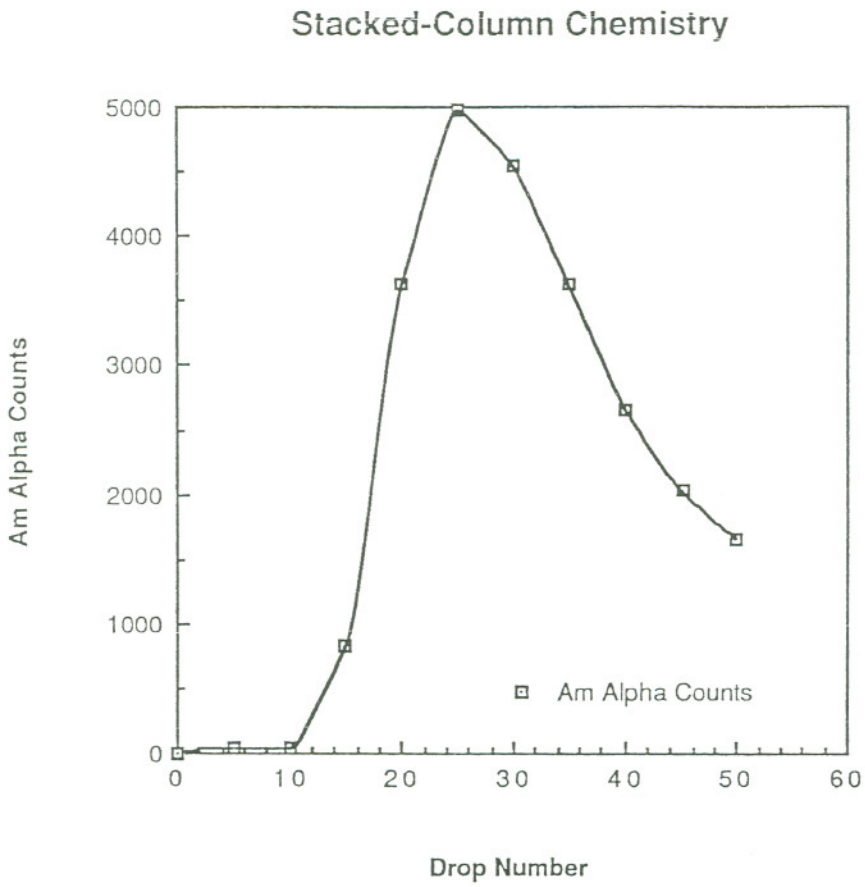

Figure 5.8: Results of the high specificity gamma measurement chemistry on a tracer mixture of ^{241}Am ($t_{1/2} = 432$ a) and ^{239}Pu ($t_{1/2} = 2.411 \times 10^4$ a).

of Equation 3.1,

$$P_{DF} = \frac{\lambda I_f / [e^{-\lambda t_1} - e^{-\lambda(t_1+t_C)}]}{D_{0,\varepsilon}}, \tag{5.2}$$

where λ is the decay constant for the fissioning species, I_f is the integrated number of fissions observed in a counting time t_C, t_1 is the time from end of bombardment to the start of the fission counting, and $D_{0,\varepsilon}$ is the initial electron-capture activity. Employing this relationship, P_{DF} can be calculated and averaged over all of the separate determinations.

Of course, once the initial electron capture activities are determined, σ_ε can be estimated from the equation

$$\sigma_\varepsilon = \frac{D_{0,\varepsilon}}{N_T\, \phi\, \mathrm{I_{theo}}\, (1 - e^{-\lambda t_{irr}})}, \tag{5.3}$$

where N_T is the effective target thickness, ϕ is the beam flux, $\mathrm{I_{theo}}$ is the branching ratio for the particular x-ray peak under analysis, and t_{irr} is the length of the irradiation. ϕ can be accurately measured, but N_T has to be estimated from the range of the compound nucleus in the target material (since the targets used in the light ion bombardments of ^{237}Np are thick compared to the range of the compound nucleus).

5.3 Correlation Study Procedures

The time correlation between the K-capture x-ray and the subsequent delayed fission was measured using aerosols collected directly without any chemical separation. The aerosols were collected on a thin foil and, after a suitable collection interval, the foil was placed before a light-tight transmission-mounted 300-mm^2 silicon surface barrier detector operated in air. The SSB detector and foil were sandwiched between two germanium γ detectors. Fission fragments (and optionally α particles) are detected in the SSB, while the x-rays are registered in the germanium detectors. In some measurements, a NaI(Tl) γ detector was also used to provide faster timing signals for the x-rays, albeit at a loss of energy resolution.

Since fission produces ~10 [HOFFMAN 74] prompt γ rays from deexcitation of the fission fragments, a high overall γ detection efficiency would reject many of the true x-ray events by summing with them. On the other hand, too low an efficiency rejects correlations by failing to detect the x-ray. By measuring the prompt γ rays from fission of a source of ^{252}Cf, the spacing between the γ detectors and the sample was adjusted to bring the summing rejection level to 50%. As long as the γ multiplicity of the εDF being studied is not grossly different from that of ^{252}Cf, this would maximize the number of detected correlations. In the final configuration, each detector subtended a solid angle of about 6.7% of 4π. A 50% summing rejection level gives an overall correlation detection efficiency of 6.7% for each detected fission. The detector configuration is shown schematically in Figure 5.9.

Fission fragment signals in the SSB detector provided a common start for two electronic time-to-amplitude converters (TACs). The stop signals for the first and second TACs were provided by the first and second γ detectors, respectively. The time window on the TACs was $\pm$500 ns. Calibrations were obtained using the prompt γ rays from the fission of ^{252}Cf and the γ rays in coincidence with the α particles from the decay of ^{249}Cf. The timing resolution of the TACs was ~25 ns FWHM, and the energy resolution of the detectors was ~1.5 keV FWHM. Upon detection of a fission event in the SSB detector, the amplitudes of the pulses (if any) in the SSB detector, the γ detectors, and the TACs were recorded in list mode with **RAGS**.

Once the data were recorded, the spectrum of x-rays in coincidence with fissions was analyzed by a maximum-likelihood method to determine both the number of x-rays observed and the most-probable $K_{\alpha 1}$ energy. In this method, the number of counts expected in channel i, Y_i, is given by

$$Y_i = (\sum_{j=1}^{5} \frac{A_j}{\sigma\sqrt{2\pi}} e^{\frac{-(i-C_j)^2}{2\sigma^2}}) + B_i, \tag{5.4}$$

where σ represents the Gaussian width of the detector response, A_j and C_j are the

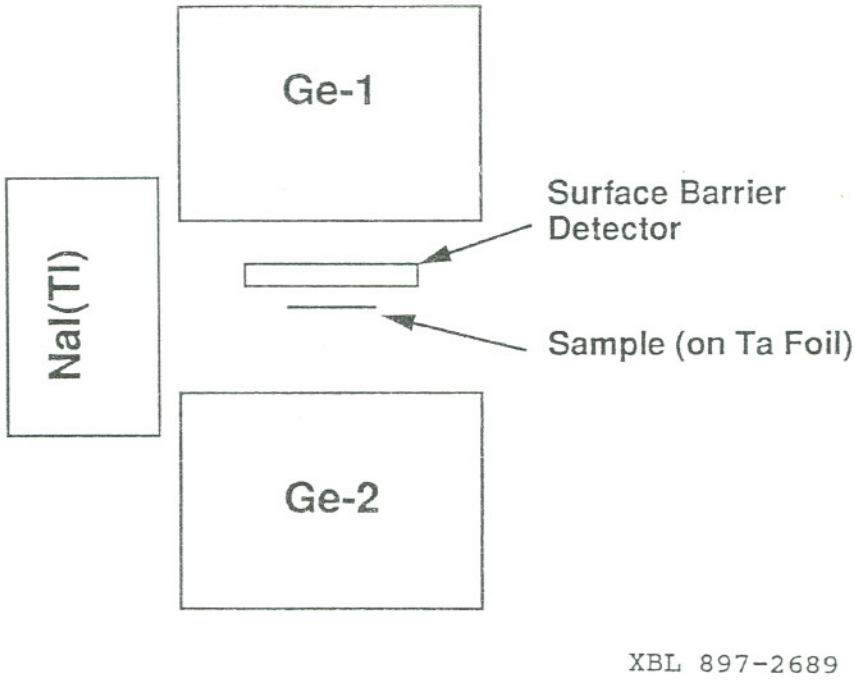

Figure 5.9: Detector configuration for the x-ray–fission time-correlation experiment on ^{234}Am.

number of expected counts and centroid in the jth peak of the K x-ray multiplet, respectively, and B_i is the expected background in channel i. The probability of observing Z_i counts in channel i when Y_i counts are expected is given by a Poisson distribution,

$$P_i = \frac{Y_i^{Z_i} e^{-Y_i}}{Z_i!}, \tag{5.5}$$

and the likelihood function is give as the product of all the probabilities

$$L = \prod_i P_i. \tag{5.6}$$

The most-probable energy and count rate for the x-rays can then be determined by maximizing L as a function of these two variables, hence the term "maximum likelihood." The expected fission prompt-γ background was determined from calibrations with a ^{252}Cf source, and the peak widths were determined from calibrations with ^{249}Cf. In the maximum-likelihood analysis of the coincidence data, the fission prompt-γ background as a function of γ energy was approximated by an exponential fit to the ^{252}Cf data.

Chapter 6

Results

6.1 ^{230}Am Results

A search was performed for ^{230}Am produced in the reaction ^{207}Pb(^{27}Al,4n) using the **MG**. Since this is an unknown isotope, its half-life was estimated to be in the range of 15 seconds to one minute, based on electron-capture systematics [LEDERER 78]. The **MG** wheel was stepped every thirty seconds, and the first detector pair was disabled for α particles for 4 seconds following the wheel motion. Over a 24-hour period, the total beam dosage was 3.445×10^4 μC of ^{27}Al^{+7}, or 3.07×10^{16} particles. The average beam flux on target was 1.6 eμA.

An α spectrum from this irradiation is shown in Figure 6.1. All peaks are attributable to transfer reaction products, *i. e.* products resulting from the exchange of a few nucleons between the target and projectile. α particles from ^{230}Am would be expected to have an energy of ~7.2 MeV (Q_α = 7.33 MeV [MÖLLER 88]), and would be difficult to observe with the high α background from the transfer products.

However, ^{230}Am has a predicted Q_ε of 5.54 MeV [MÖLLER 88], so it should have an appreciable P_{DF}. Since the transfer products are produced in large yields near the target mass only [LEYBA 89], no fissioning species should be produced by

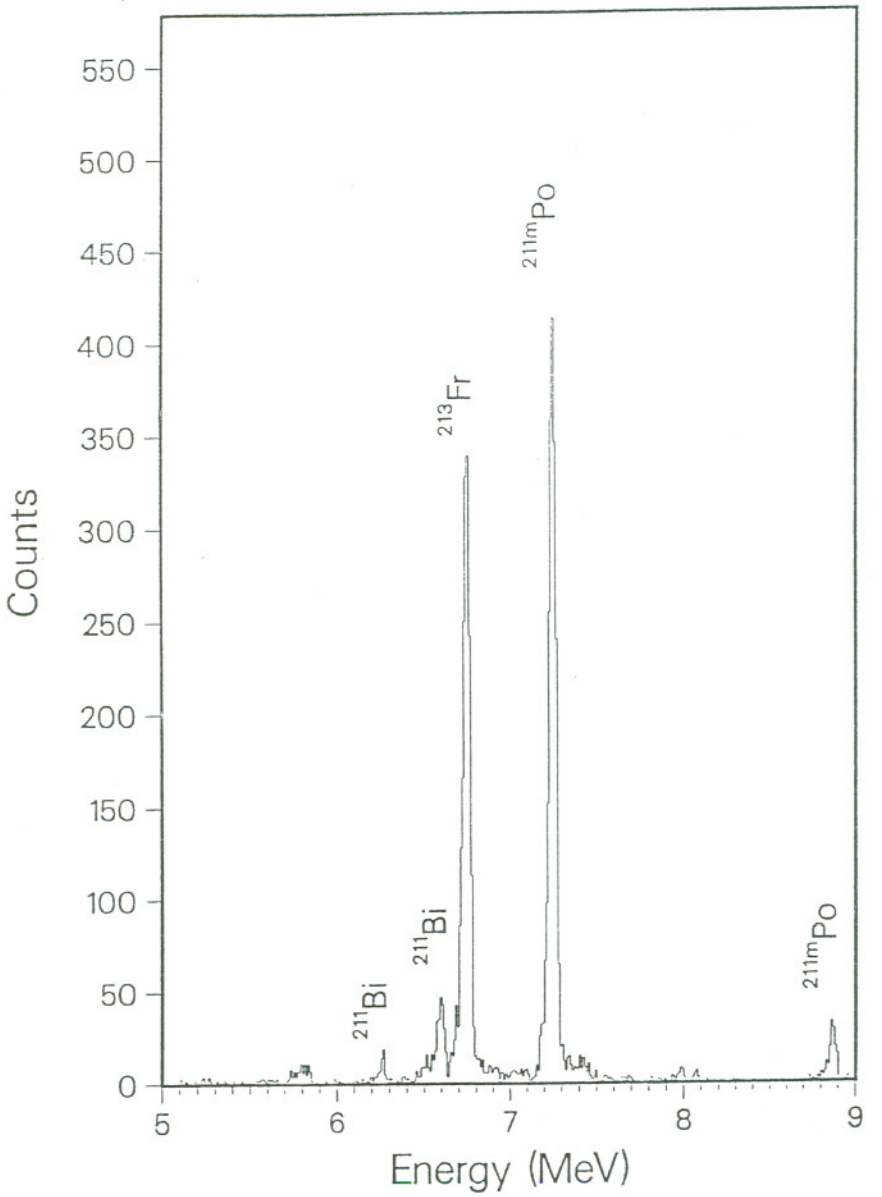

Figure 6.1: α particles observed in the irradiation of ^{207}Pb with 156-MeV ^{27}Al.

Table 6.1: Coincident fission-fragment pairs observed in the irradiation of ^{207}Pb with 156 MeV ^{27}Al. The **MG** wheel-stepping time was 30 seconds.

Pair No.	Detector Station	Lifetime (sec)
1	4	95.78
2	1	10.03
3	5	133.37
4	1	12.12
5	5	144.30
6	5	123.48

transfer reactions. Any observed fissions, therefore, should arise from some sort of compound-nucleus mechanism. This, of course, includes the charged-particle–xn exit channel as well as the xn exit channel. Since the light neptunium isotopes formed via αxn reactions also have an excellent chance of being delayed-fissioning species, an unambiguous Z and A assignment on the basis of **MG** data alone is not possible. The Z assignment could be done radiochemically, but this requires the fission production rate to be fairly large and the $t_{1/2}$ to be fairly long.

Six coincident fission-fragment pairs were observed in these irradiations, with lifetimes given in Table 6.1. Background counts before and after the irradiations indicate that less than one of these fission-fragment pairs is attributable to detector background. The lifetimes of the coincident fission-fragment events are randomly distributed among the detector stations, indicating that the half-life of the observed fission activity is much longer than the total time each foil was counted, 180 seconds. This half-life is too long to be due to ^{230}Am (which is expected to have a half-life of about 30 seconds) and must arise from some other reaction product.

The bombarding energy had been chosen to reduce the expected contribution from ^{232}Am ($\sigma_{230}/\sigma_{232} \approx 3000$ based on **SPIT**), and the fissions were not observed to decay with the ^{232}Am half-life, so it is highly unlikely that they arise from ^{232}Am

produced in the $2n$ reaction. The other americium isotopes expected to be produced at this energy, ^{229,231}Am, have lower Q_ε values than ^{230}Am, so it is unlikely that these fissions arise from these americium isotopes.

These fissions could be primarily due to charged-particle–xn reaction channels. If this is the case, then the identification of the fissioning species without radiochemical separations becomes almost impossible. Unfortunately, the very low production rate for the fissioning species precludes radiochemical assignment.

Since these fissions must arise from a source other than ^{230}Am, the region in cross-section–half-life space excluded for ^{230}Am in this reaction is shown in Figure 6.2. This curve was calculated as follows: The production of ^{230}Am can be expressed as

$$\lambda N_0 = N_T\, \phi\, \sigma_{<f>}\, (1 - e^{-\lambda t_s}), \tag{6.1}$$

where λ is the decay constant for ^{230}Am, N_0 is the number of atoms of ^{230}Am produced after an irradiation of time t_s, N_T is the target thickness, ϕ is the beam flux, and $\sigma_{<f>}$ is the apparent fission cross section for ^{230}Am ($\sigma_{<f>} = \sigma_\varepsilon P_{DF}$). The number of atoms which decay in the detector stations, N, is calculated by taking the difference between N_0 and the number of atoms remaining after the sample exits the detector stations,

$$N = N_0\, N_S\, (1 - e^{-6\lambda t_s}), \tag{6.2}$$

where N_S is the number of samples measured. The time of decay is $6t_s$, since there are six detector stations in the **MG**. The number of events detected, $N_{\rm det}$, is simply the product of the number of decays observed in the detectors and the detection efficiency, ϵ,

$$N_{\rm det} = N\epsilon. \tag{6.3}$$

One can then express $\sigma_{<f>}$ as a function of λ (and hence half-life) as

$$\sigma_{<f>} = \frac{\lambda N_{\rm det}}{N_T\, \phi\, N_S\, \epsilon\, (1 - e^{-\lambda t_s})\, (1 - e^{-6\lambda t_s})}. \tag{6.4}$$

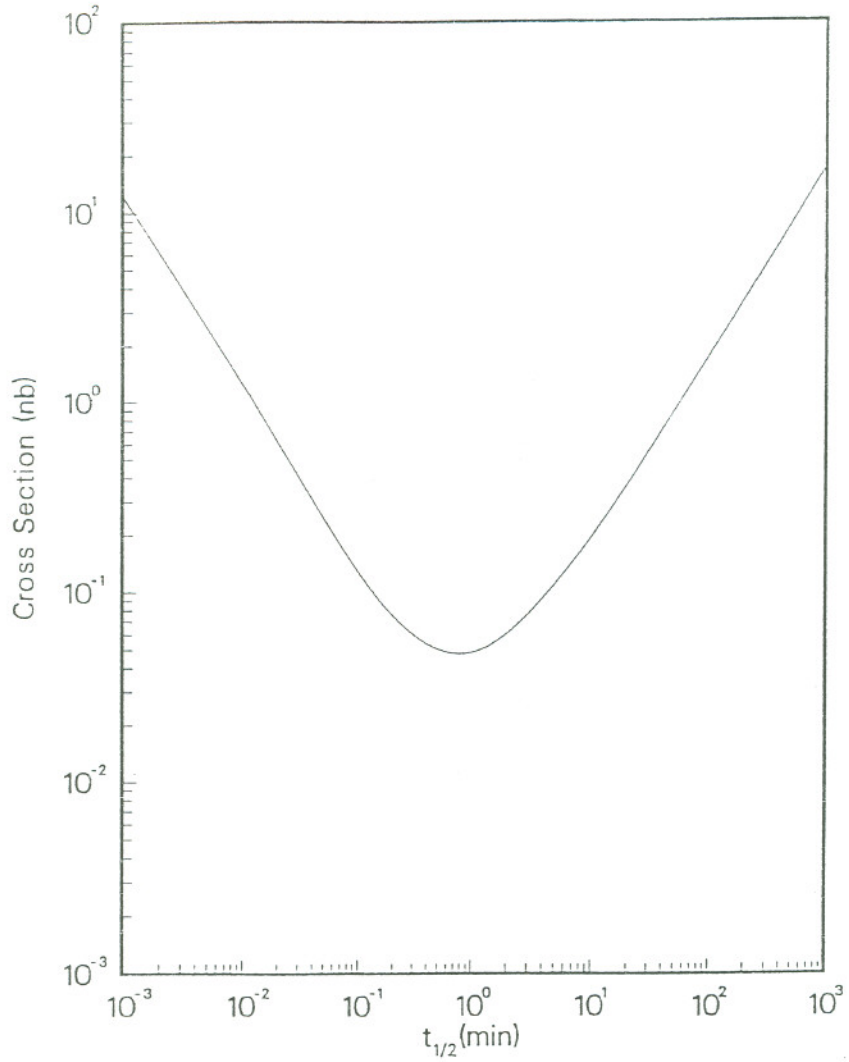

Figure 6.2: Half-life and $\sigma_{<f>}$ limitations imposed on the production of ^{230}Am in the ^{207}Pb + ^{27}Al reaction by the results of this experiment. Calculations were performed assuming all observed fissions were attributable to sources other than ^{230}Am, and five coincident fission-fragment pairs of ^{230}Am were produced but not detected.

For the calculations of the limits in Figure 6.2, it was assumed that five coincident fission-fragment pairs would have to be observed to distinguish them from the long-lived fissions, so N_{det} was taken as 5. The detection efficiency for coincident fission fragments was taken as 60%.

Based on the results of this experiment, no definitive evidence for the existence of a delayed-fission branch in ^{230}Am was found. The calculated (using **SPIT**) overall cross section for the production of ^{230}Am in this reaction is 50 nb. If its half-life is on the order of 1 minute, the upper limit on the fission cross section is 50 pb, so the upper limit on the delayed-fission probability would be 0.1% for this isotope. If the half-life is much longer or much shorter than about one minute, the upper limit would be even larger, as can be seen from Figure 6.2.

However, **SPIT** has been found to systematically underestimate $4n$ reactions where the product is highly neutron deficient by up to an order of magnitude [HAYNES 88] for light-heavy ions such as ^{12}C. If this effect is included, P_{DF} would be lowered into the range of 0.01% to 0.05% for ^{230}Am. This is, of course, a rather poor estimate, since it is not at all clear how well **SPIT** estimates the magnitude of the $4n$ cross section for heavier ions such as aluminum. It is possible that **SPIT** overestimates the overall cross section, which would increase P_{DF}. With this uncertainty in mind, the upper limit for εDF from ^{230}Am is reported as 1%. No definitive evidence for the discovery of ^{230}Am has been found.

6.2 ^{232}Am Results

6.2.1 Elemental Assignment

Using the chemical procedure described in **5.2.1**, 26 samples were processed and counted over about three hours. In each case, the aerosols were collected for three minutes and then subjected to the chemical separation. Each sample was counted continuously for approximately 18 minutes. Eleven fissions were observed in the

americium fraction, and none were observed in the Np/Pu fraction. The observed fissions decayed with a half-life consistent with the measured half-life of ^{232}Am.

Based on this distribution, the fission activity produced in the 99-MeV α irradiation of ^{237}Np was assigned to americium or delayed fission from an americium precursor.

6.2.2 On-line Results

The εDF properties of ^{232}Am were measured over a 32-hour irradiation using **MG-RAGS** as described in **5.1**. The **MG** wheel was stepped at 1.0-minute intervals so that the samples would spend approximately six half-lives between the six detector pairs. Each detector initially registered fissions and α-particles for the full interval, except the first detector station. In the first station, signals from the α particles were suppressed for the first 8 seconds following the wheel motion to allow the ^{8}B+^{8}Li ($t_{1/2} < 1$ second) α activity produced from the beryllium in the target system to decay without causing excessive system deadtime. Fission signals from this detector were not seriously affected by these activities, and were analyzed for the full interval. However, a large number of α-activities were produced in this irradiation which completely overwhelmed the region in which α-particles from ^{232}Am and its daughter were expected to appear. As a result of this, the α signals were disabled after the first wheel was removed. After each full revolution of the wheel (80 positions), the wheel was replaced with a clean one so that any build-up of long-lived spontaneous fission activities was prevented.

Fission Properties

A total of 2201 coincident fission-fragment pairs was observed in these measurements using the wheel-stepping interval of 1.0 minute. From these events, the half-life was found to be 1.31 ± 0.04 minutes, closer to the early half-life reported by Skobelev [SKOBELEV 72] than the more recent value reported by Habs [HABS 78]. The decay curve for this fission activity is shown in Figure 6.3.

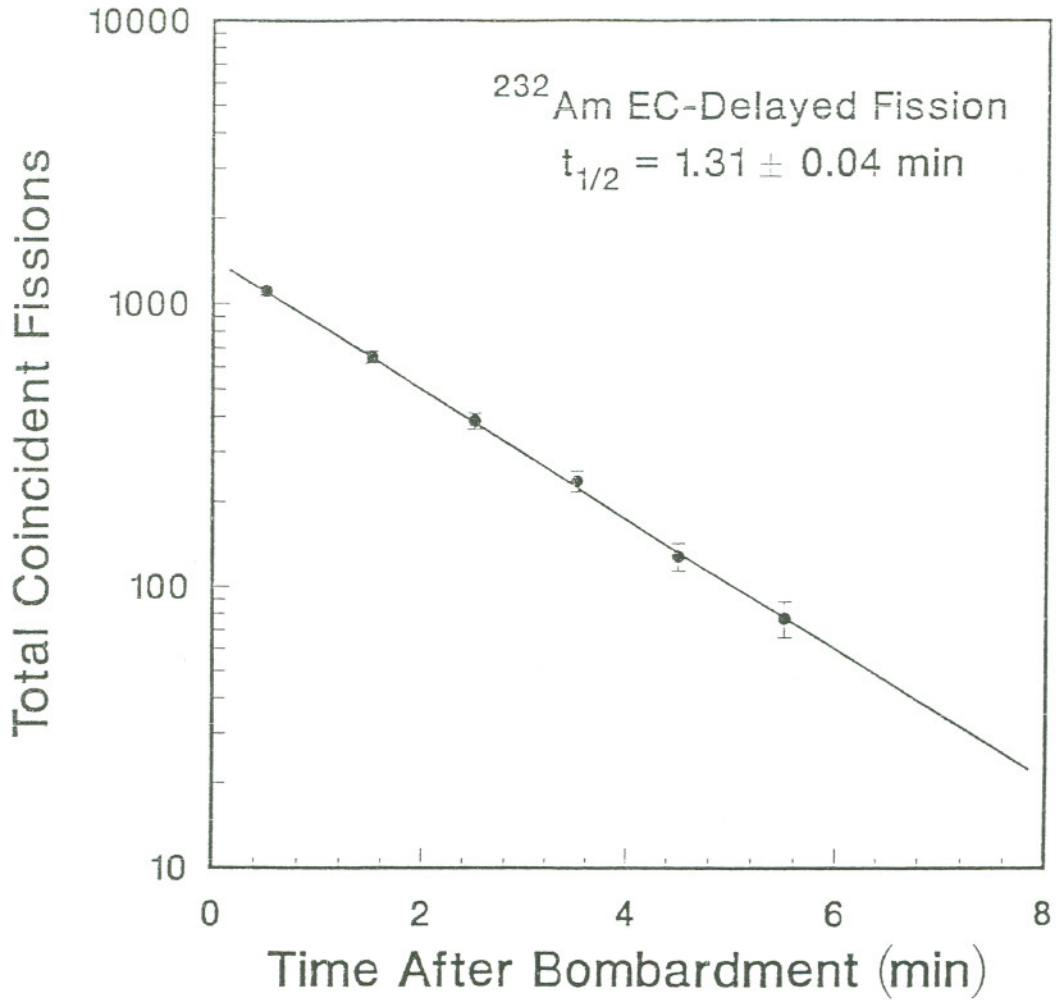

Figure 6.3: Decay curve of the ^{232}Am EC-delayed fission activity as measured on **MG-RAGS**. The wheel stepping time was 1.0 minute per station.

From the decay curve, an apparent fission cross section was estimated for the ^{232}Am εDF mode from this reaction. The effective target thickness was estimated by extrapolating low-energy recoil ranges for the compound nucleus linearly to zero energy. Recoil ranges were taken from Northcliffe and Schilling [NORTHCLIFFE 70], and extrapolated when necessary. This method gave an estimate of the effective target thickness of 100 μg/cm^2 per target. The efficiency of the aerosol-transport system was taken as 100%, although it could be lower. These assumptions result in an apparent fission cross-section of about 2.5 nb (it should be noted that this is in fact a lower limit due to the 100% efficiency assumed for the gas jet, however, other experiments have indicated normal operating efficiencies of the **LIM** system at about 80% so the 100% estimate is not grossly wrong. In these experiments, unfortunately, there was no way to directly quantify the efficiency).

The fission-fragment distributions were corrected for neutron emission using the method originated by Schmitt, Kiker, and Williams (SKW) [SCHMITT 65]. The ^{252}Cf calibration constants were taken from Weissenberger [WEISSENBERGER 86]. The neutron emission function, $\overline{\nu}(A)$, was taken as similar to that of ^{252}Cf, normalized to $\overline{\nu}_T = 2.40$ (estimated from systematics [HOFFMAN 74]).

Fission from ^{232}Am was observed to have a highly asymmetric mass distribution, with no trace of the triple-peaked mass distribution characteristic of the thorium anomaly. The mass-yield distribution is clearly two-humped, with a well-defined valley (after correction for neutron emission using the SKW [SCHMITT 65] method with the ^{252}Cf constants of Weissenberger [WEISSENBERGER 86]) with no evidence shown of a symmetric component. The total kinetic energy distribution is symmetric about 174 MeV with no evidence of multiple components. The TKE and mass-yield distributions are presented graphically in Figure 6.4. The behavior of the TKE and $\overline{\text{TKE}}$ as a function of mass fraction is shown in the TKE contour [BRANDT 63] plot in Figure 6.5. From this figure, it is noteworthy that the $\overline{\text{TKE}}$ for near symmetric mass division is about the same as the $\overline{\text{TKE}}$'s for asymmetric mass-division. The statistical significance of this point is poor (only 46 events were

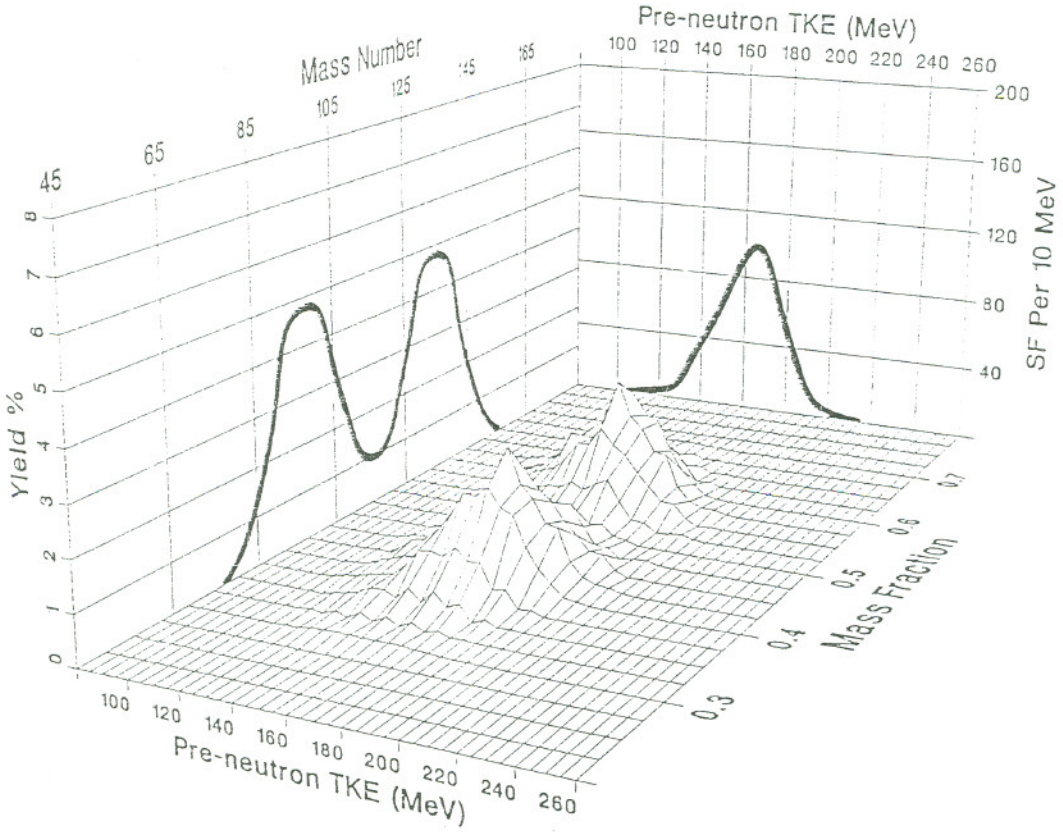

Figure 6.4: Pre-neutron emission total kinetic energy (TKE) distribution of the ^{232}Am εDF mode and pre-neutron emission mass-yield distribution.

observed at this mass division), but this behavior is unusual for light actinides. If the symmetric fragments were in the vicinity of a spherical shell, this behavior would be expected, since similar behavior has been observed in the heavy fermium region [HOFFMAN 89] where the fission fragments can approach two doubly-magic ^{132}Sn nuclei and thus have higher TKE's at symmetry. For ^{232}Pu, the symmetric fragments would be ^{116}Ag. This is too far from the Z=50 shell to expect an effect, and is quite far from the N=50 and N=82 shells. However, it may be that fission of ^{232}Pu is being affected by the half-filled shell at N=66. It has been observed that there is a strong transition from spherical to deformed nuclei at about N=60 for lighter Z elements than silver [HAMILTON 85], so the high $\overline{\text{TKE}}$ observed near symmetric mass division for ^{232}Pu may signal the gradual onset of a similar transition in the silver isotopes. Other plutonium isotopes display differences of nearly 20 MeV between symmetric mass division and the peak of the $\overline{\text{TKE}}$ curve [THIERENS 81,ALLAERT 82,THIERENS 83,WAGEMANS 84]. The fission properties of the ^{232}Am εDF mode are summarized in Table 6.2.

6.2.3 P_{DF} and σ_ε Results

Americium fractions were repeatedly isolated chemically over an irradiation period of about 24 hours in order to measure the x-rays from americium K-capture. Fission measurements were made on an alternating basis with the chemical separations. The chemically purified americium samples were repeatedly γ counted for 20 minutes each, and the fission samples were each counted for four minutes in the proportional counter, and the integrated fissions were recorded. The γ spectra were analyzed using the **SAMPO** [ROUTTI 69] computer code, and half-life analysis was performed with the **CLSQ** [CUMMING 64] code.

The initial activities determined for the americium electron-capture decay mode were corrected for detector efficiency, the individually-measured chemical yield, branching ratio, and K-fluorescence yield (taken as 97.7% [LEDERER 78]). The resulting initial disintegration rates were used for the calculation of σ_ε and P_{DF}.

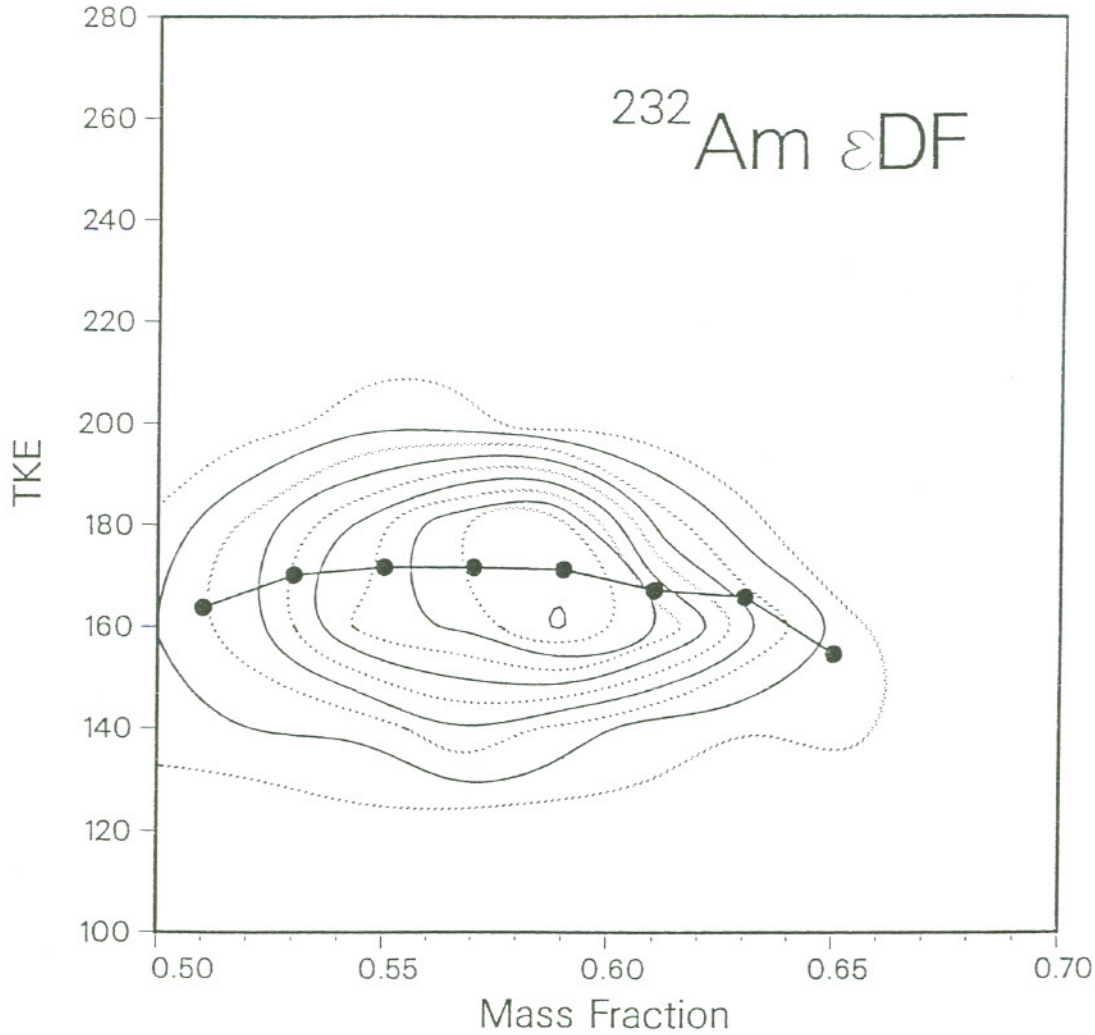

Figure 6.5: Total kinetic energy and average total kinetic energy of ^{232}Am as a function of mass fraction. The solid points are the average TKE values.

Table 6.2: Summary of the fission characteristics of the ^{232}Am εDF mode.

	SKW[a]	Weissenberger[b]
Post-neutron $\overline{\text{TKE}}$[c]	175 ± 5 MeV	173 ± 5 MeV
Pre-neutron $\overline{\text{TKE}}$	177 ± 5 MeV	174 ± 5 MeV
Post-neutron $\overline{\text{KE}}$[d] of high-energy fragment	100.6 ± 2.0 MeV	99.4 ± 1.9 MeV
Post-neutron $\overline{\text{KE}}$ of low-energy fragment	74.8 ± 2.1 MeV	73.6 ± 2.0 MeV
Pre-neutron $\overline{\text{KE}}$ of high-energy fragment	101.4 ± 2.0 MeV	100.2 ± 1.9 MeV
Pre-neutron $\overline{\text{KE}}$ of low-energy fragment	75.4 ± 2.1 MeV	74.2 ± 2.0 MeV
Average mass of the light fission fragment	98.9 ± 0.3	98.7 ± 0.3
Average mass of the heavy fission fragment	133.1 ± 0.3	133.3 ± 0.3

[a]Calculated using the Schmitt, Kiker, and Williams (SKW) [SCHMITT 65] method and constants for ^{252}Cf.
[b]Calculated using the SKW method and the constants of Weissenberger [WEISSENBERGER 86] for ^{252}Cf.
[c]Average total kinetic energy.
[d]Average kinetic energy.

The partial cross-section for ^{232}Am nuclei produced and decaying by electron capture, σ_ε, was calculated based on the following assumptions. First, the target thickness was estimated the same way as for the apparent fission cross-section, yielding an effective total target thickness 100 μg/cm^2 per target for ^{232}Am. Second, the gas-jet yield was assumed to be 100%. Third, because of the lack of discernible γ lines in the spectrum with half-lives consistent with the decay of ^{232}Am, it was assumed that the level density of the plutonium daughter was high enough that deexcitation proceeded through a series of high-energy (500-1000 keV) low-multipolarity transitions. Based on this assumption, the K x-ray production from internal conversion was taken as negligible. Of course, the last few transitions should be more highly converted, but without detailed information about the daughter level scheme any estimates on K-conversion would be near baseless. Finally, it was assumed that K-capture was by far the dominant mode of electron capture for ^{232}Am; L and M capture was neglected.

The K x-ray region from a representative γ spectrum is shown in Figure 6.6. The plutonium x-rays resulting from the electron capture of americium are weak, but visible. Half-life analysis of the Pu K x-rays revealed a two-component decay curve, with one component being consistent with 1.31 min, and the other on the order of an hour. The long component was a mixture of ^{237}Am ($t_{1/2} = 73$ min) and ^{238}Am ($t_{1/2} = 1.63$ hr), and the short was ^{232}Am. The K x-rays were fitted with two components using **CLSQ**, with the short component being set at 1.31 min and the long component allowed to vary to produce the best fit. An example of such a fit is shown in Figure 6.7.

The resulting initial count rates of the ^{232}Am electron-capture decay mode were converted to D_0 values for the calculation of P_{DF} by Equation (5.2). Employing this relationship and averaging over all of the separate determinations yielded a value of P_{DF} of $(6.9 \pm 1.0) \times 10^{-4}$ at the 1σ (68%) confidence level. From these D_0 values, σ_ε was also found to be 1.3 ± 0.2 μb at the 1σ confidence level. Individual measurements are given in Table 6.3.

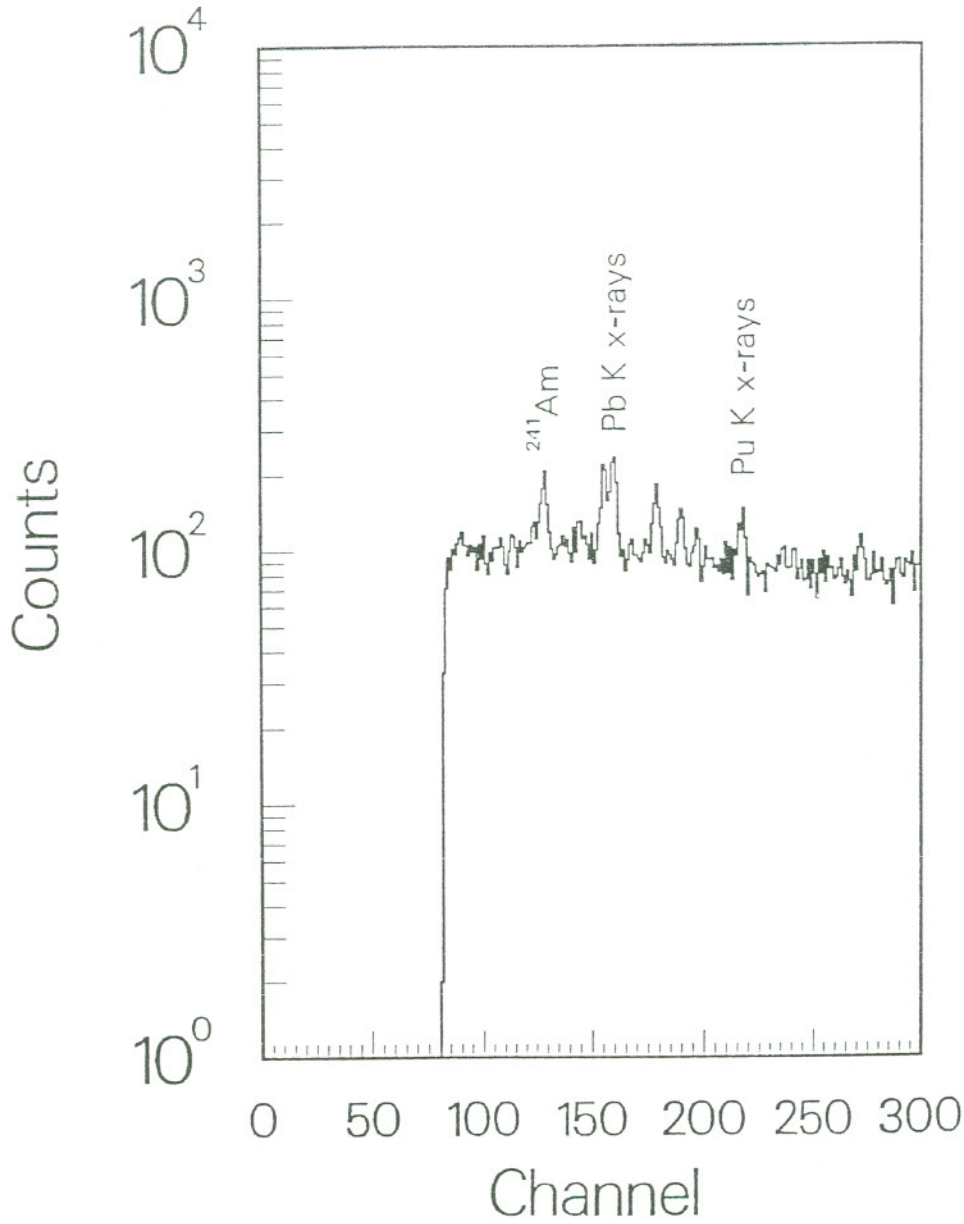

Figure 6.6: The K x-ray region of the gamma spectrum of a chemically purified ^{232}Am sample.

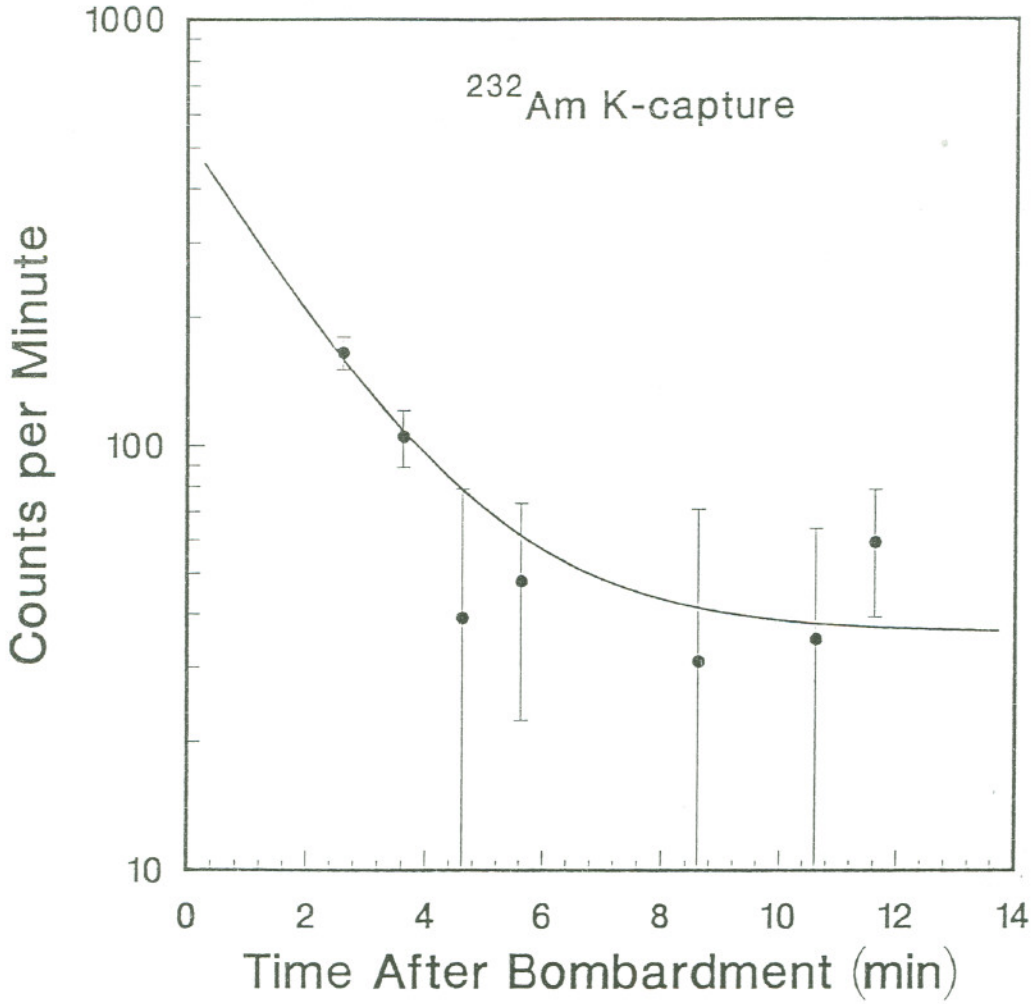

Figure 6.7: Representative half-life fit for the plutonium $K_{\alpha 1}$ x-ray observed in the chemically purified ^{232}Am sample.

Table 6.3: Individual measurements of P_{DF} for ^{232}Am.

$D_{0,\varepsilon}$	I_f[a]	$P_{DF}/10^{-4}$
2894 ± 35%	1.0 ± 0.7	2.71 ± 78%
8480 ± 16%	1.5 ± 0.9	1.39 ± 62%
2777 ± 42%	0.5 ± 0.5	1.41 ±108%
4201 ± 26%	4.5 ± 1.5	8.39 ± 42%
64 ± 1700%	1.0 ± 0.7	1.22 ± 1701%
3480 ± 31%	1.5 ± 0.9	3.38 ± 68%
3734 ± 33%	3.0 ± 1.2	6.29 ± 52%
1150 ± 144%	1.5 ± 0.9	10.2 ± 156%
2266 ± 53%	3.5 ± 1.3	12.1 ± 65%
2340 ± 153%	2.5 ± 1.1	8.37 ± 159
53 ± 3000%	3.5 ± 1.3	518 ± 3000%
3382 ± 33%	4.5 ± 1.5	10.4 ± 47%
3383 ± 25%	5.0 ± 1.6	11.6 ± 41%
2066 ± 81%	3.5 ± 1.2	13.3 ± 89%
7021 ± 24%	3.0 ± 1.2	3.35 ± 47%
5614 ± 52%	2.5 ± 1.1	3.49 ± 68%
745 ± 153%	2.5 ± 1.1	26.0 ± 159%
2086 ± 46%	1.0 ± 0.7	3.75 ± 84%
9500 ± 19%	1.0 ± 0.7	0.82 ± 73%
6287 ± 27%	1.0 ± 0.7	1.25 ± 75%
3234 ± 53%	2.5 ± 1.1	6.05 ± 69%
4854 ± 28%	1.5 ± 0.9	2.42 ± 66%
1355 ± 57%	2.5 ± 1.1	14.5 ± 72%
1521 ± 114%	1.0 ± 0.7	5.15 ± 134%

[a] I_f for the P_{DF} measurement of ^{232}Am is the average of the preceding and succeeding fission measurements.

This value for P_{DF} is approximately a factor of twenty smaller than the value reported by Habs *et al.* [HABS 78], and nearly a factor of a hundred smaller than the estimate of Kuznetsov [KUZNETSOV 79]. However, their P_{DF} values rely on evaporation codes to estimate σ_ε whereas our measurement uses nearly thirty separate experimental determinations of σ_ε through the plutonium K x-rays. Of course, this method of measuring P_{DF} is sensitive to K-conversion of γ rays, but it would require a cascade of 20 γ rays that are 100% converted *per electron capture* to account for the discrepancy. It seems much more likely that the evaporation codes become unreliable for predicting the magnitude of the cross section when such a large number of neutrons are evaporated. ^{232}Am was formed by the ^{237}Np$(\alpha, 9n)$ reaction in the study by Habs *et al.* [HABS 78], and the data used by Kuznetsov involved the reaction ^{230}Th$(^{10}$B$, 8n)^{232}$Am [KUZNETSOV 79].

6.2.4 X-ray–Fission Results

Samples were collected from the gas-jet system at two-minute intervals, and then these samples were placed in the counting chamber for the correlation studies. Figure 6.8(A) shows the x-ray and γ spectrum of those events in prompt coincidence with the fission signal. The data in Figure 6.8(C) is the logarithm of a maximum-likelihood fit L of an idealized x-ray spectrum (shown in Figure 6.8(B)) to the observed data as a function of the $K_{\alpha 1}$ position.

From the likelihood functions, the most probable $K_{\alpha 1}$ energy was found to be 103.8 ± 0.3 keV for the ^{232}Am εDF mode, in excellent agreement with the plutonium $K_{\alpha 1}$ energy of 103.76 keV [LEDERER 78]. The total number of K x-rays was found to be 42 ± 8 by allowing the intensity of the ideal spectrum to vary within the maximum-likelihood analysis. Observed and expected x-ray intensities are given in Table 6.4.

The number of x-ray–fission coincidences relative to the total number of fissions was consistent with the detector geometries. The number of fissions in coincidence with prompt γ rays from the deexcitation of fission fragments relative to the total

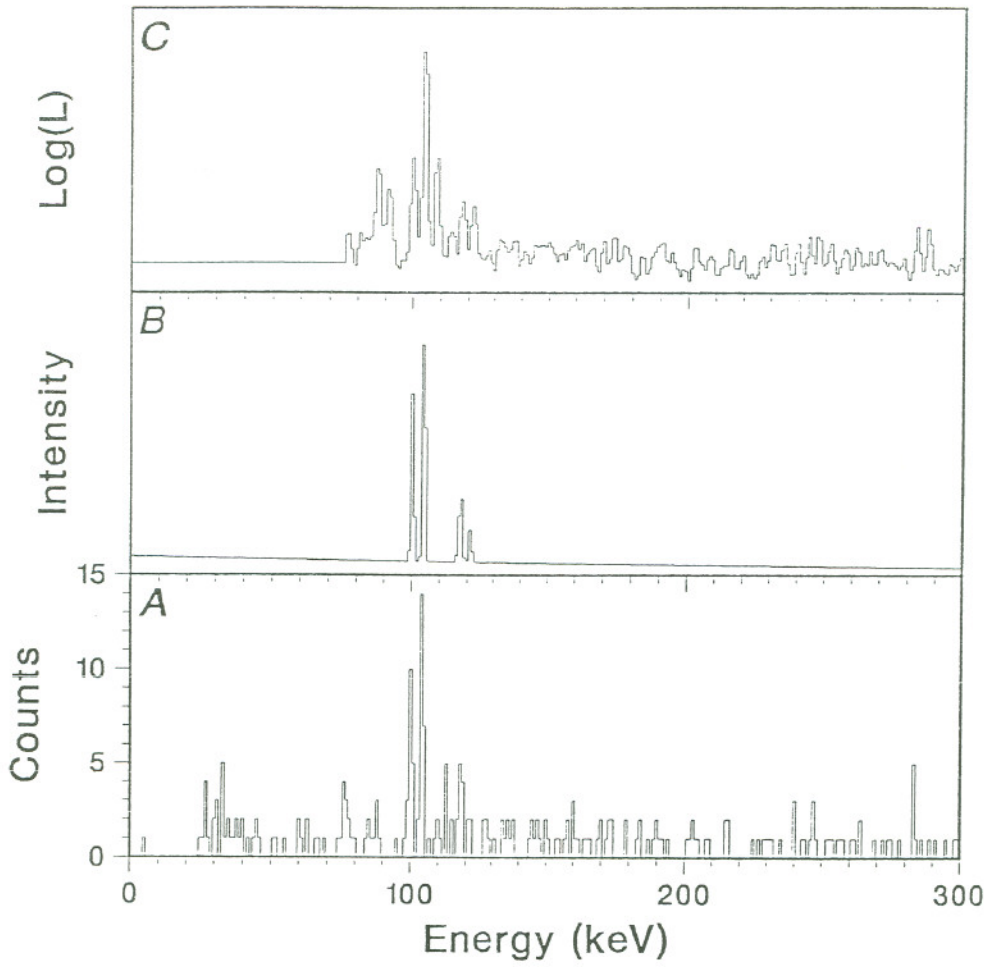

Figure 6.8: X-ray–fission correlation results for ^{232}Am. *A*: X-rays and γ rays in coincidence with delayed fission from ^{232}Am. *B*: An idealized plutonium K x-ray spectrum, based on the measured detector resolution and prompt γ-ray continuum. *C*: The likelihood function for the position of the ideal spectrum (*B*) in the data (*A*), as a function of the $K_{\alpha 1}$ position.

Table 6.4: Observed and expected x-ray intensities from the correlated x-ray–fission data for ^{232}Am. Expected x-ray intensities are taken from the **Table of Isotopes** [LEDERER 78].

X-ray	E/keV	I_{theo}	No. Observed[a]	I_{obs}
Pu $K_{\alpha 2}$	99.55	0.299	19	0.33 ± 0.09
Pu $K_{\alpha 1}$	103.76	0.479	23	0.40 ± 0.10
Pu $K_{\beta 1'}$	116.9	0.162	11	0.19 ± 0.06
Pu $K_{\beta 2'}$	120.6	0.060	4	0.07 ± 0.04

[a]Approximately 15 ± 4 of the observed events are attributable to the prompt γ-ray continuum for the ^{232}Am study.

---

number of fissions observed indicate that the γ multiplicity of ^{232}Am εDF is similar to that of ^{252}Cf. No evidence was observed for fission delay times longer than the best timing resolution of this experiment, about 8 ns. The fact that plutonium x-rays can be seen requires that the lifetime of the fissioning state be longer than the time it takes the orbital electrons to cascade down and fill a K-vacancy. The time required for this is on the order of 10^{-17} seconds [SCOFIELD 74]. We can therefore set boundaries on the excited states' half-lives of 10^{-8} ns $< t_{\frac{1}{2}} < 8$ ns for ^{232}Pu. If the nucleus is truly heavily damped in the second well for low energies (as is commonly assumed [HABS 78,GANGRSKIĬ 80,HALL 89D], and supported by experimental measurements [GOERLACH 78]), then these limits are also limits on the lifetimes of the shape isomer ^{232f}Pu. These limits are consistent with the half-life systematics of plutonium shape isomers (See Figure 3 of [POENARU 89]), from which one would expect the half-life of ^{232f}Pu to be in the range of 1 to 10 picoseconds.

6.3 ^{234}Am Results

6.3.1 Elemental Assignment

Using the chemical procedure described in **5.2.1**, 38 samples were processed and counted over about four hours. In each case, the aerosols were collected for three minutes and then subjected to the chemical separation. Each sample was counted for approximately 18 minutes. Twenty-seven fissions were observed in the americium fraction, and one was observed in the Np/Pu fraction. The one fission in the second fraction is consistent with the amount of americium expected to tail into this fraction. The 6.46-MeV α group attributed [ELLIS-AKOVALI 83] to ^{234}Am was also observed in the americium fraction.

Based on these results, we have assigned the $\sim$ 2-min fission activity produced in this reaction to americium.

6.3.2 On-line Results

The εDF and α-decay properties of ^{234}Am were measured over a forty hour irradiation using **MG-RAGS** as described in **5.1**. The **MG** wheel was advanced one position every 2.50 minutes, so that the samples would spend approximately six half-lives between the six detector pairs. Each detector registered α particles and fissions for the full 2.50 minutes, except the first detector station. In the first station, signals from the α particles were suppressed for the first 12 seconds following the wheel motion. This allowed the ^{8}B+^{8}Li ($t_{1/2} < 1$ second) α activity produced from the beryllium target backings to decay without causing excessive system deadtime. Fission signals from this detector were not seriously affected by these activities, and were analyzed for the entire 2.50 minutes. After one full revolution of the wheel (80 positions), the wheel was replaced with a clean one so that any build-up of long-lived spontaneous fission activities was prevented.

Fission Properties

A total of 1188 coincident fission fragment pairs was observed in these measurements. From these events, a more accurate value of the half-life was obtained than previously [KUZNETSOV 66,KUZNETSOV 67,SKOBELEV 72,SOMERVILLE 77] reported. The half-life was found to be 2.32 ± 0.08 minutes, slightly shorter than found in the previous reports. The decay curve for this fission activity is shown in Figure 6.9.

From the decay curve, we can estimate an apparent fission cross section for the ^{234}Am εDF mode from this reaction. The effective target thickness was estimated by extrapolating low-energy recoil ranges from Northcliffe and Schilling [NORTHCLIFFE 70] linearly to zero energy. This method gave an estimate of the effective target thickness of 75 μg/cm^2 per target. The efficiency of the aerosol-transport system was taken as 100%, although it could be lower. These assumptions result in a lower limit on the apparent fission cross-section of about 0.2 nb.

Fission from ^{234}Am was observed to have a highly asymmetric mass distribution. The data were corrected for neutron emission with a neutron emission function $\overline{\nu}(A)$ similar to that for ^{252}Cf, normalized to $\overline{\nu}_T = 2.4$. Pre- and post-neutron values are given in Table 6.5. Figure 6.10 shows the TKE and mass-yield distributions of the ^{234}Am εDF mode after corrections for neutron emission. The TKE distribution is symmetric, and shows only one component. The behavior of the TKE and $\overline{\text{TKE}}$ as a function of mass fraction is shown in the TKE contour [BRANDT 63] plot in Figure 6.11.

Alpha Decay Properties

The 6.46-MeV α group [ELLIS-AKOVALI 83] of ^{234}Am was observed in the on-line alpha spectra, along with a number of other peaks resulting from other reactions with the ^{237}Np target material, or with lead and bismuth impurities in the targets. An α spectrum from the MG, with the major groups identified, is shown in Figure 6.12. Unfortunately, the large amount of short-lived β activity produced in this

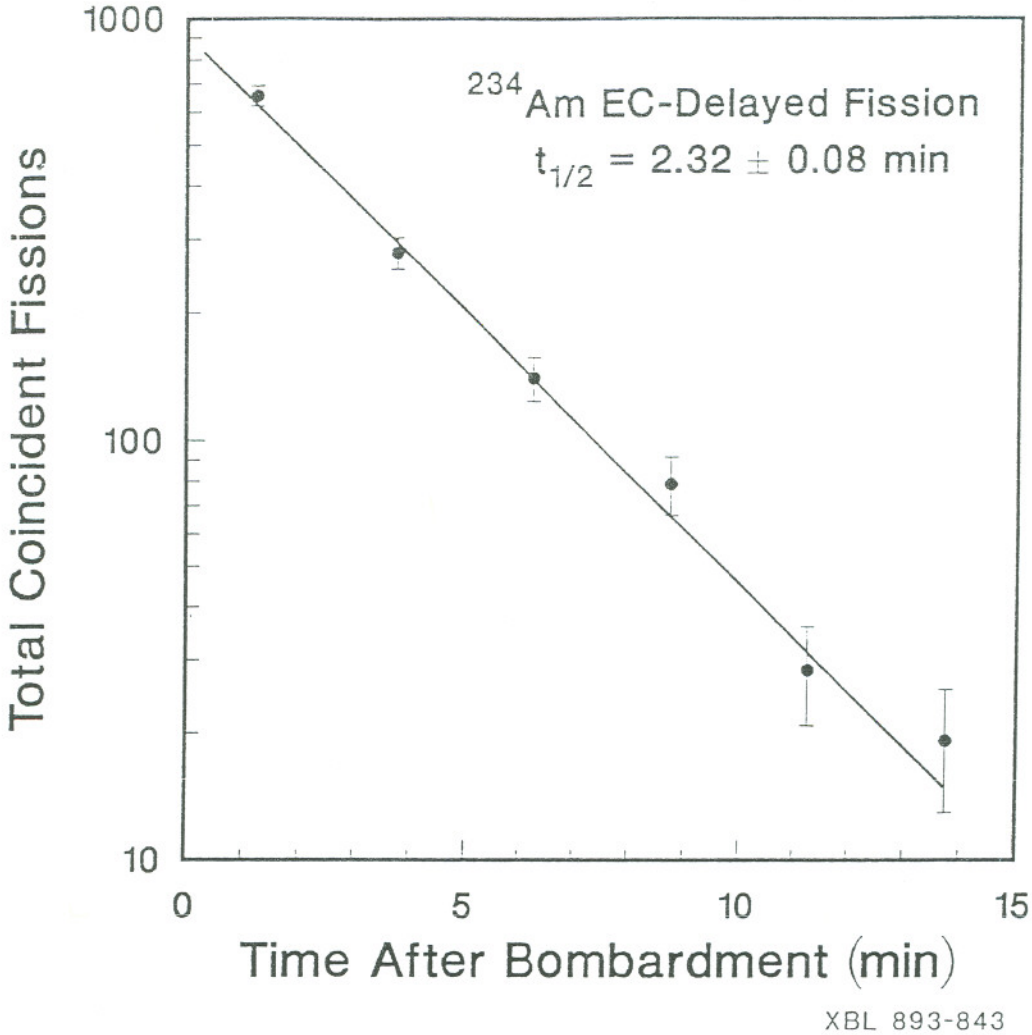

Figure 6.9: Decay curve of the ^{234}Am EC-delayed fission activity as measured on MG-RAGS. The wheel stepping time was 2.50 minutes.

Table 6.5: Summary of the fission characteristics of the ^{234}Am εDF mode.

	SKW[a]	Weissenberger[b]
Post-neutron $\overline{\mathrm{TKE}}$[c]	173 ± 5 MeV	171 ± 5 MeV
Pre-neutron $\overline{\mathrm{TKE}}$	175 ± 5 MeV	173 ± 5 MeV
Post-neutron $\overline{\mathrm{KE}}$[d] of high-energy fragment	99.8 ± 2.0 MeV	98.6 ± 2.0 MeV
Post-neutron $\overline{\mathrm{KE}}$ of low-energy fragment	73.5 ± 1.4 MeV	72.3 ± 1.5 MeV
Pre-neutron $\overline{\mathrm{KE}}$ of high-energy fragment	100.6 ± 2.0 MeV	99.4 ± 2.0 MeV
Pre-neutron $\overline{\mathrm{KE}}$ of low-energy fragment	74.1 ± 1.4 MeV	72.9 ± 1.5 MeV
Average mass of the light fission fragment	99.1 ± 0.1	99.0 ± 0.1
Average mass of the heavy fission fragment	134.8 ± 0.1	135.0 ± 0.1

[a]Calculated using the Schmitt, Kiker, and Williams (SKW) [SCHMITT 65] method and reference values for ^{252}Cf.
[b]Calculated using the SKW method and the reference values of Weissenberger [WEISSENBERGER 86] for ^{252}Cf.
[c]Average total kinetic energy.
[d]Average kinetic energy.

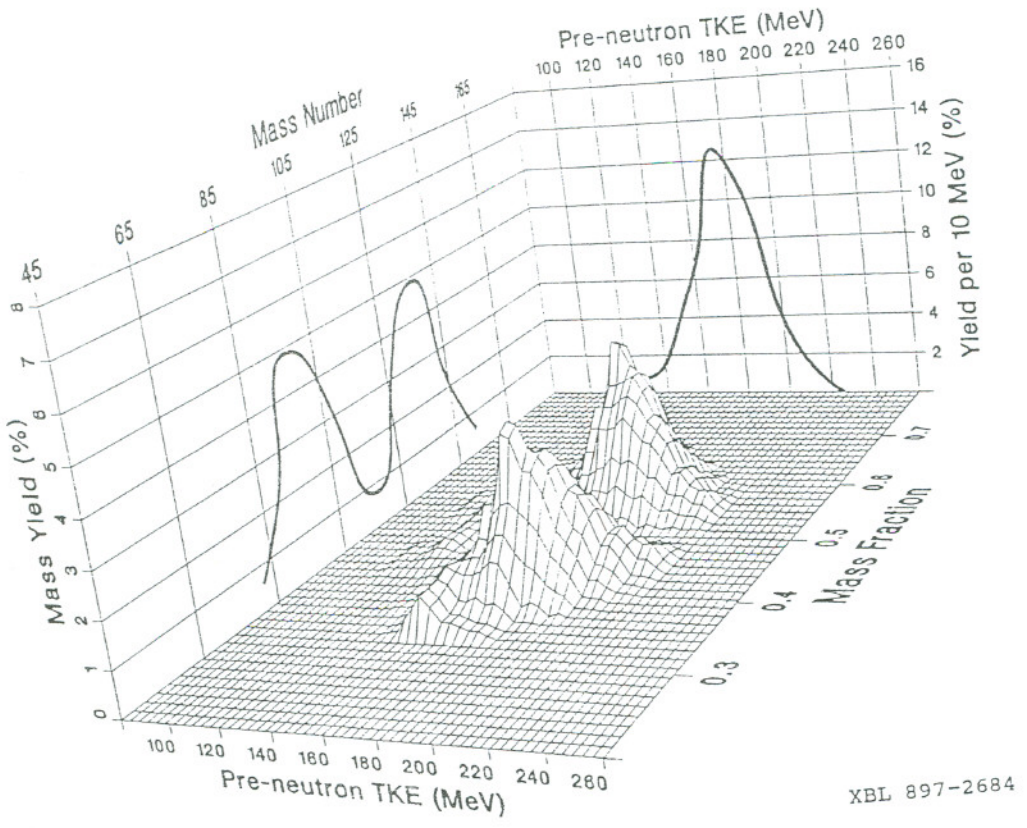

Figure 6.10: Pre-neutron emission total kinetic energy (TKE) distribution of the ^{234}Am εDF mode and pre-neutron emission mass-yield distribution.

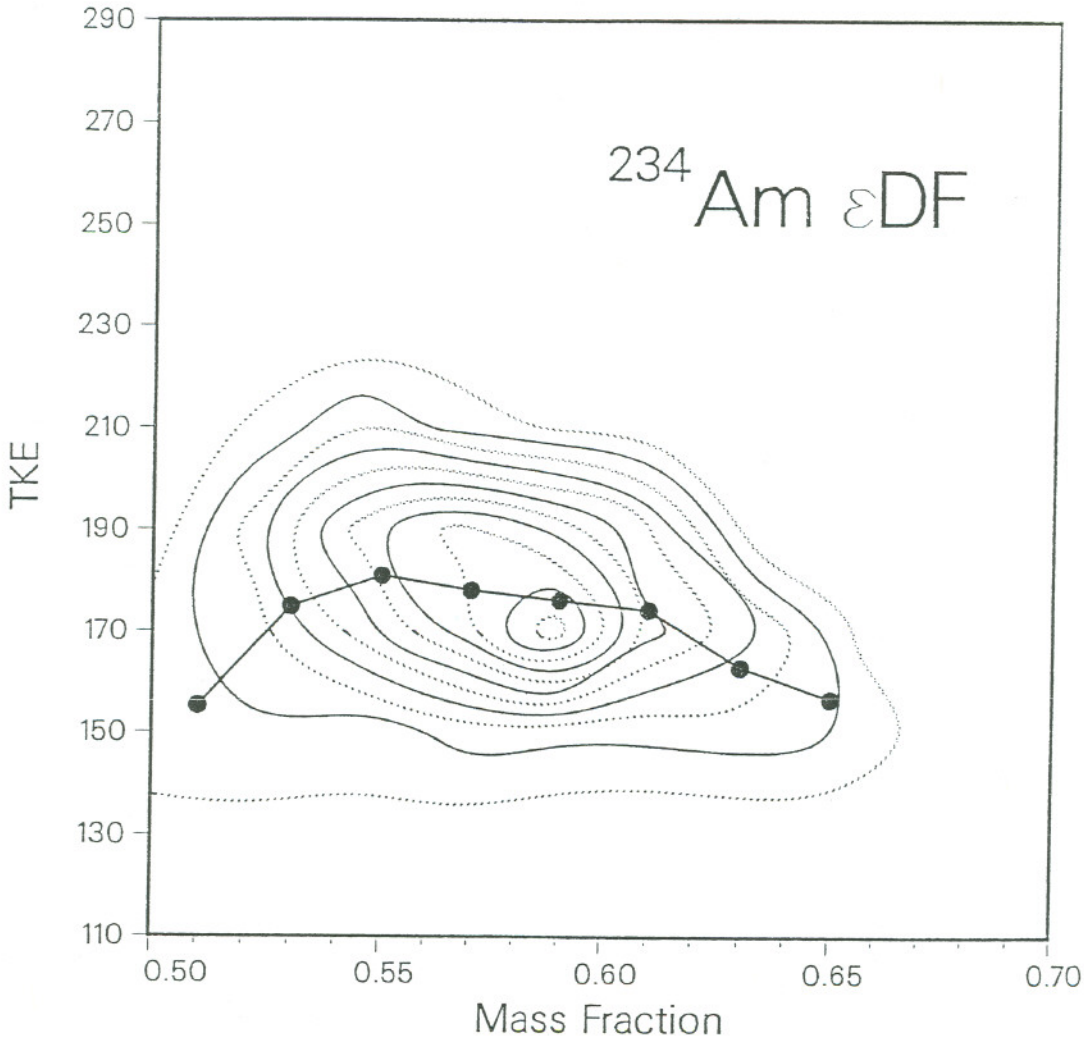

Figure 6.11: Total kinetic energy and average total kinetic energy of ^{234}Am as a function of mass distribution. The solid points are the average TKE values.

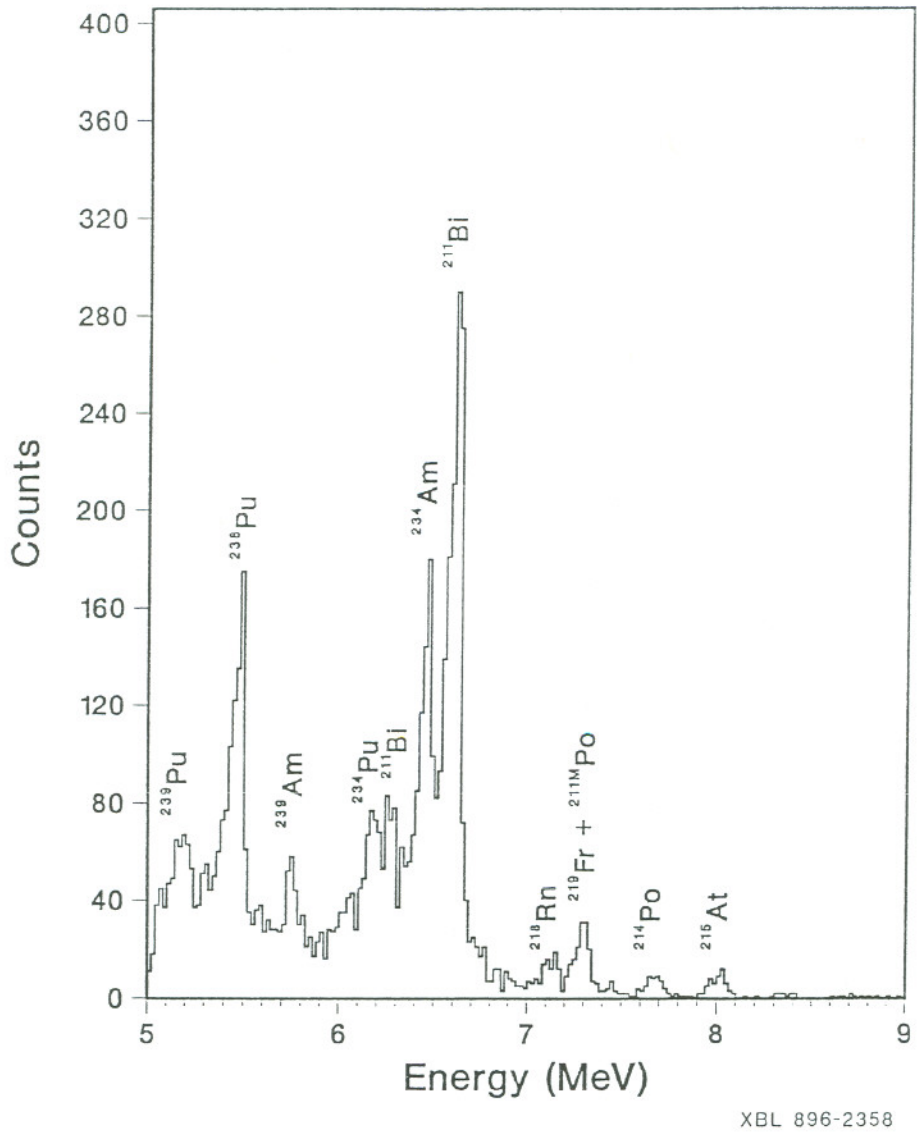

Figure 6.12: Alpha spectrum from the on-line studies of ^{234}Am produced by the ^{237}Np(α,xn) reaction and measured by the MG. This spectrum is taken from the second detector station, with a stepping time of 2.50 minutes. Major peaks are identified.

reaction reduced the α resolution of the first detector station to such a poor value that the α data from this detector station had to be omitted from the subsequent decay analysis. Peaks in the α spectrum were integrated by a simple sum of counts, and contributions from nearby peaks were estimated by hand.

The 6.46-MeV α peak was observed to decay with two half-life components, with one component about 2.3 minutes and the second too long to be measured accurately in this experiment. After correction of the decay data to represent the same number of samples, half-life analysis was performed using the **EXFIT** [GREGORICH 85] computer code. The 2.32-minute component is assigned to ^{234}Am, and the long component is attributed to tailing (lower-energy scattered α particles) of the ^{211}Bi peak into the ^{234}Am peak. The long component cannot be due to a long-lived isomeric state in ^{234}Am decaying by IT to the ground state. Such a state would also yield a long component in the delayed fissions, which is not observed. The decay of the 6.46-MeV α group is shown in Figure 6.13. Comparison of the initial activities of the ^{234}Am α and εDF branches yields an alpha-to-fission ratio of 5.8$\pm$0.4. Using the same assumptions about effective target thickness and transport yields, the partial cross-section for ^{234}Am produced by this reaction and decaying by alpha emission was found to be 1.1 nb.

6.3.3 P_{DF} and σ_ε Results

Americium fractions were repeatedly isolated chemically over an irradiation period of about four hours. Fission measurements were made in the same period on an alternating basis with the chemical separations. The chemically purified americium samples were γ counted repeatedly for approximately 40 minutes each. The fission samples were counted for one ten-minute period each in the proportional counter, and the integrated fissions were recorded. The γ spectra were analyzed using the **SAMPO** [ROUTTI 69] computer code, and half-life analysis was performed with the **CLSQ** [CUMMING 64] code.

Figure 6.14 shows the γ rays observed in a representative spectrum from this

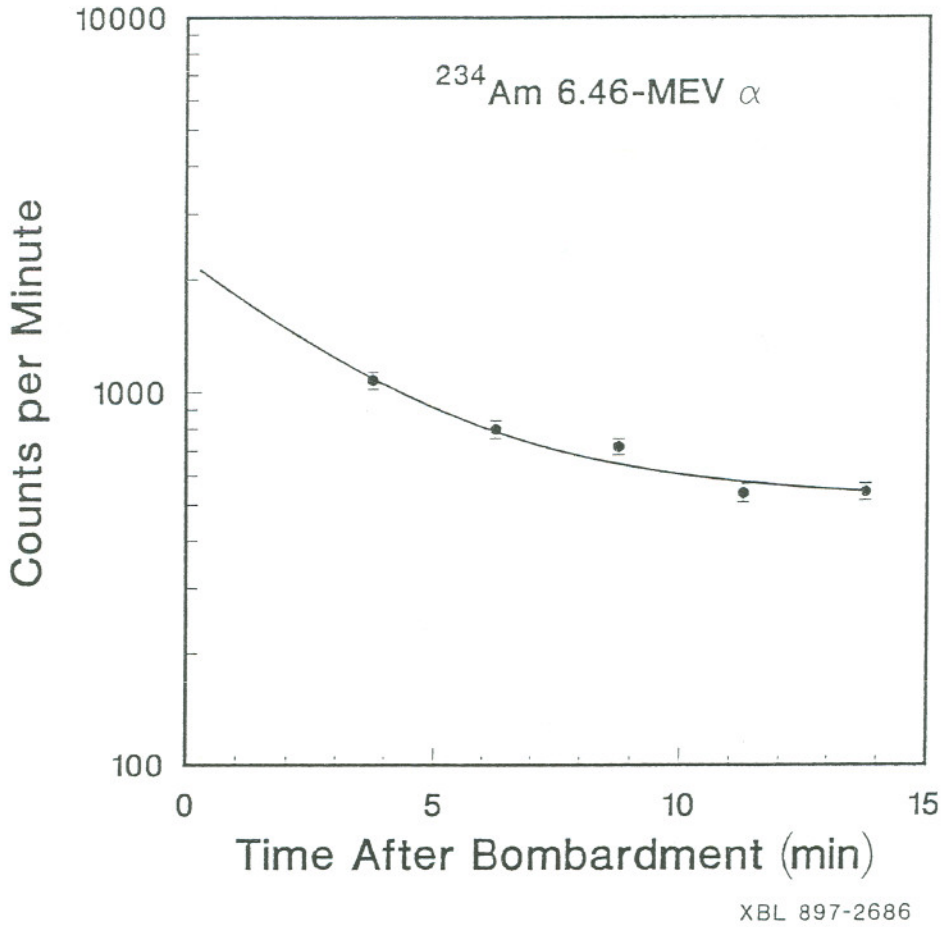

Figure 6.13: Decay curve of the 6.46 MeV α group from the on-line α and fission measurements using the MG.

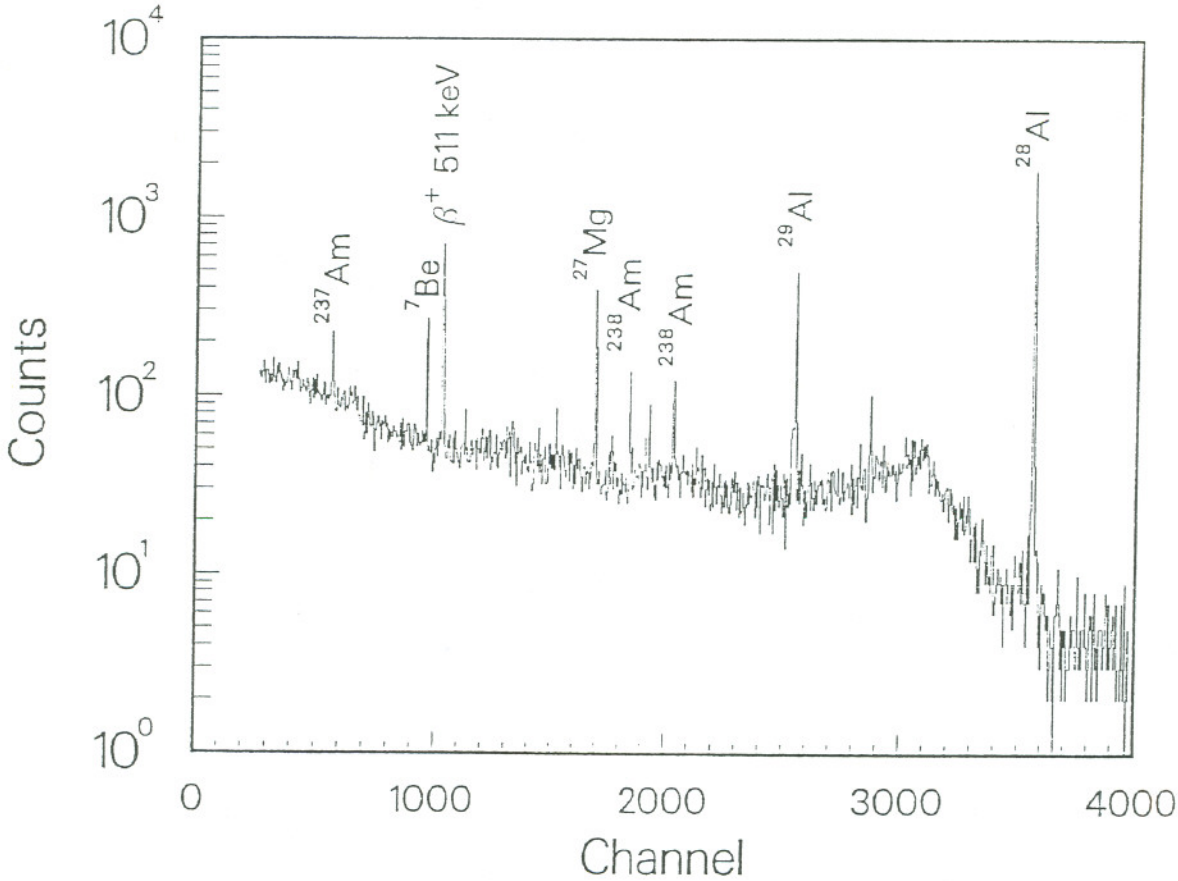

Figure 6.14: Gamma rays in the range of 0 to 2 MeV observed in a chemically purified sample of americium. The K x-ray region is expanded and shown in Figure 6.15.

experiment. Some ^{237}Am and ^{238}Am were visible within the spectra, probably produced by non-compound-nucleus reactions. A small amount of ^{7}Be, which was produced from the target backings, followed the americium, as did small amounts of ^{28,29}Al and ^{27}Mg. The aluminum and magnesium were most likely produced by scattered beam on the aluminum target-holder cards. Half-life analysis confirmed the assignment of these peaks.

The K x-ray region from the spectrum used for Figure 6.14 is expanded and shown in Figure 6.15. The plutonium x-rays resulting from the electron capture of americium are clearly visible. The only other peaks in this region are lead K x-rays and the 59.5-keV γ ray from the ^{241}Am yield tracer.

Half-life analysis of the Pu K x-rays revealed a two-component decay curve, with one component being short (about 2-3 minutes), and the other on the order of an hour. The long component was a mixture of the ^{237}Am ($t_{1/2} = 73$ min) and ^{238}Am ($t_{1/2} = 1.63$ hr), and the short one was ^{234}Am. The K x-rays were fitted with two components using **CLSQ**, with the short component being set at 2.32 minutes and the long component allowed to vary. An example of such a fit is shown in Figure 6.16. The resulting initial activities of the ^{234}Am electron-capture decay mode were corrected for detector efficiency, chemical yield, and K-fluorescence yield (taken as 97.7% [LEDERER 78]). The resulting initial disintegration rates were used for the calculation of σ_ε and P_{DF}.

The electron-capture cross-section was calculated based on the following assumptions. First, the target thickness was estimated the same way as for the apparent fission cross-section, yielding an effective total target thickness of 900 μg/cm^2. Second, the gas-jet yield was assumed to be 100%. Third, it was assumed that the level density of the daughter was high enough that deexcitation proceeded through a series of high-energy ($\sim$500-1000 keV) low-multipolarity transitions. Based on this assumption, the K x-ray production from internal conversion was taken as negligible. Of course, the last few transitions should be more highly converted, but without detailed information about the level scheme of ^{234}Pu any estimates on

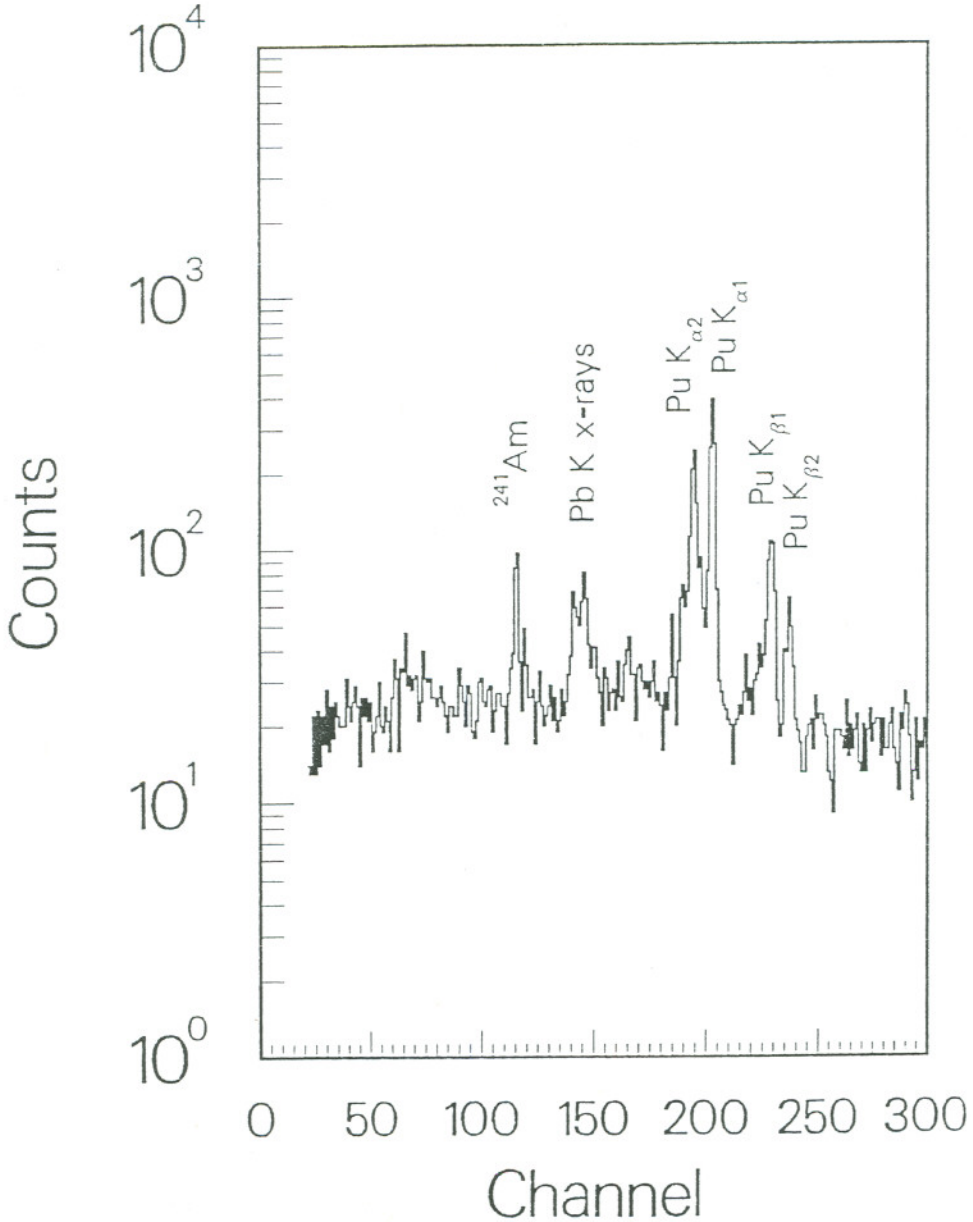

Figure 6.15: The K x-ray region of the gamma spectrum of a chemically purified ^{234}Am sample.

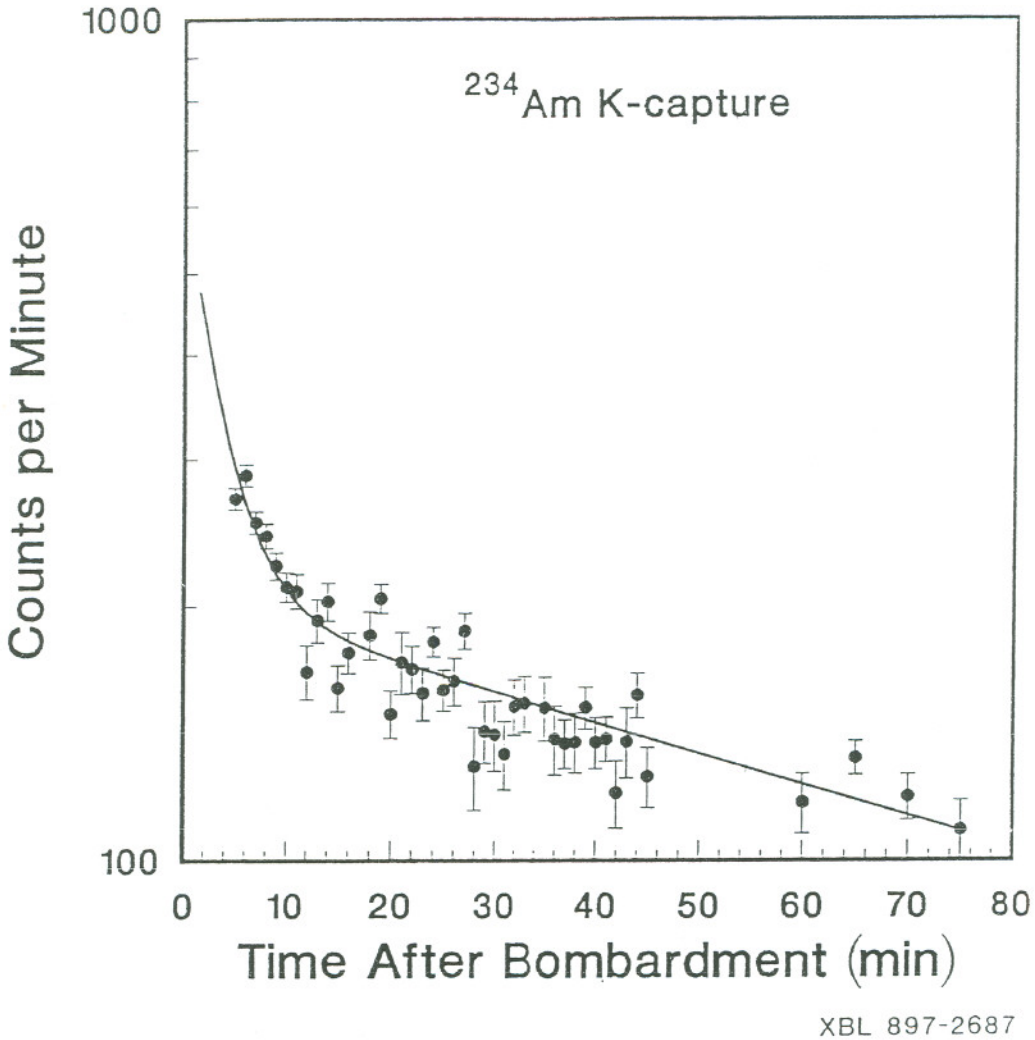

Figure 6.16: Half-life fit for the plutonium K x-rays observed from the chemically purified ^{234}Am sample.

Table 6.6: Individual P_{DF} determinations for ^{234}Am. P_{DF} was calculated in each case by Equation 5.2.

$D_{0,\varepsilon}$	$I_f{}^a$	$P_{DF}/10^{-5}$
16694 ± 13%	4 ± 2	7.17 ± 52%
15502 ± 15%	4 ± 2	7.74 ± 52%
15157 ± 12%	3.5 ± 1.3	6.93 ± 39%
11606 ± 20%	3 ± 1.7	7.74 ± 39%
18929 ± 17%	2 ± 1.4	3.18 ± 72%
19636 ± 16%	5 ± 2.3	7.65 ± 48%

[a] I_f for the P_{DF} measurement of ^{234}Am is the fission measurement immediately following the chemical separation.

K-conversion would be near baseless. Finally, the K/L-capture ratio was taken as being very large (this assumption and the third assumption err in opposite directions - hopefully, they approximately cancel). With the above assumptions, σ_ε was determined to be 5.4 ± 1.3 μb at the 1σ (68%) confidence level.

The delayed fission probability was calculated from the electron-capture initial activities and the number of fissions observed in the subsequent fission sample, according to Equation 5.2. The beam flux was held at a constant 7 eμA throughout the experiment, with less than 5% deviation, so that ϕ does not appear in the calculation. Employing Equation 5.2, P_{DF} was calculated and averaged over all of the separate determinations. This yielded a value of P_{DF} of $(6.6 \pm 1.8) \times 10^{-5}$ at the 1σ (68%) confidence level. Table 6.6 lists the individual values obtained.

Using the delayed-fission probability as the ratio of fissions to EC decays and the α-to-fission ratio determined in **6.3.2** above, the α-to-EC ratio was found to be $(3.9 \pm 1.2) \times 10^{-3}$.

6.3.4 X-ray–Fission Results

Samples were collected from the gas-jet system every four minutes and then placed in the counting chamber for the correlation studies. Approximately 1500 samples were processed in this manner. Figure 6.17(A) shows the x-ray and γ spectrum of those events in prompt coincidence with the fission signal. Figure 6.17(C) is the logarithm of a maximum-likelihood fit L (from Equation (5.6)) of an idealized x-ray spectrum (shown in Figure 6.17(B)) to the observed data. In Figure 6.17(C), the logarithm of the likelihood is plotted as a function of the $K_{\alpha 1}$ position of the ideal spectrum. From the likelihood functions, the most probable $K_{\alpha 1}$ energy was found to be 103.6 $\pm$ 0.5 keV, in excellent agreement with the plutonium $K_{\alpha 1}$ energy of 103.76 keV. The total number of K x-rays was found to be 32 $\pm$ 6 by allowing the intensity of the ideal spectrum (Y) to vary within the maximum-likelihood analysis. Observed and expected x-ray intensities for plutonium are given in Table 6.7.

The number of x-ray–fission coincidences relative to the total fissions was consistent with the detector geometries. As with ^{232}Am, the number of fissions in coincidence with prompt γ rays from the fission fragments relative to the total number of fissions indicated that the γ multiplicity of ^{234}Am εDF is about the same as that of ^{252}Cf. No evidence was observed for fission delay times longer than the best timing resolution of these experiments, about 3 ns using a NaI(Tl) detector. The fact that plutonium x-rays can be seen requires that the lifetime of the fissioning state be longer than the time it takes the orbital electrons to cascade down and fill a K-vacancy. The time required for this is on the order of 10^{-17} seconds [SCOFIELD 74]. We can therefore set boundaries on the excited state half-life of 10^{-8} ns $< t_{\frac{1}{2}} <$ 3 ns. If the nucleus is truly 100% damped in the second well (as it was assumed in Equation 3.7), then these limits are also limits on the lifetime of the shape isomer ^{234f}Pu. These limits are consistent with the half-life systematics of plutonium shape isomers (See Figure 3 of [POENARU 89]), from which one would expect the half-life of ^{234f}Pu to be in the range of 1 to 100 picoseconds.

The coincidence γ data in Figure 6.17 also show what appear to be true peaks

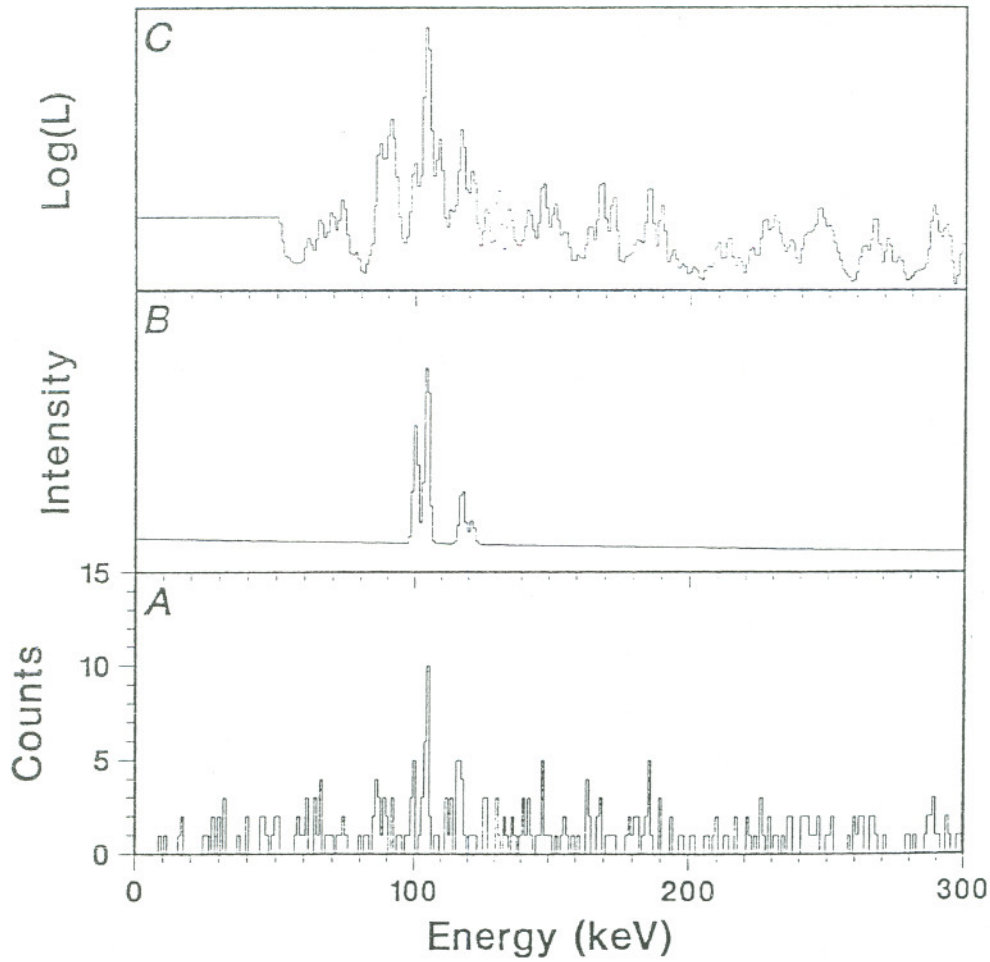

Figure 6.17: X-ray–fission correlation results. *A*: X-rays and γ rays in coincidence with delayed fission from ^{234}Am. *B*: An idealized plutonium K x-ray spectrum, based on the measured detector resolution and an expected prompt γ-ray continuum. *C*: The likelihood function for the position of the ideal spectrum (*B*) in the data (*A*), as a function of the $K_{\alpha 1}$ position.

at about 112, 147, 168, and 185 keV. These peaks are very weak, but prompt γ rays from fission fragments do not display such structure (prompt γ rays from fission tend to follow an exponential structure in energy [HOFFMAN 74]). It is possible that these γ rays are a result of the level structure of ^{234}Pu in the second well. If this is the case, the correlation of these γ rays supports the hypothesis that the second well is strongly damped. Unfortunately, the poor statistics of the γ-γ-fission-time correlation data (even taking all data in the hardware time window of 1 μs) precludes constructing a level scheme for ^{234f}Pu.

6.4 ^{236}Am Results

6.4.1 On-line Measurements

A search was performed for an εDF mode in the unknown isotope ^{236}Am ($t_{1/2}$ estimated at 10 - 15 minutes) using the **MG**. The reaction ^{3}He + ^{237}Np was chosen for this attempt to discover the new isotope. ^{3}He has a smaller momentum than an α particle of the same energy (and hence less of the target material is useful for producing the compound nucleus products because of their shorter recoil range), but the predicted cross section for the (^{3}He,4n) reaction is considerably larger than the 5n reaction channel using α particles. The low recoil momentum for the compound nucleus led to an estimate of the effective target thickness of 28 μg/cm^2 per target, or 280 μg/cm^2 total.

The recoiling reaction products, after attaching to KCl aerosols, were collected on the **MG** wheel. The wheel was stepped at 3.0 minute intervals, and the first detector station was disabled for α particles for the first twelve seconds after the wheel motion. This allowed all the short-lived α activities produced from the beryllium target backings to decay. Over a twelve hour irradiation, the total beam dosage to the targets was 0.5977 C of ^{3}He^{+2}, or 1.86×10^{18} particles. The average beam flux was 13.5 eμA.

The α particles observed in this irradiation are shown in Figure 6.18. With the exception of the peak at 6.41 MeV, the major peaks are identified as known activities, and their identification is supported by half-life analysis. The peak at 6.41 MeV is potentially attributable to ^{236}Am (Q_α = 6.51 MeV [MÖLLER 88]), and its decay shows two half-life components. The short component decays with a half-life consistent with the 3.73-minute half-life observed in the radiochemical separations (see **6.4.2** below), and the long component was too long to be measured accurately with a three minute stepping time. The decay curve of this α group is shown in Figure 6.19.

This α activity is assigned to ^{236}Am for the following reasons: First, it cannot be the 6.46-MeV group of ^{234}Am. There is barely enough incident energy to overcome the reaction Q-value needed to produce ^{234}Am (-33 MeV), and the predicted production cross section for ^{234}Am at the highest energy on target (38 MeV) is about 10 nb. Using the measured α branching ratio for ^{234}Am of 3.9×10^{-3}, the production rate from ^{234}Am at this energy should be about three orders of magnitude lower than the observed rate. The energy of the α group is also lower than the ^{234}Am group by about 50 keV. This is too great a difference to be accounted for by random error. Second, the known isotopes in the vicinity of ^{236}Am either have too low a Q_α or do not match the observed half-life. The third and final other possibility, ^{235}Am, is an unlikely assignment because of its 6.44-MeV Q_α. This would indicate a maximum α energy of 6.33 MeV, significantly lower than the observed 6.41 MeV. The 6.41-MeV α group was also observed in the americium fraction in radiochemical separations, further supporting the assignment of this activity to ^{236}Am.

From the decay curve, the cross section for producing the 3.7-min component of the 6.41-MeV α group was determined to be 133 ± 13 nb. The long component matches no known α activity which can be produced in this reaction, and background measurements indicate that it does not arise from detector or wheel contamination. There is not enough ^{211}Bi produced to account for the long compo-

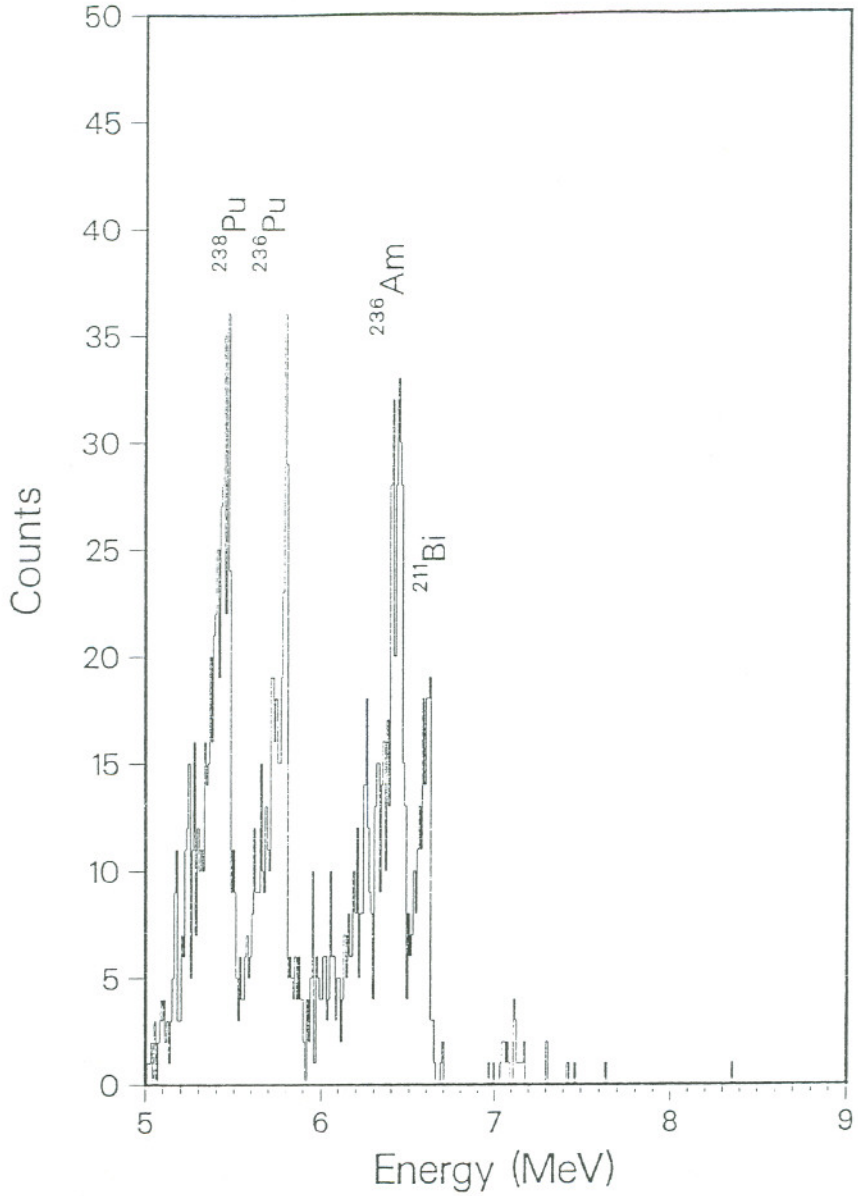

Figure 6.18: Representative spectrum of the α particles observed in the irradiation of ^{237}Np with ^{3}He in the search for ^{236}Am.

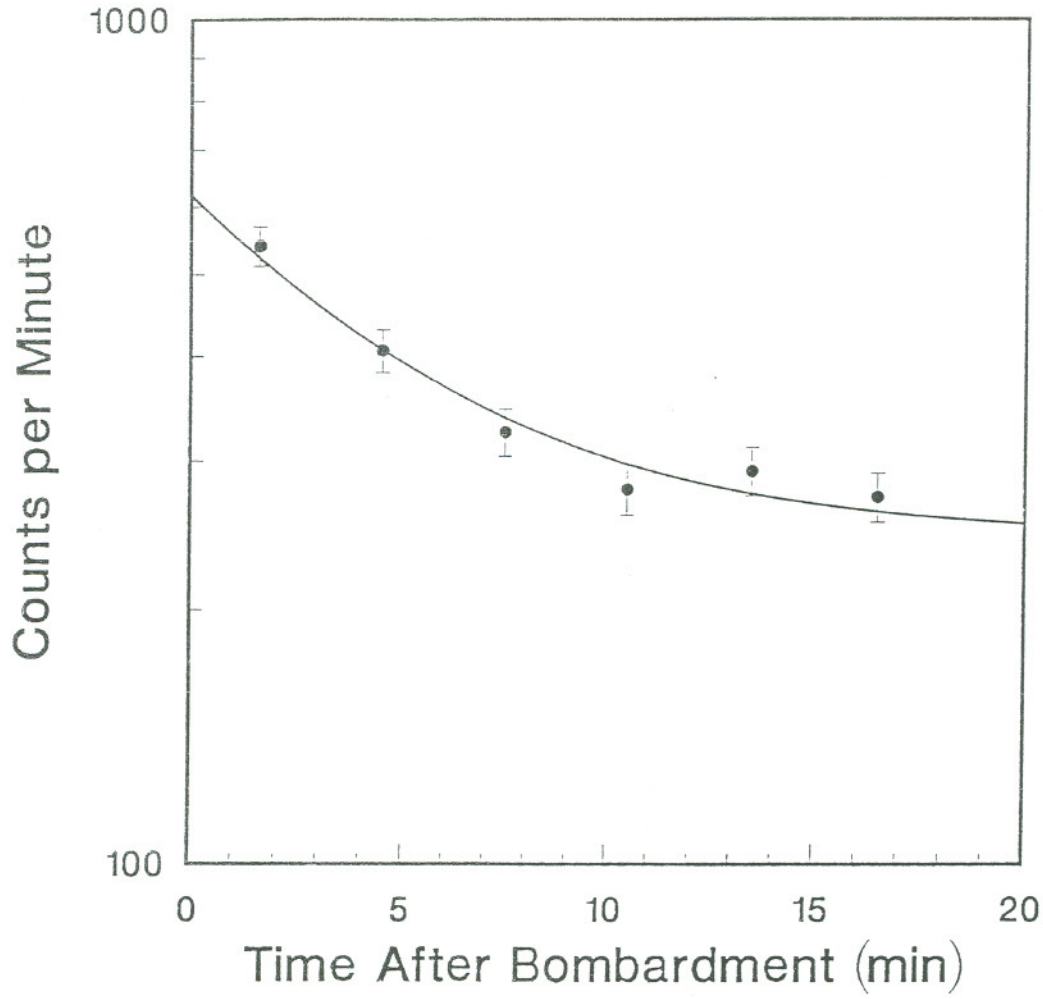

Figure 6.19: Decay curve of the 6.41-MeV α group observed in the irradiation of ^{237}Np with ^{3}He. The short component is assigned to ^{236}Am, and the long component may be attributable to ^{236m}Am.

nent by peak overlap. It is possible that the long component arises from a long-lived isomer in ^{236}Am which decays primarily by α emission. The peak at 6.41 MeV is rather broad for a single α-energy component, so it could hide 2 or more separate α groups. However, the α energies of the two components must be very close together, within 100 keV. There is insufficient evidence to definitely assign the long-lived component to ^{236m}Am, although it is a reasonable hypothesis.

Fifteen coincident fission-fragment pairs were observed in the course of this irradiation. The lifetimes of these fissions, relative to the end of bombardment, is given in Table 6.8. A background of the detectors taken immediately before the experiment indicated a background rate of two coincident fission fragments per day with no wheel in the **MG**, and the background during the measurement should be lower because the wheel collimates the detectors relative to one another, reducing the coincidence detection geometry for fissions arising from sources other than the polypropylene foils. Since the data in Table 6.8 were taken in 12 hours, it is possible that one of the fission-fragment pairs is due to this background. However, as in the case of ^{230}Am, the fissions are observed at a very low level and have a half-life much longer than the residence time in the detector stations, 18 minutes. Since the above α data and the γ data (discussed below) support the hypothesis that ^{236}Am has a half-life of 3.7 minutes, these fissions cannot be attributed to ^{236}Am. No fissions were observed in the elemental assignment chemistry either, indicating that the fissions probably arise from a lower Z element.

Since the observed fissions cannot be attributed to ^{236}Am, the region in cross section - half-life space which has been excluded by this experiment is shown in Figure 6.20.

6.4.2 Radiochemical Measurements

Both the short and long chemical separations were performed on the fission activity over a 12-hr period. No fissions were observed in either of the fractions from the short chemistry, nor were any observed in the direct catches which alternated

Table 6.7: Observed and expected x-ray intensities from the correlated x-ray–fission data for ^{234}Am. Expected x-ray intensities are taken from the **Table of Isotopes**. [LEDERER 78].

X-ray	E/keV	I_{theo}	No. Observed[a]	I_{obs}
Pu $K_{\alpha 2}$	99.55	0.299	10	0.20 ± 0.07
Pu $K_{\alpha 1}$	103.76	0.479	22	0.45 ± 0.12
Pu $K_{\beta 1'}$	116.9	0.162	14	0.29 ± 0.09
Pu $K_{\beta 2'}$	120.6	0.060	3	0.06 ± 0.04

[a]Approximately 18 of the observed events are attributable to the prompt γ-ray continuum.

Table 6.8: Coincident fission-fragment pairs observed in the experiment to produce ^{236}Am.

Pair No.	Detector No.	Lifetime (sec)
1	5	806.82
2	4	714.57
3	3	466.37
4	6	1037.45
5	4	607.25
6	2	288.52
7	5	854.67
8	2	260.90
9	5	763.60
10	4	632.68
11	3	367.82
12	1	153.97
13	4	699.75
14	1	174.20
15	3	405.30

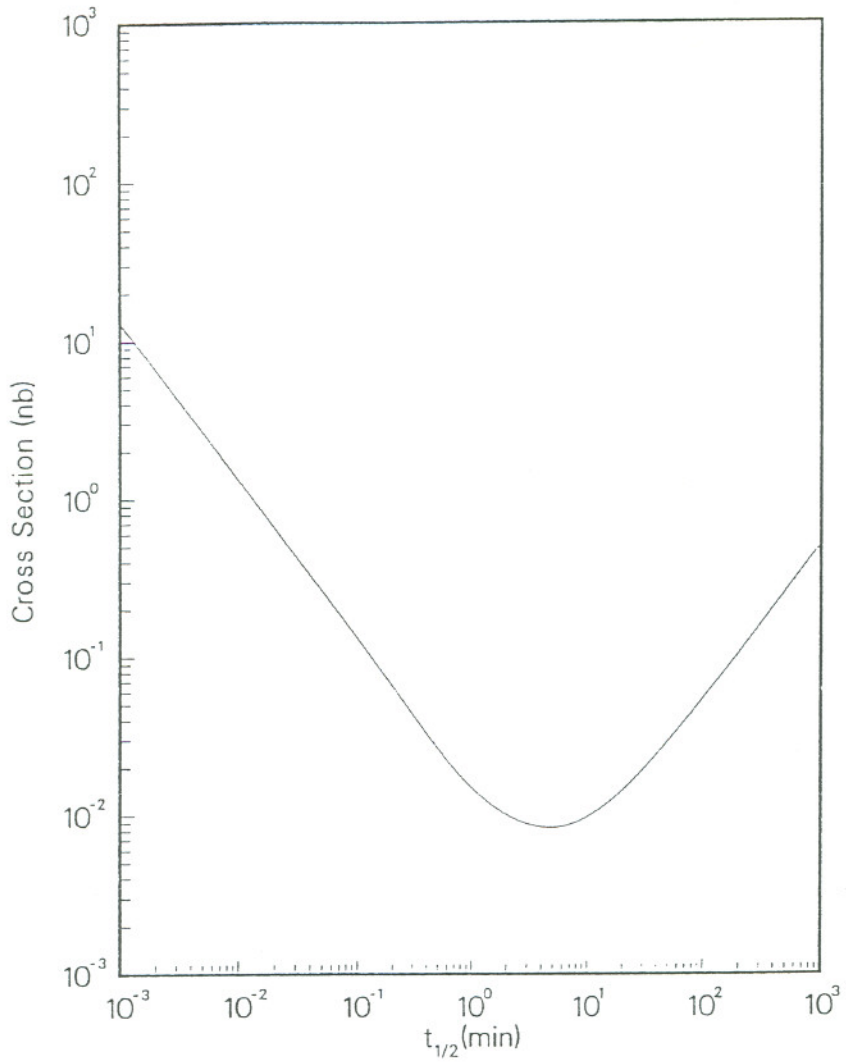

Figure 6.20: Half-life and $\sigma_{<f>}$ limitations imposed on the production of ^{236}Am in the ^{237}Np + ^{3}He reaction by the results of this experiment. Calculations were performed assuming all observed fissions were attributable to sources other than ^{236}Am, and five coincident fission-fragment pairs of ^{236}Am could be produced but not detected.

with the long chemistry. However, because of the very low fission production rate observed on the **MG**, only about two fissions could be expected in these sample in this period. Since none were observed, there is no data on a radiochemical Z assignment.

However, the x-ray analysis of samples from the long chemistry were much more fruitful. The plutonium K x-rays from americium K-capture were clearly visible in the γ spectra, as an example shows in Figures 6.21 and 6.22. The primary contaminants are the same ones observed before, isotopes of beryllium, magnesium, and aluminium. Half-life analysis confirmed these assignments.

Half-life analysis of the plutonium K x-rays revealed a two-component decay curve, as expected. The long component is attributable to a mixture of ^{237}Am and ^{238}Am, as has been observed before. The short component is assigned to ^{236}Am, since that is expected to be the only short-lived americium produced in large quantities. From the calculated excitation function (shown in Figure 6.23), there could be a maximum of about 15% as much ^{235}Am as ^{236}Am produced in this energy range. Because of this uncertain contribution, the quoted error on the final half-life determined for ^{236}Am has been arbitrarily doubled.

Thirty-nine determinations of the half-life of the short component yielded a value of 3.73 ± 0.28 minutes for ^{236}Am (fitted with **CLSQ**). The various measurements are given in Table 6.9. A representative half-life fit is shown in Figure 6.24. Calculation of σ_ε using Equation (5.3) yielded 320 ± 35 μb. Using the estimated upper limit on $\sigma_{<f>}$ from Figure 6.20 of 8 pb, the upper limit on P_{DF} is calculated to be 2.5×10^{-8}. Using the on-line α data, the branching ratio for the 6.41-MeV α group of the 3.73-minute ^{236}Am was determined to be $(4.2 \pm 0.6) \times 10^{-4}$.

The observed half-life is somewhat shorter than expected for ^{236}Am, yielding a $\log ft$ value of 5.2 for this decay. Such a low $\log ft$ value strongly implies that the EC transition in ^{236}Am is allowed (even though actinides usually have fast forbidden transitions, a $\log ft$ of 5.2 is considerably lower than the 6 or higher usually found for such transitions), with $\Delta I^{\Delta\pi} = 0^{\mathrm{No}}$. Such a transition would

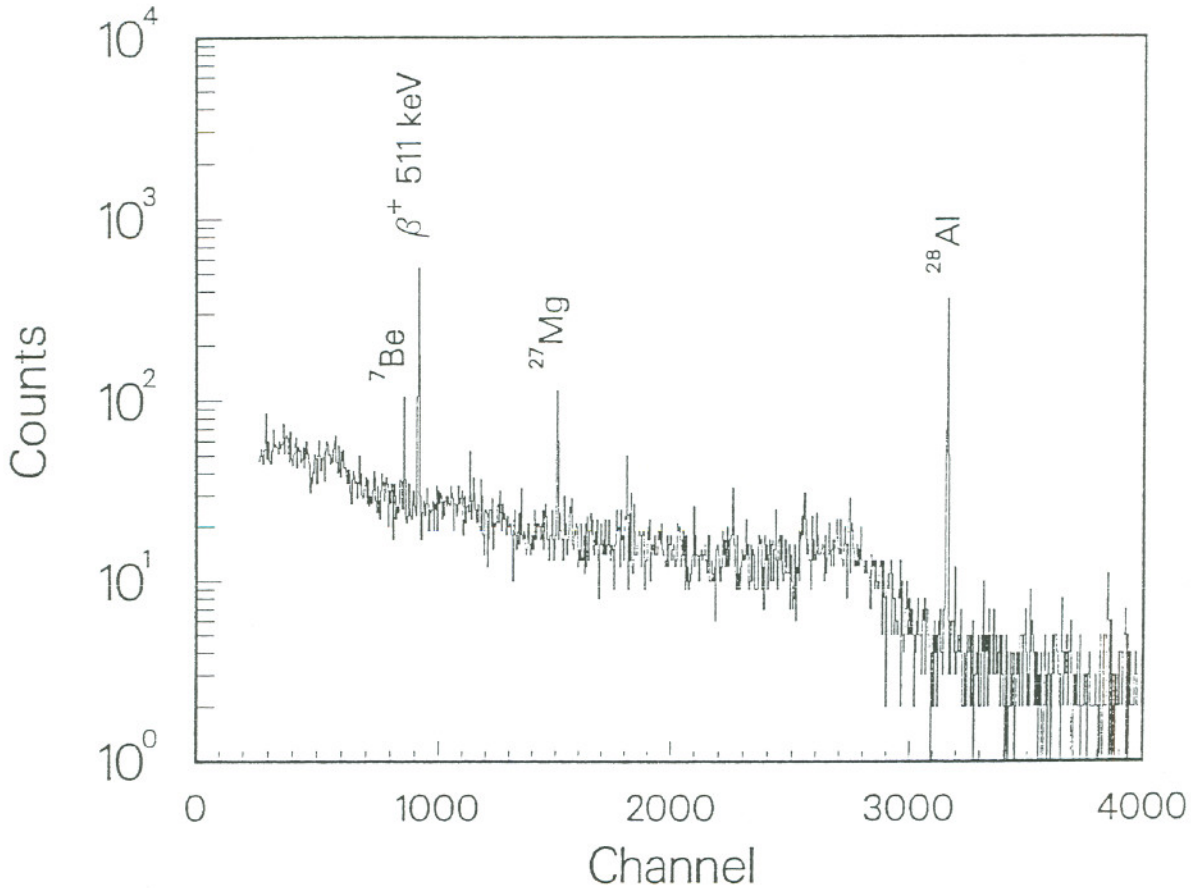

Figure 6.21: Gamma rays observed in the americium sample from the long chemistry, produced in the irradiation of ^{237}Np with ^{3}He. Major contaminants are labelled. The K x-ray region is expanded and shown in Figure 6.22.

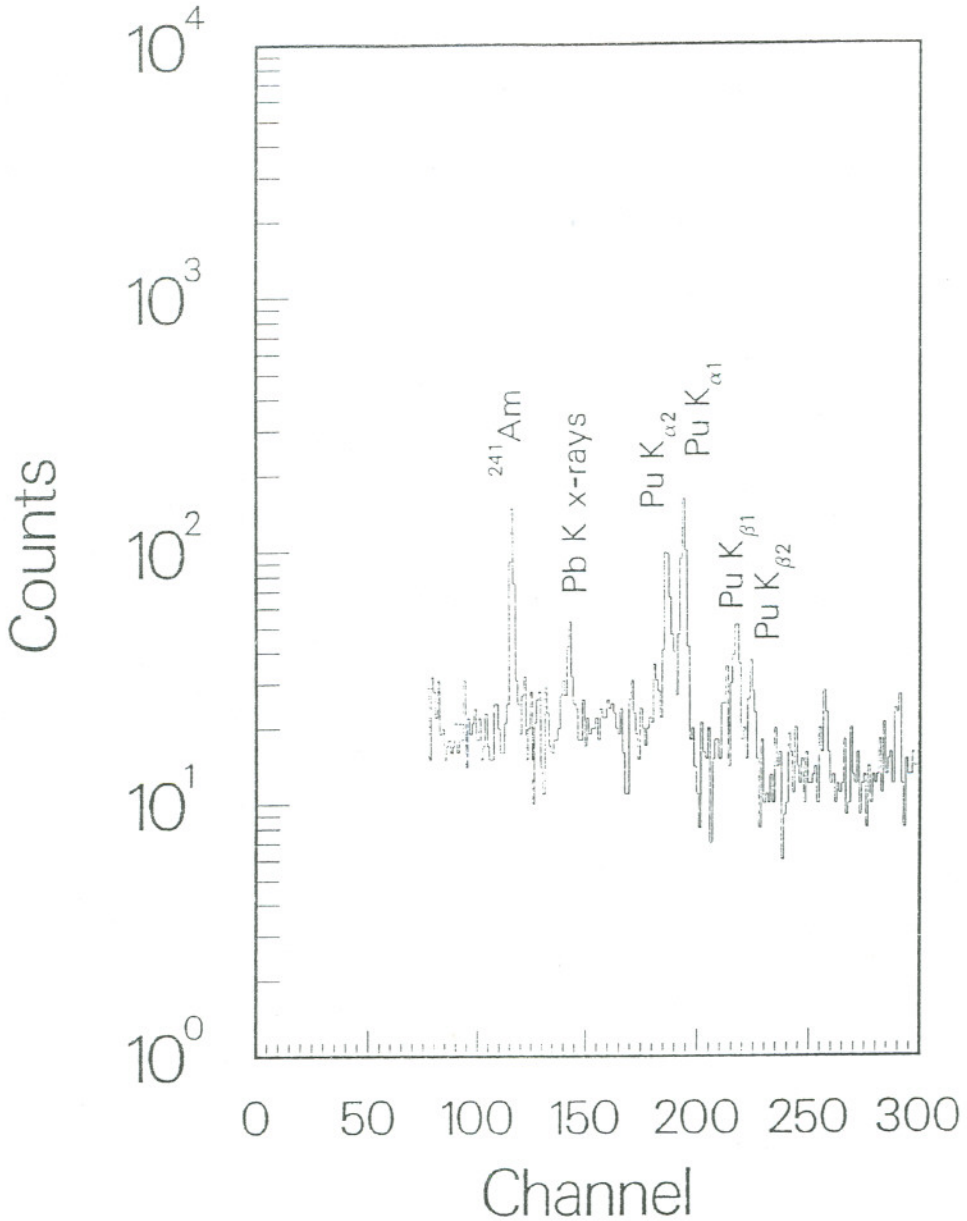

Figure 6.22: The K x-ray region from Figure 6.21.

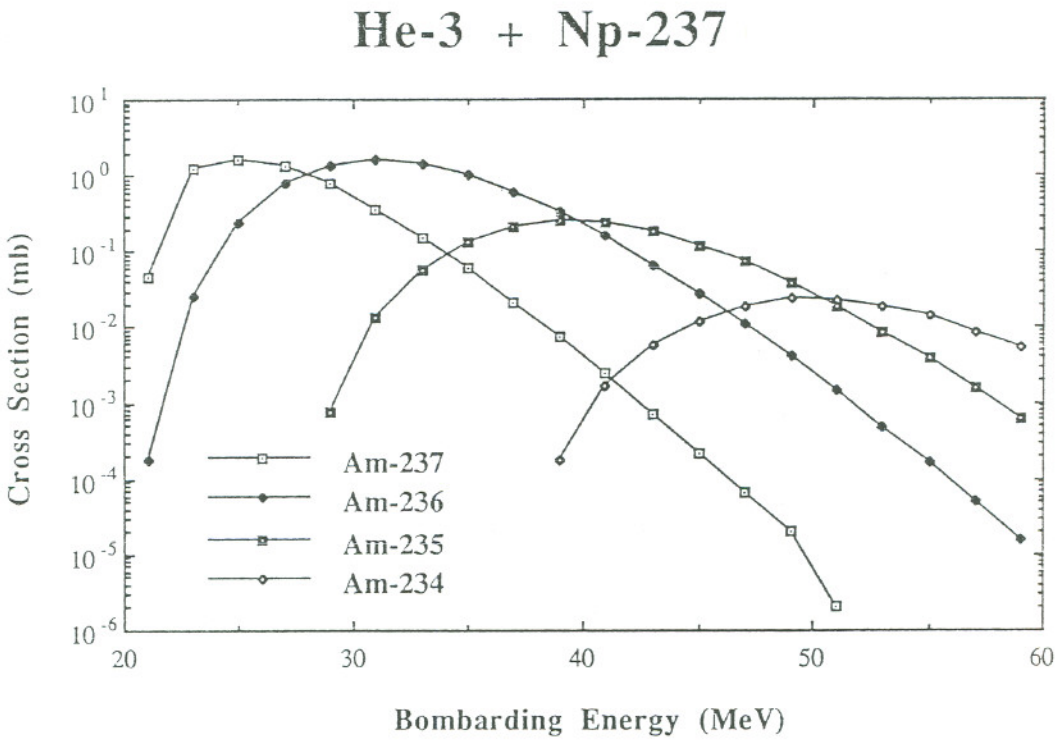

Figure 6.23: Calculated excitation functions for compound nucleus products in the reactions of ^{3}He with ^{237}Np. The energy range of the ^{3}He in the targets was 33-39 MeV.

Table 6.9: Individual $t_{1/2}$ determinations for ^{236}Am based on its K-capture x-rays.

Point No.	Source	$t_{1/2}$ (min)	Point No.	Source	$t_{1/2}$ (min)
1	$K_{\alpha 2}$	7.4 ± 6.0	21	$K_{\beta 2'}$	3.8 ± 2.5
2	$K_{\alpha 1}$	2.22 ± 0.45	22	$K_{\alpha 1}$	2.16 ± 0.39
3	$K_{\beta 2'}$	3.9 ± 8.6	23	$K_{\alpha 2}$	6.8 ± 6.6
4	$K_{\alpha 2}$	2.33 ± 0.84	24	$K_{\alpha 1}$	3.47 ± 0.47
5	$K_{\alpha 1}$	5.8 ± 1.1	25	$K_{\alpha 2}$	2.5 ± 1.5
6	$K_{\beta 2'}$	3.5 ± 1.3	26	$K_{\alpha 1}$	3.92 ± 0.85
7	$K_{\alpha 2}$	4.2 ± 1.8	27	$K_{\beta 2'}$	3.1 ± 2.2
8	$K_{\alpha 1}$	3.48 ± 0.78	28	$K_{\alpha 2}$	2.41 ± 0.93
9	$K_{\beta 2'}$	4.7 ± 1.6	29	$K_{\alpha 1}$	3.03 ± 0.45
10	$K_{\alpha 2}$	4.99 ± 1.9	30	$K_{\alpha 1}$	3.12 ± 0.42
11	$K_{\alpha 1}$	3.71 ± 0.63	31	$K_{\alpha 2}$	5.6 ± 2.5
12	$K_{\alpha 2}$	3.5 ± 1.4	32	$K_{\alpha 1}$	4.22 ± 0.47
13	$K_{\alpha 1}$	3.26 ± 0.54	33	$K_{\alpha 1}$	3.52 ± 0.49
14	$K_{\beta 2'}$	1.6 ± 0.6	34	$K_{\alpha 2}$	2.81 ± 0.66
15	$K_{\alpha 1}$	4.7 ± 1.9	35	$K_{\alpha 1}$	3.54 ± 0.4
16	$K_{\alpha 2}$	3.1 ± 1.4	36	$K_{\beta 2'}$	7.6 ± 2.2
17	$K_{\alpha 1}$	3.56 ± 0.64	37	$K_{\alpha 2}$	9.7 ± 3.4
18	$K_{\alpha 1}$	2.5 ± 0.61	38	$K_{\alpha 1}$	4.02 ± 0.48
19	$K_{\alpha 2}$	2.49 ± 0.94	39	$K_{\beta 2'}$	11.1 ± 4.4
20	$K_{\alpha 1}$	3.78 ± 0.73			

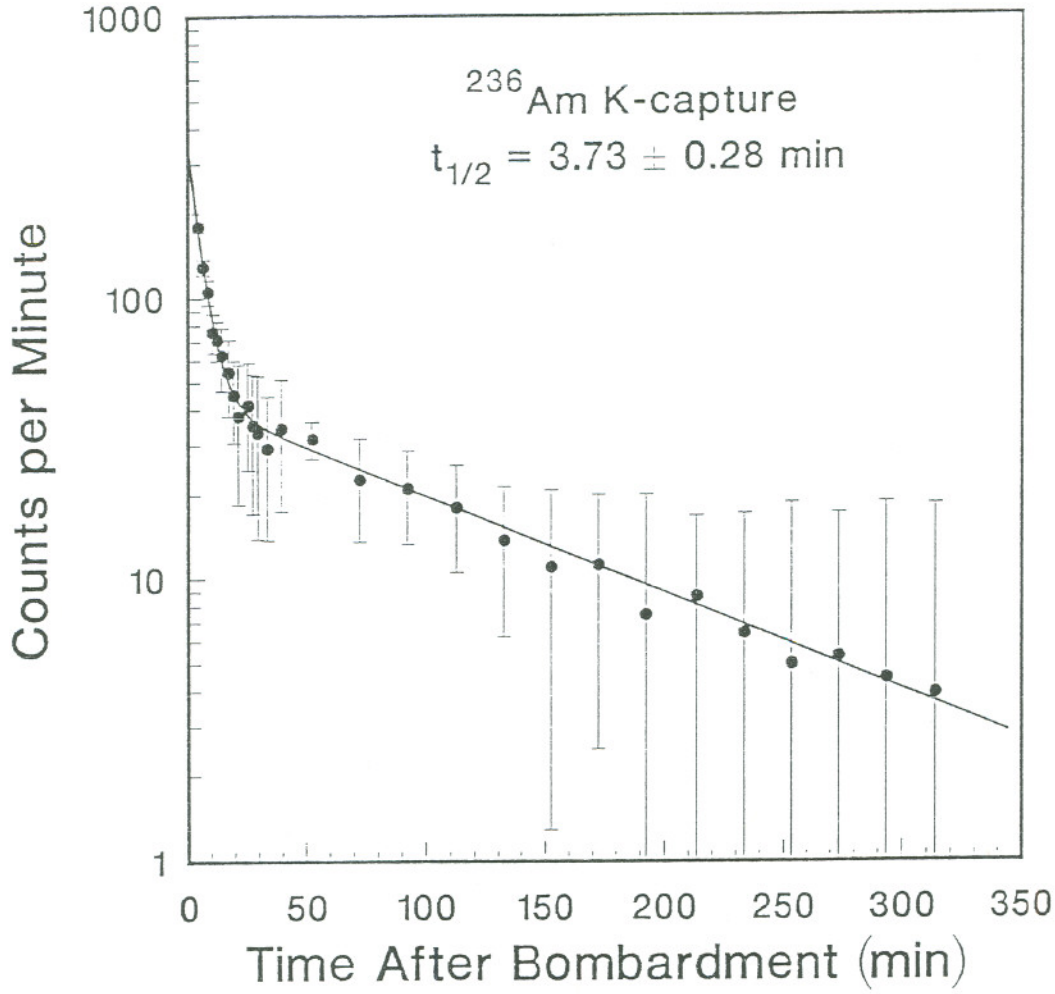

Figure 6.24: Half-life fit from a representative data set of the plutonium x-rays observed in the irradiation of ^{237}Np with ^{3}He.

not be expected for ^{236}Am *a priori*, for the expected neutron and proton states in this nucleus are $\frac{5}{2}^+[633]\downarrow$ and $\frac{5}{2}^-[523]\downarrow$, respectively. This leads one to expect a ground-state configuration of 0^- for ^{236}Am. However, there is low-lying intrinsic proton state with the configuration $\frac{5}{2}^+[642]\uparrow$ in the americium nuclei. If this state has dropped below the $\frac{5}{2}^-$ state in ^{236}Am, then its ground-state configuration could be 0^+, leading to an allowed electron capture decay. This is also supported by the extremely low P_{DF} limit.

Chapter 7

Conclusions

Light americium isotopes were produced using multiple ^{237}Np targets irradiated with α particles. The half-lives of ^{232}Am and ^{234}Am were determined as 1.31 ± 0.04 minutes and 2.32 ± 0.08 minutes, respectively, using a rotating-wheel system at the Lawrence Berkeley Laboratory 88-Inch Cyclotron. No evidence for the existence of the unknown isotope ^{230}Am was found, and an upper limit on its delayed-fission probability was estimated at 1% from predicted production cross sections. The previously unknown isotope ^{236}Am was discovered, and found to have a half-life of 3.73 ± 0.28 minutes by measurements of the plutonium x-rays arising from the americium K-capture. An upper limit on εDF from this isotope was set at 2.5×10^{-8}. Evidence for an α branch in this isotope was also presented. From the half-life of ^{236}Am, a ground-state configuration of 0^+ was postulated.

The fission properties of the εDF mode in ^{232}Am and ^{234}Am were measured. These are the first delayed-fissioning nuclei for which measurements of the fission properties have been made. These are also the first nuclei for which both the fission and the EC branch leading to the fission have been directly measured.

The highly asymmetric mass-division and symmetric TKE distributions for both ^{232}Am and ^{234}Am show no trace of the thorium anomaly. Therefore, the transition region between "normal" double-humped mass distributions and the triple-humped

distribution of the thorium anomaly must begin with lighter elements for this neutron number. Unfortunately, the lighter isotones have considerably smaller Q_ε values. This may reduce εDF in those nuclei to a level too low to measure their fission properties.

The $\overline{\text{TKE}}$ values of 174 MeV and 175 MeV for the ^{232}Am and ^{234}Am εDF modes, respectively, are comparable to the predicted $\overline{\text{TKE}}$'s [VIOLA 66,UNIK 74] for ground state fission from the daughter plutoniums, as shown in Figure 7.1. The εDF mode provided a mechanism for studying the fission properties of nuclei far from stability near their ground states. No other technique currently exists which would allow the study of near-ground-state fission from specific nuclei this far from β-stability.

The observation of x-ray–fission correlations in this experiment unequivocally proves that the decay is indeed EC-delayed fission. These are the first εDF processes for which direct proof has been obtained. The only other time-correlated proof of a delayed-fission process is for βDF in ^{256m}Es [HALL 89B].

The x-ray–fission data also provide a most intriguing prospect, that of studying the level structure of the daughter shape isomers. If the nucleus is strongly damped in the second well, then γ decay must occur after the inner barrier has been penetrated and before scission. This γ-decay will of course take place between levels in the second well, the shape isomer. The highly specific coincidence requirement, along with the lack of structure in the fission prompt γ ray emission, would allow detection of γ transitions between levels in the second well (provided, of course, that the second well is at least partially populated by states above the lowest state in the well). Figure 7.2 tantalizingly shows what appears to be true peaks in both the ^{232}Am and ^{234}Am spectra. With better statistics in the data and the addition of a γ-γ coincidence gate, it might be possible to construct a fairly complete level scheme for this shape isomer.

However, to study the level structure of the second well efficiently, it may be necessary to use a multiple-germanium-detector array such as **HERA** [DIAMOND 86]

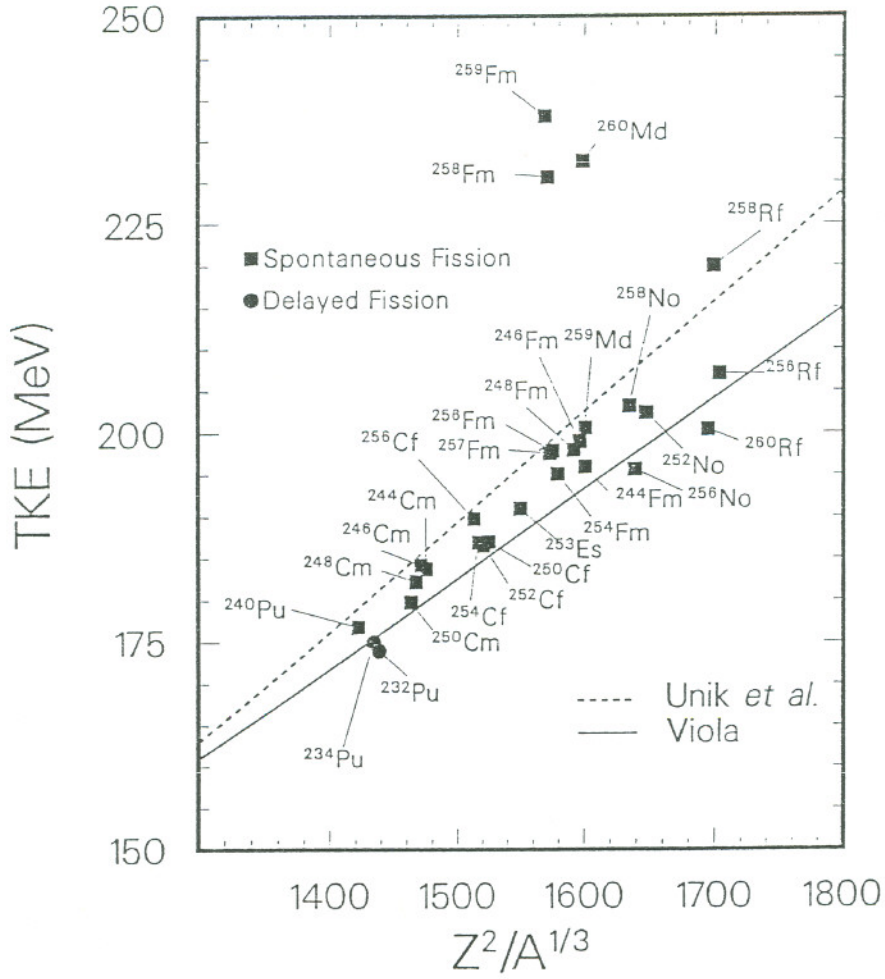

Figure 7.1: Average total kinetic energy as a function of $Z^2/A^{1/3}$. The solid line is a linear fit of Viola [VIOLA 66], and the dashed line is from Unik *et al.* [UNIK 74]. Ground-state (spontaneous) fission data for the trans-berkelium actinides are taken from Hoffman and Somerville [HOFFMAN 89], and data for the lighter actinides are from Hoffman and Hoffman [HOFFMAN 74]. $Z^2/A^{1/3}$ for the americium delayed fission is calculated for the plutonium daughter, since that is the fissioning nucleus.

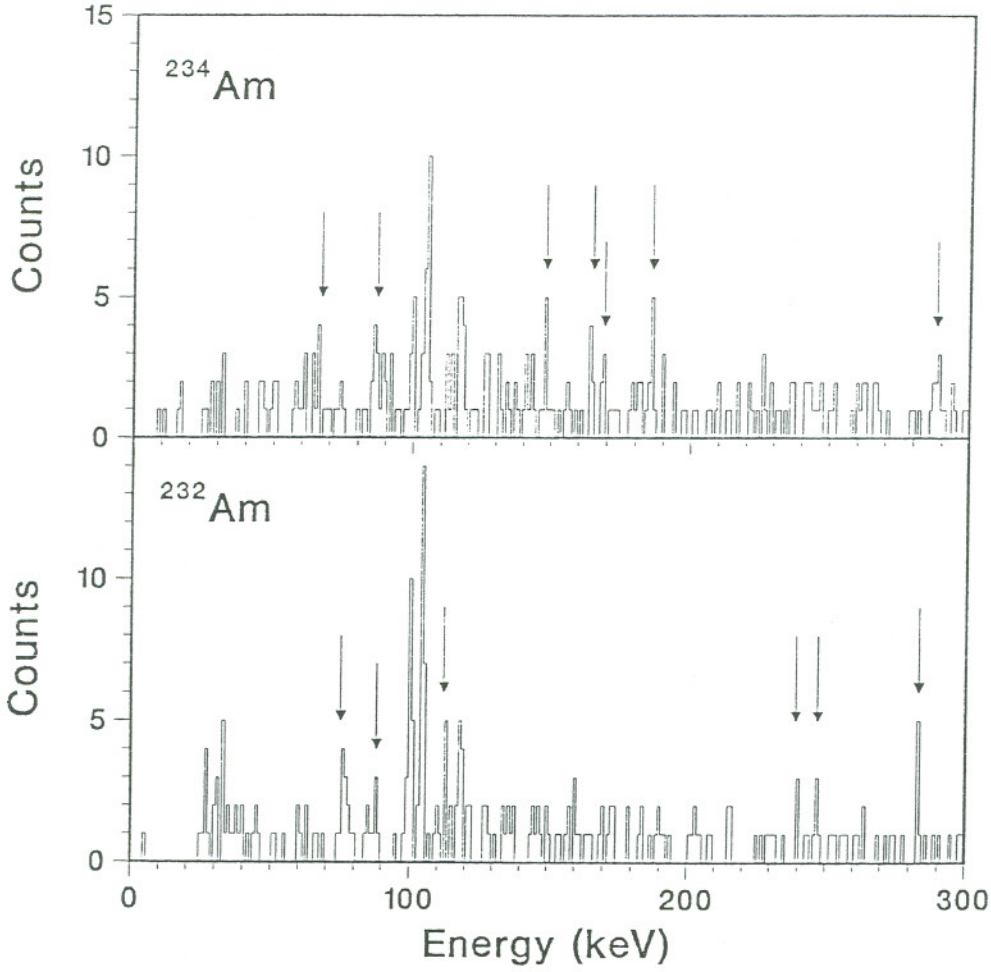

Figure 7.2: Experimental x-ray-fission coincidence data for ^{232}Am and ^{234}Am. Anomalous background peaks which could arise from γ transitions in the second well are marked with arrows.

or the proposed **GAMMASPHERE** [DELAPLANQUE 88]. A multiple-detector array is required to cover a large fraction of 4π with each individual detector subtending approximately 1% of 4π to overcome problems created by the high prompt γ-ray multiplicity intrinsic to fission.

If such an experiment is performed in such an array, it should be possible to construct the level scheme of the second well in ^{232}Am and ^{234}Am by triggering the γ detectors on the fission. Since the background γ rate from the beryllium-backed targets is only about 10^3 per second, random correlations should not pose a problem. In fact, the only significant background will arise from the fission prompt γ-ray continuum.

Appendix A

X-ray - Fission Code

```
      PROGRAM MLHX
C
C     THIS PROGRAM LOOKS AT THE SPECTRUM OF GAMMAS AND X-RAYS
C     IN COINCIDENCE WITH FISSIONS.  IT COMPARES THIS SPECTRUM
C     WITH THAT EXPECTED FOR FOUR GAUSSIANS (KA1, KA2, KB1, KB2)
C     AND DOES A MAXIMUM-LIKELIHOOD FIT USING THE GAUSSIAN
C     DETECTOR RESPONSE OVER THE MULTIPLET AND A POISSON
C     DISTRIBUTION AT EACH POINT ON THE GAUSSIANS.
C     WITH THE CALIBRATIONS USED, 1 CHANNEL = 0.25 keV.
      INTEGER*2     CC              !KA1 CENTRAL CHANNEL
      REAL*4        AMPKA1          !AMPLITUDE OF KA1 PEAK
      REAL*4     AMPKA2     !AMPLITUDE OF KA2 PEAK
      REAL*4     AMPKB1     !AMPLITUDE OF KB1 PEAK
      REAL*4     AMPKB2     !AMPLITUDE OF KB2 PEAK
      REAL*4     KXEXP(-100:100) !EXPECTED COUNTS IN KX REG
      CHARACTER*14  INFILE     !NAME OF XRAY HISTOGRAM
      CHARACTER*14  OUTFIL     !NAME OF CHI**2 HISTOGRAM
      INTEGER*2     HIST(0:2047)    !THE XRAY HISTOGRAM
      REAL*4     RH(0:2047)     !REAL REP. OF HIST(I)
      INTEGER*2     INREC     !RECORD NUMBER IN INPUT FILE
      REAL*4     LLH(0:2047)     !LOG OF LIKELIHOOD FUNCTION
      REAL*4     TOTX     !THE TOTAL NUMBER OF XRAYS
      INTEGER*2     IDIOT     !A "DUMMY" VARIABLE
      INTEGER*2     I     !GENERIC COUNTER
      REAL*4     SIG2     !SIGMA**2 OF GAUSSIAN PEAKS
      REAL*4     MINLLH     !SMALLEST LOG LIKELIHOOD
      REAL*4     MAXLLH     !LARGEST LOG LIKELIHOOD
      REAL*4     SCALER     !SCALING FACTOR FOR OUTPUT
      REAL*4     LFAC(0:100)     !LN OF FACTORIALS
```

```
      REAL*4     BKGD     !BACKGROUND PER CHANNEL
      REAL*4     LLHB(0:2047)    !PROB PER CHANNEL IN BKGD REG
C
C     CALCULATE THE LOGS OF THE FACTORIALS
C
      LFAC(0) = 0
      DO 10 I=1,100
 10   LFAC(I) = LFAC(I-1) + LOG( FLOAT(I) )
      BKGD = 0.1
C
C     GET THE INPUT FILE AND OPEN IT
C
 100  WRITE(5,110)
 110  FORMAT('  WHAT IS THE NAME OF THE X-RAY SPECTRUM? ',$)
      READ(5,'(A14)',ERR=100) INFILE
      OPEN(UNIT=1,ACCESS='DIRECT',FILE=INFILE,RECL=2050,STATUS='OLD',
     XREADONLY)
C
C     READ IN THE HISTOGRAM
C
 120  WRITE(5,130) INFILE
 130  FORMAT(' WHICH RECORD IN ',A14,' TO BE USED? ',$)
      READ(5,*,ERR=120) INREC
      READ(1,REC=INREC)(IDIOT,I=1,4),(HIST(I), IDIOT, I=0,2047)
C
C     COPY HISTOGRAM INTO A REAL REPRESENTATION
C
      DO 132 I=0,2047
 132  RH(I) = FLOAT( HIST(I) )
C
C     GET TOTAL NUMBER OF X-RAYS AND CALCULATE THE EXPECTED SPECTRUM
C     THIS INCLUDES 0.1 COUNT PER CHANNEL BACKGROUND
C
 140  WRITE(5,150)
 150  FORMAT('  HOW MANY X-RAYS WILL BE ASSUMED? ',$)
      READ(5,*,ERR=140) TOTX
 160  WRITE(5,170)
 170  FORMAT('  WHAT IS THE FWHM IN THE X-RAY REGION (keV)? ',$)
      READ(5,*,ERR=160) SIG2
      SIG2 = (SIG2/2.345*4.)**2
      AMPKA1=.478698*TOTX/2.5066/SIG2**.5
      AMPKA2=.299186*TOTX/2.5066/SIG2**.5
      AMPKB1=.106271*TOTX/2.5066/SIG2**.5
      AMPKB2=.059837*TOTX/2.5066/SIG2**.5
      AMPKB3=.056008*TOTX/2.5066/SIG2**.5
      DO 180 I=-100,100
         KXEXP(I)=AMPKA2*EXP(-((FLOAT(I)+16.84)**2.)/SIG2/2.
```

```
         KXEXP(I)=KXEXP(I)+AMPKA1*EXP(-((FLOAT(I)+00.00)**2.)/SIG1/2.)
         KXEXP(I)=KXEXP(I)+AMPKB1*EXP(-((FLOAT(I)-54.00)**2.)/SIG1/2.)
         KXEXP(I)=KXEXP(I)+AMPKB2*EXP(-((FLOAT(I)-67.36)**2.)/SIG1/2.)
         KXEXP(I)=KXEXP(I)+AMPKB3*EXP(-((FLOAT(I)-50.04)**2.)/SIG1/2.)
 180  KXEXP(I) = KXEXP(I) + BKGD
      WRITE(5,200)
 200  FORMAT(1X,'    KA2    KA1    KB1    KB2')
      DO 210 I = 0,16
 210  WRITE(5,220)KXEXP(I-25),KXEXP(I-8),KXEXP(I+43),KXEXP(I+59)
 220  FORMAT(1X,4(E11.5,1X))
C
C     GET THE OUTPUT FILE AND OPEN IT
C
 230  WRITE(5,240)
 240  FORMAT('  NAME OF LOG LIKELIHOOD OUTPUT HISTOGRAM? ',$)
      READ(5,'(A14)',ERR=230) OUTFIL
      OPEN(UNIT=2,ACCESS=DIRECT,FILE=OUTFIL,RECL=2050,STATUS='NEW')
C
C     DO THE MAXIMUM-LIKELIHOOD STUFF
C
C     CALCULATE THE PROBABILITIES FOR BACKGROUNS REGIONS
C
      MINLLH = 1.E+37
      DO 290 I=0,2047
 290  LLHB(I)=RH(I)*LOG(BKGD)-BKGD-LFAC(HIST(I))
C
C     STEP THROUGH ALL POSSIBLE VALUES OF KA1 CENTRAL CHANNEL
C
      DO 300 CC=200,1800
         LLH(CC)=0
         DO 310 I=100,CC-29
 310     LLH(CC)=LLH(CC)+LLHB(I)
         DO 320 I=-30,80
 320     LLH(CC)=LLH(CC)+RH(CC+I)*LOG(KXEXP(I))-KXEXP(I)-
     X   LFAC(HIST(CC+I))
         DO 330 I=CC+81, 1900
 330     LLH(CC)=LLH(CC)+LLHB(I)
         IF(LLH(CC).LT.MINLLH)THEN
            MINLLH=LLH(CC)
         ENDIF
         IF(MOD(CC,100).EQ.0)WRITE(5,333)CC,LLH(CC)
 333  FORMAT(' CHANNEL=',I4,' LOG LIKELIHOOD=',E12.6)
 300  CONTINUE
 340  WRITE(5,350)MINLLH
 350  FORMAT(' MIN LOG LIKELIHOOD = ',E9.3,' SCALING FACTOR? ',$)
      READ(5,*)SCALER
      DO 360 I=0,2047
```

```
 360  LLH(I) = LLH(I) + SCALER
C
C     FILL IN THE PARTS OF THE SPECTRUM THAT HAVEN'T BEEN USED
C
      DO 370 I=0,199
 370  LLH(I)=LLH(200)
      DO 380 I=1801,2047
 380  LLH(I)=LLH(1800)
      IDIOT=0
      WRITE(2,REC=1)JINT(SCALER),IDIOT,IDIOT,(JINT(LLH(I)),I=0,2047)
      CLOSE(1)
      CLOSE(2)
      STOP
      END
```

Bibliography

[ALLAERT 82] E. Allaert, C. Wagemans, G. Wegener-Penning, A. J. Deruytter, and R. Barthélémy, *Nucl. Phys. A380*, 61 (1982).

[AUMANN 74] D. C. Aumann and G. Müllen, *Nucl. Inst. Meth. 115*, 75–81 (1974).

[BAAS-MAY 85] A. Baas–May, J. V. Kratz, and N. Trautmann, *Z. Physik A 322*, 457 (1985).

[BEDOV 56] V. B. Bedov and V. N. Kosyakov, *Proc. Int'l Conf. Peaceful Uses of Atomic Energy 7*, 369–373 (1956).

[BERLOVICH 69] É. E. Berlovich and Yu. P. Novikov, *Dok. Akad. Nauk SSSR 185*, 1025 (1969) [*Sov. Physics—Doklady 14*, 349 (1969)].

[BHANDARI 89] B. S. Bhandari and A. S. Al-Kharam, *Phys. Rev. C 39*, 917 (1989).

[BLONS 84] J. Blons, C. Mazur, D. Paya, M. Ribrag, and H. Weigmann, *Nucl. Phys. A414*, 1 (1984).

[BRANDT 63] R. Brandt, S. G. Thompson, R. C. Gatti, and L. Phillips, *Phys. Rev. 131*, 2617 (1963)

[BROWNE 89] E. Browne, B. Sur, E. B. Norman, H. L. Hall, R. A. Henderson, K. T. Lesko, R. M. Larimer, and D. C. Hoffman, *Nucl. Phys. A*, in press.

[BURBIDGE 57] E. M. Burbidge, G. R. Burbidge, W. A. Fowler, and F. Hoyle, *Rev. Mod. Phys. 29*, 547 (1957).

[CUMMING 64] J. B. Cumming, *NAS-NS 3107*, 25 (1963). Also, *Brookhaven National Laboratory Report No. BNL-6470* (1963).

[DELAPLANQUE 88] "GAMMASPHERE - A Proposal for a National Gamma Ray Facility," M.-A. Delaplanque and R. M. Diamond, eds., *Lawrence Berkeley Laboratory Publication No. PUB-5202* (1988).

[DIAMOND 86] R. M. Diamond, *in* **Nuclei Off the Line of Stability**, R. A. Meyer and D. S. Brenner, eds., (ACS Symposium Series, Washington, DC, 1986) 341.

[ELLIS-AKOVALI 83] Y. A. Ellis-Akovali, *Nucl. Data Sheets 40*, 523 (1983).

[EVANS 72] J. E. Evans, R. W. Lougheed, M. S. Coops, R. W. Hoff and E. K. Hulet, *Nucl. Inst. Meth. 102*, 389–401 (1972).

[GANGRSKIĬ 78] Yu. P. Gangrskiĭ, G. M. Marinescu, M. B. Miller, V. N. Samoyusk, and I. F. Kharisov, *Yad. Fiz. 27*, 894 (1978) [*Sov. J. Nucl. Phys. 27*, 475 (1978)].

[GANGRSKIĬ 80] Yu. P. Gangrskiĭ, M. B. Miller, L. V. Mikhaĭlov, and I. F. Kharisov, *Yad. Fiz. 31*, 306 (1980) [*Sov. J. Nucl. Phys. 31*, 162 (1980)].

[GOERLACH 78] U. Goerlach, D. Habs, M. Just, V. Metag, P. Paul, H. J. Specht, and H. J. Maier, *Z. Physik A 287*, 171 (1978).

[GREGORICH 85] K. E. Gregorich, *Ph. D. Thesis* (1985). Also, *Lawrence Berkeley Laboratory Report No. 20192* (1985).

[HABS 78] D. Habs, H. Klewe–Nebenius, V. Metag, B. Neumann, and H. J. Specht, *Z. Physik A 285*, 53 (1978).

[HALL 89A] H. L. Hall, M. J. Nurmia, D. C. Hoffman, *Nucl. Inst. Meth. A276*, 649 (1989).

[HALL 89B] H. L. Hall, K. E. Gregorich, R. A. Henderson, D. M. Lee, D. C. Hoffman, M. E. Bunker, M. M. Fowler, P. Lysaght, J. W. Starner, and J. B. Wilhelmy, *Phys. Rev. C 39*, 1866 (1989).

[HALL 89C] H. L. Hall, K. E. Gregorich, R. A. Henderson, C. M. Gannett, R. B. Chadwick, J. D. Leyba, K. R. Czerwinski, B. Kadkhodayan, S. A. Kreek, D. M. Lee, M. J. Nurmia, and D. C. Hoffman, submitted to *Phys. Rev. Lett.* Also, *Lawrence Berkeley Laboratory Report No. 27425* (1989).

[HALL 89D] H. L. Hall, K. E. Gregorich, R. A. Henderson, C. M. Gannett, R. B. Chadwick, J. D. Leyba, K. R. Czerwinski, B. Kadkhodayan, S. A. Kreek, D. M. Lee, M. J. Nurmia, D. C. Hoffman, C. E. A. Palmer, and P. A. Baisden, submitted to *Phys. Rev. C.* Also, *Lawrence Berkeley Laboratory Report No. 27510* (1989).

[HAMILTON 85] J. H. Hamilton, P. G. Hansen, and E. F. Zganjar, *Rep. Prog. Phys. 48*, 631 (1985).

[HAYNES 88] G. R. Haynes, J. D. Leyba, and D. C. Hoffman, *private communication* (1988).

[HILL 53] D. L. Hill and J. A. Wheeler, *Phys. Rev. 89*, 1102 (1953).

[HINGMANN 85] R. Hingmann, W. Kuehn, V. Metag, R. Novotny, A. Ruckelshausen, H. Stroeher, F. Hessberger, S. Hofmann, G. Muenzenberger, and W. Reisdorf, *Gessellschaft für Schwerionenforschung, Darmstadt, Report No. GSI 85–1*, 88 (1985).

[HOFF 86] R. W. Hoff, *in* **Weak and Electromagnetic Interactions in Nuclei,** H. V. Klapdor, ed., Springer-Verlag (Heidelburg, 1986), 207.

[HOFF 88] R. W. Hoff, *Inst. Phys. Conf. Ser. No. 88/J. Phys. G:Nucl. Phys. 14 Suppl.*, S343 (1986).

[HOFFMAN 74] D. C. Hoffman and M. M. Hoffman, *Ann. Rev. Nucl. Sci. 24*, 151 (1974).

[HOFFMAN 89] D. C. Hoffman and L. P. Somerville, *in* **Charged Particle Emission from Nuclei Vol. III**, D. N. Poenaru and M. Ivaşcu, eds., (CRC Press, Boca Raton, Fla., 1989) 1.

[HORNSHØJ 75] P. Hornshøj, B. R. Erdal, P. G. Hansen, B. Jonson, K. Aleklett, and G. Nyman, *Nucl. Phys. A239*, 15 (1975).

[HUBERT 80] F. Hubert, A. Fleury, R. Bimbot, and D. Gardes, *Ann. Phys., Fr. 5*, 1 (1980).

[ITKIS 88] M. G. Itkis, V. N. Okolovich, and A. Ya. Rusanov, *Fiz. Elem. Chastits At. Yadra 19*, 701 (1988) [*Sov. J. Part. Nucl. 19*, 301 (1988)].

[KLAPDOR 79] H. V. Klapdor, C.-O. Wene, I. N. Isosimov, and Yu. W. Naumow, *Z. Physik A 292*, 249 (1979).

[KLAPDOR 81] H. V. Klapdor, T. Oda, J. Metzinger, W. Hillebrandt, and F. K. Thielman, *Z. Physik A 299*, 213 (1981).

[KODAMA 75] T. Kodama and K. Takahashi, *Nucl. Phys. A239*, 489 (1975).

[KONECNY 73] E. Konecny, H. J. Sprecht, and J. Weber, *Phys. Lett. 45B*, 329 (1973).

[KRATZ 73] K. L. Kratz and G. Herrmann, *Z. Physik 263*, 435 (1973).

[KUZNETSOV 66] V. I. Kuznetsov, N. K. Skobelev, and G. N. Flerov, *Yad. Fiz. 4*, 279 (1966) [*Sov. J. Nucl. Phys. 4*, 202 (1967)].

[KUZNETSOV 67] V. I. Kuznetsov, N. K. Skobelev, and G. N. Flerov, *Yad. Fiz. 5*, 271 (1967) [*Sov. J. Nucl. Phys. 5*, 191 (1967)].

[KUZNETSOV 79] V. I. Kuznetsov, *Yad. Fiz. 30*, 321 (1979) [*Sov. J. Nucl. Phys. 30*, 166 (1979)].

[LAZAREV 80] Yu. A. Lazarev, Yu. Ts. Oganessian, and V. I. Kuznetsov, *Joint Institutes for Nuclear Research, Dubna, Report No. JINR-E7-80-719* (1980).

[LAZAREV 87] Yu. A. Lazarev, Yu. Ts. Oganessian, I. V. Shirokovsky, S. P. Tretyakova, V. K. Utyonkov, and G. V. Buklanov, *Europhys. Lett. 4*, 893 (1987).

[LEDERER 78] C. M. Lederer, V. M. Shirley, E. Browne, J. M. Dairiki, R. E. Doebler, A. A. Shihab-Eldin, L. J. Jardine, J. K. Tuli, and A. B. Buyrn, **Table of Isotopes** (John Wiley & Sons, New York, 1978).

[LEYBA 89] J. D. Leyba, R. A. Henderson, H. L. Hall, C. M. Gannett, R. B. Chadwick, K. R. Czerwinski, B. Kadkhodayan, S. A. Kreek, G. R. Haynes, K. E. Gregorich, D. M. Lee, M. J. Nurmia, and D. C. Hoffman, *to be published, 1989.*

[MEYER 89] B. S. Meyer, W. M. Howard, G. J. Matthews, K. Takahashi, P. Möller, and G. Leander, *Phys. Rev. C 39*, 1876 (1989).

[MÖLLER 88] P. Möller, W. D. Myers, W. J. Świątecki, and J. Treiner, *At. Data Nucl. Data Tables 39*, 225 (1988).

[MOLTZ 80] D. M. Moltz, J. M. Wouters, J. Äystö, M. D. Cable, R. F. Parry, R. D. von Dincklage and J. Cerny, *Nucl. Inst. Meth. 172*, 519–525 (1980).

[MÜLLEN 75] G. Müllen and D. C. Aumann, *Nucl. Inst. Meth. 128*, 425–428 (1975).

[NORTHCLIFFE 70] L. C. Northcliffe and R. F. Schilling, *Nucl. Data Tables A 7*, 233 (1970).

[POENARU 89] D. N. Poenaru, M. S. Ivaşcu, and D. Mazilu, *in* **Charged Particle Emission from Nuclei Vol. III**, D. N. Poenaru and M. Ivaşcu, eds., (CRC Press, Boca Raton, Fla., 1989) 41.

[ROUTTI 69] J. T. Routti and S. G. Prussin, *Nucl. Inst. Meth. 72*, 125 (1969).

[SCHMITT 65] H. W. Schmitt, W. E. Kiker, and C. W. Williams, *Phys. Rev. 137*, B837 (1965).

[SCOFIELD 74] J. H. Scofield, *At. Data Nucl. Data Tables 14*, 121 (1974)

[SHALEV 77] S. Shalev and G. Rudstam, *Nucl. Phys. A275*, 76 (1977).

[SKOBELEV 72] N. K. Skobelev, *Yad. Fiz. 15*, 444 (1972) [*Sov. J. Nucl. Phys. 15*, 249 (1972)].

[SOMERVILLE 77] L. P. Somerville, A. Ghiorso, M. J. Nurmia, and G. T. Seaborg, *Lawrence Berkeley Laboratory Nuclear Science Division Annual Report, 1976-1977, Report No. LBL-6575*, 39 (1977).

[SPECHT 74A] H. J. Specht, *Rev. Mod. Phys. 46*, 773 (1974).

[SPECHT 74B] H. J. Specht, *Phys. Scripta 10A*, 21 (1974).

[THIERENS 81] H. Thierens, A. De Clerq, E. Jacobs, D. De Frenne, P. D'hondt, P. De Gelder, and A. J. Deruytter, *Phys. Rev. C 23*, 2104 (1981).

[THIERENS 83] H. Thierens, A. De Clerq, E. Jacobs, M. Piessens, P. D'hondt, D. De Frenne, *Phys. Rev. C 27*, 1117 (1983).

[UNIK 74] J. P. Unik, J. E. Gindler, L. E. Glendenin, K. F. Flynn, A. Gorski, and R. K. Sjoblom, *in* **Proceedings of the 3rd IAEA Symposium on the Physics and Chemistry of Fission, 1973, Vol. 2** (International Atomic Energy Agency, Vienna, 1974), 19.

[VANDENBOSCH 73] R. Vandenbosch and J. R. Huizenga, **Nuclear Fission**, Academic Press (New York, 1973).

[VIOLA 66] V. Viola, *Nucl. Data, Sect. B 1*, 391 (1966).

[WAGEMANS 84] C. Wagemans, E. Allaert, A. Deruytter, R. Barthélémy, and P. Schillebeeckx, *Phys. Rev. C 30*, 218 (1984).

[WILD 88] J. Wild, *Private communication* (1988).

[WEISSENBERGER 86] E. Weissenberger, P. Geltenbort, A. Oed, F. Gönnenwein, and H. Faust, Nucl. Inst. Meth. A248, 506 (1986).

[WENE 74] C.-O. Wene and S. A. E. Johansson, *Phys. Scripta 10A*, 156 (1974).

[WENE 75] C.-O. Wene, *Astron. & Astrophys. 44*, 233 (1975).

LAWRENCE BERKELEY LABORATORY
TECHNICAL INFORMATION DEPARTMENT
1 CYCLOTRON ROAD
BERKELEY, CALIFORNIA 94720